UNIVERSITY OF CALIFORNIA
RIVERSIDE

Development of Particulate Matter Mass Measurement Methods for Atmospheric Air Quality Monitoring and Very Low Vehicle Emissions

A Dissertation submitted in partial satisfaction
of the requirements for the degree of

Doctor of Philosophy

in

Mechanical Engineering

by

Liem T. Pham

December 2017

Dissertation Committee:
Dr. Heejung Jung, Chairperson
Dr. Kambiz Vafai
Dr. Roya Bahreini

The Dissertation of Liam T. Pham is approved:

Committee Chairperson

University of California, Riverside

Acknowledgments

I would like to dedicate this part of my dissertation and have moment to thank all the agencies, companies, and individuals who helped made this dissertation possible. I would like to thank the University of California, Riverside for providing me this opportunity to study in the Department of Mechanical Engineering and financial support that I needed to complete this program. I want to thank the Center of Environmental Research and Technology (CE-CERT) for providing me an interdisciplinary learning environment and the necessary resources to conduct my research.

I want to show appreciation to the University of California Transportation Center (UCTC) and National Center for Sustainable Transportation (NCST) for the fellowship I received. I want to show appreciation to Dr. Arthur Miller for allowing me to use their CPCs. I acknowledge the National Science Foundation (Grant #: 1233038) for supporting this research. I acknowledge TSI, MSP, AVL, Horiba, Sierra Instruments, Sick, California Air Resources Board, and Motor Trend for allowing us to use their equipment and vehicles for the cabin air project. I want to thank Nick Molden, Sam Boyle, Jesus Flores, and Alan Lau from Emission Analytics for their time and effort in obtaining the vehicles, setting up the instruments, and conducting the tests. I also want to acknowledge the funding from the Coordinating Research Council under the E99-2 project. I acknowledge Mark Villela, Daniel Gomez, Kurt Bumiller, Edward O'Neil, Don Pacocha, Lauren Ackock, and Grace Johnson of the University of California, Riverside for their contributions in conducting the emissions testing for this program and the lab experience that I gained through interactions with them.

Without the tremendous support from my colleagues and mentors at CE-CERT and the Mechanical Engineering Department, this dissertation would not be possible. I want to thank my labmates whom are Michael Grady, Yang Li, Yue Lin, Desireé Smith, and Eli Brewer, Michael Han, and Dr. Chengguo Li for their insights and support. I also want to thank other colleagues from other groups, Dr. Ji (Jill) Luo, Dr. Derek Price, Dr. Mary Kacarab, Jiacheng (Joey) Yang, Daniel Sandez, Yu (Jade) Jiang, Xinze (Eric) Peng, Weihan Peng, Paul Van Rooy, Patrick Roth, William Lichtenberg, Christos Stamatis. I also want to thank to my mentors whom are Dr. Kent Johnson, Dr. Tom Durbin, Dr. George Scora, Dr. Gouyuan Wu, and Dr. Jian (Eric) Xue. I want to thank Dr. Roya Bahreini, and Dr. Kambiz Vafai for serving in my committee and providing beneficial feedbacks. I also want to especially thank Dr. David Cocker, Dr. Akua Asa-Awuku, and Dr. Kelley Barsanti for allowing me to attend their weekly group meeting where I had a chance to learn and be exposed to many research areas.

I want to give a special gratitude to my advisor, Dr. Heejung Jung, who had been there to guide me through this journey for the last five years. He provided guidance, knowledge, and financial support for me to thrive in this research area. He is a great role model, both in the academia and simply as a person. Lastly, I would like to thank my family for their relentless, unconditional support and encouragement for which I am forever grateful. Without them, this would not be possible. Thank you all.

The work in Chapter 2 was published in Journal of Aerosol Science 2016, 102, 96 –104.

To my family and parents,

Pham Ngoc Rinh and Dong Thi Tam

ABSTRACT OF THE DISSERTATION

Development of Particulate Matter Mass Measurement Methods for Atmospheric Air Quality Monitoring and Very Low Vehicle Emissions

by

Liem T. Pham

Doctor of Philosophy, Graduate Program in Mechanical Engineering
University of California, Riverside, December 2017
Dr. Heejung Jung, Chairperson

The public raises concerns about the exposure to particulate matter (PM) which has been strongly associated with illness and mortality. However, most of the studies relied on the measurements from stationary monitoring sites, which cannot capture the actual PM exposure for those at or near the source. In this study, both stationary and comprehensive mobile monitoring platforms were developed to measure PM concentration and traffic conditions on some major highways in Southern California. The main objective is to develop a set of alternative metrics that measure particle concentrations as well as particle size. Measurement of particle size distributions are useful but doing so to monitor a wide region is not practical. The use of a particle counter and a diffusion charger was investigated as a relatively simple means to measure spatiotemporally-resolved particle concentrations over a wide region using a mobile platform. While the condensation particle counter and electrical aerosol detector respectively measure particle number and particle active surface area concentrations, the ratio of surface area over number provides an additional information of particle size

which is important for particle transport. Particle size distributions measured by scanning mobility particle sizer during ambient monitoring were used to verify the concept. The study found that alternative metrics (number, surface area, and ratio of surface area over number) can be used to monitor spatiotemporally resolved particle concentrations over a wide region.

Gravimetric sampling methods on a chassis dynamometer were studied in accordance to Code of Federal Regulations. This study evaluated commercially available partial flow dilutors with a focus on their equivalency with the standard constant volume sampler system and the ability to provide reproducible measurements at low PM emission levels. As PM standards for light-duty vehicles are becoming more stringent, improving the confidence and understanding the mass measurement methods become one of the main goals for the industry and regulatory agencies. Simultaneous testing was conducted with three partial flow dilutors over the Federal Test Procedure and US06 drive cycles. The Federal Test Procedure had means that were statistically different for two of the three partial flow dilutors. As for the US06 tests, the mean differences were not statistically different. The performance of all partial flow dilutors also showed repeatable and accurate level of proportionality, which could easily meet the Code of Federal Regulations 1066 and 1065 requirements for all tests performed.

Table of Contents

List of Figures

List of Tables

Definitions/Abbreviations

σ	Standard Deviation	σ_g	Geometric Standard Deviation of the Lognormal Distribution
AQE	Air Quality Egg	Bag	Phase of the FTP Bag Measurement System
CARB	California Air Resources Board	CAST	Combustion Aerosol STandard
CE-CERT	College of Engineering-Center for Environmental Research and Technology	CFR	Code of Federal Regulations
CMD	Count Median Diameter	CO	Carbon Monoxide
CO_2	Carbon Dioxide	CPC	Condensation Particle Counter
CVS	Constant Volume Sampling	DF	Dilution Factor
DMM	Dekati Mass Monitor	EAD	Electrical Aerosol Detector
EC	Elemental Carbon as Defined by NIOSH Methods	EFM	Exhaust Flow Meter
EMFAC	EMission FACtors	USEPA	United States Environmental Protection Agency
EEPS	Engine Exhaust Particle Sizer	E10	10% ethanol in gasoline blend by weight
EV	Electric Vehicles	FFV	Filter Face Velocity
FTP	Federal Test Procedure	GDI	Gasoline Direct Injection
GMDs	Geometric Mean Diameters	GSD	Geometric Standard Deviation
ID	Inner Diameter	ISO	International Organization for Standardization
$\boldsymbol{Kn}$	Knudsen Number	LDVs	Light Duty Vehicles
LEV	Low-Emission Vehicle	MCM	Mass Concentration Monitor
MFC	Mass Flow Controller	MOVES	Motor Vehicle Emission Simulator
MSS	Micro Soot Sensor	NAAQS	National Ambient Air Quality Standards
NCST	National Center for Sustainable Transportation	NIOSH	National Institutes of Safety and Health method
NIST	National Institute for Standards and Technology	NOx	Nitrogen Oxides
NSAM	Nanoparticle Surface Area Monitor	OC	Organic Carbon

o.d.	Outer Diameter	PAH	Polycyclic Aromatic Hydrocarbons
OPS	Optical Particle Sizer	PFD	Partial Flow Dilution System
PFI	Conventional Port Fuel Injection	PHEM	Passenger Car and Heavy-Duty Emission Model
PM	Particulate Matter	PSD	Particle Size Distribution
PTFE	Polytetrafluoroethylene	SCAQMD	South Coast Air Quality Management District
SO_2	Sulfur Dioxide	SEE	Standard Error Estimate
SMPS	Scanning Mobility Particle Sizer	SwRI	Southwest Research Institute
TB	Tunnel Blank	TECS	Tailored Electrode Concentration Sensor
US06	US06 Test Cycle	UCR	University of California at Riverside
UFP	Ultrafine Particle	UCTC	University of California Transportation Center
VERL	Vehicle Emissions Research Laboratory	VISSIM	Verkehr In Städten - SIMulationsmodell
VOC	Volatile Organic Compound	VSP	Vehicle Specific Power
WHDC	Heavy-Duty On-Highway Engines		

1 Introduction

Traffic congestion has been the daily norm in many metropolitan areas. The associated socio-economic issues, such as the waste in energy consumption and air pollution, have received increasing attentions from the public. The major pollutants emitted by vehicles include carbon monoxide (CO), volatile organic compounds (VOCs), nitrogen oxides (NO_x), particulate matter (PM), and polycyclic aromatic hydrocarbons (PAHs) [1]. It is estimated by the U.S. Environmental Protection Agency (USEPA) that the nationwide CO, NO_x, PM (including PM2.5 and PM10), and sulfur dioxide (SO_2) emissions due to transportation activities were about 36.30, 7.16, 0.49, 0.34 and 0.10 million metric tons, respectively, in Year 2014 [2]. Of all these commonly-seen air pollutants, PM has been strongly associated with illness and mortality, such as respiratory inflammation, allergy, and asthma attacks, as indicated in many studies [3, 4, 5, 6]. For example, California Air Resources Board (CARB) estimated that annually about 9,200 people in California die prematurely as a result of exposure to PM2.5 [7]. Other detrimental health effects caused by the exposure to PM may include respiratory and cardiovascular morbidity [8, 9]. In addition, the ultrafine particles (less than 100 nanometers in diameter) whose dominant sources are diesel engine powered vehicles [10], have been considered to be more toxic by many researchers due to their unique physical properties, interactions with tissues and cells, and the potential for translocation beyond the lung [11]. The National Ambient Air Quality Standards (NAAQS) set by USEPA suggest that the annual mean for primary PM2.5 should not exceed 12 $\mu g/m^3$ and the temporal average of PM10 within any 24-hour period should not exceed 150 $\mu g/m^3$ [12].

Although a substantial body of research has been focused on assessment of public exposure to PM and the associated health effects, most of the measurement data were obtained from stationary monitoring sites which are not close enough to the sources, such as highways. For example, AIRNOW.GOV gives a general trend of where the highest PM concentrations are regionally, but it does not give enough details at finer scale to show the highest concentrations on and near highways. In recognition of this issue, EPA's new air pollution rules require air pollution monitoring near road starting Jan 2014. For example, South Coast Air Quality Management District has implemented four air pollution monitoring stations in the proximity of major highways to monitor nitrogen oxides, fine particulate matter (soot), and carbon monoxide [13]. This implementation is to assess public's real exposure to these air pollutants. There are nearly one million people living within 300 feet from major highways in the South Coast Air Basin [14]. This may lead to discrepancy from the actual PM exposure for those people who are in or near the sources, e.g., travelers in the traffic flow [15]. This raises concerns for the real exposure when people are near sources such as being on the road and living near the highways. It was reported that the average time an American spent traveling in car is nearly 1 hour everyday [16]. Furthermore, previous studies estimated that in-cabin exposures to ultrafine particles (UFPs) might be 10 times higher than ambient levels and were responsible for 10 – 50% of total daily UFP exposure for Los Angeles commuters [17]. In consideration of all these concerns, USEPA's new air pollution rules require near-road monitoring starting from January 2014. Such effort significantly improves the accuracy in measuring the PM concentration near the mobile sources. However, the measurements are highly restricted

by the locations and sparsity of surveillance stations, resulting in difficulty to capture spatial variations of in-/near-source PM concentration.

A common approach to resolve this issue is to monitor PM concentrations using mobile platforms to get temporally and spatially resolved information. Many different researchers had reported particle concentrations and size distributions using particle sizing instruments, such as Scanning Mobility Particle Sizer (SMPS, TSI Inc.) installed on a mobile platform [18, 19, 20, 21, 22]. They provided detailed size distribution information, which is useful for research. However, particle size distribution measurement is not appropriate for a routine monitoring over a wide region. It is much more costly than other types of measurements for data collection and analysis. It is also difficult to present particle size distributions (PSDs) to show spatiotemporal evolution and distribution. Ranjan and Dhaniyala pointed out that a total number concentration is often sufficient to monitor particle exposure level [23].

Another approach is to monitor particle concentrations using multiple units of low cost particle sensors. Air Quality Egg (AQE) monitors NO_2 and CO gases globally using low cost sensors. Currently there is no true "low-cost" PM sensor commercially available. Many of available low-cost PM sensors use light scattering to detect particles, which is not appropriate to detect UFPs. A PM mass sensor is being developed by researchers at UC Berkeley [24]. This sensor has the potential to become a true low-cost PM sensor, which is also sensitive to ultrafine particles. Unfortunately, this sensor is currently not available in the market.

The model-based approach can be implemented but it heavily relies on detailed traffic conditions and emissions models [25]. Based on the resolution of available traffic information, microscopic, mesoscopic or macroscopic motor emission models such as MOVES [26], EMFAC [27], and PHEM [28], can be applied to estimate the tailpipe PM emissions. For example, Hausberger et al. applied a self-developed emission model for mobile sources to the traffic data at a test intersection to assess the traffic related PM emissions [29]. Abou-Senna et al. used VISSIM to simulate real-world traffic condition and predict the mobile source emissions using MOVES model [30]. In Hao et al. 2015, the authors developed a statistical model to estimate the vehicle speed trajectory based on sparse mobile sensor data from the probe vehicle, and estimated the PM emissions by applying a microscopic emission model [31]. Compared to the stationary measurement-based approach, the model-based one can be applied to the in-/near-source PM emissions assessment at a much larger scale in a much more economical manner. However, the model accuracy and reliability for on-road traffic is still questionable, since most models were developed using dynamometer tests from standard drive cycles, which may not necessarily apply well to real-world driving due to the effects of road grades, driving behavior, fleet composition, and traffic conditions.

The first chapter proposes and validates alternative metrics to monitor spatiotemporally resolved particle concentrations using relatively simple instruments: a particle counter and a particle surface instrument. There are a few promising commercially available instruments for ambient particle monitoring in real time. A condensation particle counter (CPC) has been widely used to measure number-based particle concentrations. A

diffusion charger is another promising instrument. The response of a diffusion charger is proportional to the effective surface area for acquiring electrical charge by the diffusion of ions produced in a corona discharge. Particle active surface area is a good metric to correlate with health effects.

The deficiency of using a single metric is that it can not provide information regarding particle size. Particle transport such as particle lung deposition is a strong function of particle size. None of single metrics such as mass, surface area, and number give such information. There are previous studies to use combination of a particle surface instrument and a particle counter for ambient air monitoring in an attempt to extract information regarding particle size. Ntziachristos et al. reported the mean diameter obtained from the ratio of Nanoparticle Surface Area Monitor (NSAM, TSI) and CPC measurements were in good agreement with the SMPS arithmetic mean diameter from particle size distributions [32]. The NSAM and Electrical Aerosol Detector (EAD, TSI) are similar instruments, because of their fundamental measurement techniques. On the other hand, Frank et al. conducted calibration tests using a CAST (Combustion Aerosol STandard) system and reported that EAD/CPC and SMPS have a poor agreement in terms of the mean particle diameter and total aerosol length [33]. They attributed the difference in the mean particle size determined by the SMPS against the EAD/CPC method to the difference in concentrations measured by the CPC and SMPS rather than any difference in the characteristics of the three instruments (SMPS, EAD and CPC). They reported that the EAD and SMPS measurements were consistent with each other, because it was assumed that both instruments were affected by the same diffusion loss. Although Frank et al. was

mainly focused on comparing the particle mean diameter, they did not look into the relationship between particle size distribution and EAD/CPC ratio. Frank et al. overlooked characteristics of the EAD such as power law dependence and could not properly extract information contained in EAD/CPC ratio [33].

For the measurement-based approach, mobile PM monitoring or Lagrangian PM monitoring has become an attractive strategy, as it allows to cover long spatial range with high temporal resolution and to conduct real-time assessment on human exposure to in-/near-source PM concentration. For example, Fruin et al. used a mobile monitoring platform including a SMPS, to measure particle counts and size distributions [19]. There are other commercially available instruments for ambient particle monitoring in real time. CPC can effectively measure number-based particle concentration but not detailed information on particle size. EAD can measure aerosol active surface area of particles and has $d^{1.13}$ dependence between 10nm and 1μm. Most of these studies have been only focused on spatially-limit measurements of PM characteristics due to the significant cost for real-world experimentation. Very few studies have investigated the relationship between traffic conditions and in-/near-source PM concentrations (e.g., on highways).

The last section of this dissertation will investigate the ability to accurately characterize low levels of PM emissions from light-duty vehicles (LDVs). It is becoming more of an issue as the certification standards for vehicle emissions continue to become more stringent. Vehicle exhaust emissions have typically been measured using a Constant Volume Sampler (CVS) in the past. A CVS captures the whole exhaust flow while maintaining constant volumetric flow. This enables calculation of emission rates by the

product of concentrations measured at the CVS and its constant volume flow rate. Another approach that can be used to sample vehicle exhaust is a partial flow diluter (PFD). A PFD uses a different approach by taking only a small fraction of the vehicle exhaust flow proportional to the exhaust flow at all times [34, 35, 36, 37, 38, 39]. PFDs offer potentially significant cost savings, sampling flexibility, and performance benefits compared to the full flow CVS tunnel. PFDs have been more prevalent for the measurement of emissions of large engines, since it becomes impractical to utilize a CVS for engines with very high exhaust volumes. PFDs play an important role for on-road testing such as Europe's Real Driving Emission regulations due to their compact size. PFDs are of particular interest to quantify very low PM mass because of its potential to reduce adsorption artifacts. While the surface to volume ratio is higher for PFD, it is much easier to maintain the surface of the dilution tunnel clean leading to less adsorption artifact. More importantly, PFDs normally would take samples upstream of the transfer line, which would reduce the potential impacts of the storage-release effects of organic vapor from the walls [34].

The performance of PFD systems in comparison with full CVS systems has been evaluated in a number of studies over the past two decades. In the early 2000s, there was concern in the U.S. over allowing the use of PFDs for the measurement of PM mass for heavy-duty diesel engines over transient cycles as part of the International Organization for Standards (ISO) 16183 document. In conjunction with the development of this document, a study was conducted at the Southwest Research Institute (SwRI) to evaluate PFDs that were commercially available in the 2001 timeframe, including a AVL SPC, a Horiba MDLT, and a Sierra BG2 [35]. The findings of this work showed that PFDs

measured lower PM emissions rates than the CVS, which was attributed to the slow response of the PFDs to changes in the exhaust flow rate during transient operation. In other work in Europe, Schweizer and Stein evaluated PFDs as a subproject of worldwide certification procedure for heavy-duty on-highway engines (WHDC) [37]. The results of this study showed better agreement between the PFDs and CVS, with no consistent and statistically significant difference between the two systems, and that different PFD sampling parameters that were investigated had no or only minor influence on particulate mass and composition.

PFDs received greater attention with the implementation of significantly reduced PM emission standards for heavy-duty engines in the U.S. in 2007. A series of improvements to the gravimetric filter PM mass measurement method were implemented in 40 CFR, Part 1065 [40] as part of the development of the 2007 PM standards. The use of PFDs for PM measurements was among the provisions included in 40 CFR Part 1065. In conjunction with the implementation of the 2007 PM standards, a comprehensive E-66 study was conducted by Khalek et al. to evaluate and improve low level PM sampling for heavy-duty engines [41, 42, 43]. The E-66 study included an investigation of a number of commercially available PFDs for heavy-duty applications [43]. The results showed a considerable improvement in the performance of the PFDs compared to SwRI's previous 2002 work [35], including proportional sampling with a response time of 200 ms or less and correlations between engine exhaust flow and sample flow that showed correlations coefficients greater than 99 percent and a standard error of better than 5%. The PFDs were also able to show comparable performance with the CVS at PM levels below 10% of the

2007 standard for both steady state and transient operation. However, Khalek et al. investigated partial flow dilution as it applies to heavy-duty engine dynamometer emissions measurements, and there are numerous differences between heavy-duty engine dynamometer and light-duty chassis dynamometer testing.

There is also considerable interest in the potential for using PFDs for emissions measurements for light-duty vehicles (LDVs). This is particularly in light of the reductions of the PM standards from 10 to 3 mg/mi in 2017 as part of the USEPA Tier 3 and the California Lower Emission Vehicle (LEV) III regulations, with a further reduction to 1 mg/mi in 2025 as part of the California LEV III requirements [44, 45]. PM measurement for light duty vehicle in the US is based on Part 1066, which is being revised currently. Part 1066 permits the use of PFD for light duty vehicle PM measurement [46]. As PM emission levels and sampling environments are different between heavy duty and light duty, Foote et al. investigated two commercially available PFDs in 2013 for light duty vehicles [34]. They reported their PM mass results with PFD-A correlated well, while the PM mass with PFD-B underestimated compared to that from CVS. It was unclear why one of the PFDs underestimated the gravimetric PM mass relative to the CVS system, and further investigation was suggested. Ntziachristos and Samaras also conducted extensive evaluations of PFDs for both LDVs and light-duty engines [47]. Their results also showed that the PFDs had promise for low PM measurements for a wide range of engine sizes and applications. More recently, a comprehensive E-99 study of PM mass measurements from LDVs was conducted to evaluate increasing filter face velocity (FFV) (from 100 to 175), reducing dilution ratio (DR) (from 7 to 3), using cumulative vs. individual filters, and

comparing 3-bag and 4-bag Federal Test Procedure (FTP) tests [48]. A commercially available PFD was also evaluated in that study. The results for the PFD indicated reasonable performance relative to the full flow dilution tunnel, but only included a single commercially available unit. The focus of this study was to evaluate commercially available partial flow dilutors with a focus on their equivalency with the standard constant volume sampler system and the ability to provide reproducible measurements at low PM emission levels.

2 Alternative metrics for spatially and temporally resolved ambient particle monitoring

2.1 Introduction

This study aims to investigate particle active surface area concentration, particle number concentration, and their ratio as alternative metrics for spatially and temporally resolved ambient particle monitoring. A CPC and an EAD were used to monitor PN (particle number), PS (particle active surface area), and its ratio for this study. The study reports theoretical background and physical meaning of the EAD/CPC ratio. Data obtained from ambient air was analyzed to validate the concept. This method can be applied to mobile monitoring for a wide region using multiple platforms simultaneously considering relatively inexpensive instrumentation and convenience of data processing and presentation.

2.1 Theory

2.1.1 Background

Particles are charged by diffusion of ions and the charges carried by particles are detected by an electrometer in a unipolar diffusion charger equipped with an electrometer. The response of a diffusion charger is well predicted by diffusion charging theories, but some discrepancies exist for small particles. Pui et al. showed experimental data agree well with Fuchs charging theory above 10 nm [49]. Biskos et al. compared Fuchs charging theory with experimental data and calculation results by the birth-and-death theory [50]. They found the experimental results agree well with Fuchs charging theory while the

calculation fits well with the experimental results between 10 and 300 nm. On the other hand, Filippov compared Fuchs charging theory to Monte Carlo simulation and found out the agreement is down to 30 nm due to difference in treating ionic velocity distribution [51]. Keller et al. defined active surface area as the part of surface area that is responsible for exchanging energy and momentum in contrast to passive surface area which does not interact with carrier gas and diffusing species [52]. This active surface area is a similar concept to Fuchs surface area, which was first defined by Pandis et al. [53]. Keller et al. proposed scaling laws which relate mass transfer coefficient to mobility and diffusion constant [52]. They concluded the influence of image force is negligible above 20 nm for diffusion charging.

Pui et al. determined the mean free path of the dominant ion species for diffusion charging as 14.5 nm [49]. This makes the range of continuum and transition regime wider but makes free molecular regimes narrower for the size range of interest between 10 nm to 1 μm. Fuchs or active surface area is proportional to d_p^x where the exponent x is 1 for $Kn \ll 1$ and 2 for $Kn \gg 1$ for the mass transfer of diffusing species. In the transition regime, the exponent x varies as a function of Kn. Response of a diffusion charger can be approximated as a power of particle diameter for the range of measurement interest. Jung and Kittelson characterized various particle surface instruments including two diffusion chargers and reported $d^{1.13}$ and $d^{1.36}$ for the size range, 30-150 nm, for EAD and LQ1-DC [54]. TSI also conducted similar research on EAD and they reported that $d^{1.13}$ relationship can be extended up to 1 μm size [55]. This approximation of using a fixed exponent value

as opposed to varying exponent values as a function of particle size gives an opportunity to use particle moment average as an intermediate monitoring metric.

This study used an EAD and its response function, $d^{1.13}$, as an example of a response of an aerosol surface instrument. Other diffusion chargers may have slightly different fixed or varying response curve as a function of particle size. One can also adjust response of the aerosol surface instrument using the concept Ranjan and Dhaniela reported for the Tailored Electrode Concentration Sensor (TECS) [23]. Therefore, the analysis following the remainder of the paper can be applicable to any particle surface instrument and not limited to the EAD.

2.1.2 Moment Average

The moment average of power of p with respect to particle diameter, d, is determined as

$$d_{\bar{p}} = \left[\frac{\sum_i n_i d_i^p}{N} \right]^{\frac{1}{p}} \qquad \text{(Equation 2-1)}$$

where n_i is number concentration for size bin i, d_i is the diameter of the size bin i, and N is the total particle number concentration [56].

The response of the EAD in ampere is assumed to be proportional to $d^{1.13}$ for the size range of our interest (10 nm to 1μm). It can be expressed as

$$EAD\ response[A] = 0.0211eQ\sum_i n_i \cdot d_i^{1.13} \qquad \text{(Equation 2-2)}$$

where e is electron charge (=$1.602 \cdot 10^{-19}$ coulomb), Q is sample flow rate in cm^3/s. The coefficient, 0.0211, is one of the two parameters that define the EAD's power law charging efficiency taken from TSI [57]. Equation 2-2 can be further simplified as

$$EAD\ response[A] = c \cdot \sum_i n_i d_i^{1.13} \qquad \text{(Equation 2-3)}$$

where $c = 0.845 \cdot 10^{-19}\left[\frac{cm^3 \cdot A}{n_c}\right]$ and n_c is the number of charge.

EAD also outputs in mm/cm^3 after normalizing the signal against that of 1 μm diameter particle. TSI assumed 41 unit charges per particle for d_p=1μm, then the EAD response becomes

$$EAD\ response_{d_p=1\mu m}[A] = \sum_i n_i\left[\frac{particles}{cm^3}\right] \cdot 41\left[\frac{n_c}{particle}\right] \cdot 1.602 \cdot 10^{-19}\left[\frac{Coulomb}{n_c}\right] \cdot 25\left[\frac{cm^3}{s}\right]$$

$$EAD\ response_{d_p=1\mu m}[A] = 1642 \cdot 10^{-19} \sum_i n_i \qquad \text{(Equation 2-4)}$$

Equation 2-3 divided by Equation 2-4 multiplied by 1000 gives EAD response in mm/cm^3 as

$$EAD\ response[mm/cm^3] = 0.5146 \sum_i n_i d_i^{1.13} \qquad \text{(Equation 2-5)}$$

The diameter of average particle active surface area for a given particle size distribution can be obtained as a function of EAD/CPC ratio as

$$d_{\overline{1.13}} = \left[\frac{\sum_i n_i d_i^{1.13}}{N}\right]^{\frac{1}{1.13}} = \left[\frac{1}{c} \cdot \frac{EAD\ response}{CPC\ response}\right]^{\frac{1}{1.13}} = \left(\frac{1}{c}\right)^{\frac{1}{1.13}} \cdot \left(\frac{EAD\ response}{CPC\ response}\right)^{\frac{1}{1.13}}$$

(Equation 2-6)

The value of c can be chosen depending on the unit of EAD response as shown above.

2.1.3 Equivalent lognormal particle size distribution

As none of single metrics contain information about particle size, it is the goal of this study to extract particle size information from the ratio of PS/PN i.e. EAD/CPC ratio in this study. It should be noted ambient particle size distributions are typically bimodal and are frequently fitted by lognormal distributions. Two geometric mean diameters (GMDs) and two geometric standard deviation (GSDs) are needed to fully describe this bimodal distribution. It requires more than PN and PS measurement to determine these four parameters in real time. This study aims to determine a unimodal lognormal distribution which has an equivalent active surface area measured by EAD. The GMD of the unimodal lognormal distribution provides mean size information of the real particle size distribution, which is useful to assess transport of particles.

The size information, i.e. the geometric mean diameter of the equivalent lognormal particle size distribution, is indicative of the extent of bimodality in real particle size distribution. For example, if the GMD is very small, then it suggests a strong presence of nucleation mode. Also, if the GMD is near where typical accumulation mode particles present, then it means the nucleation mode is insignificance. If the GMD is neither too small nor very close to the typical GMD of accumulation mode, then it means both nucleation and accumulation mode particles contribute to the distribution to a similar extent with respect to particle active surface area. However, this cannot distinguish a unimodal distribution with intermediate mean diameter from a 50-50 bimodal distribution with small and large particles. The advantage of this method is that it is based on particle active surface

area, which is a good indication for health effect and it is relatively or a lot simpler than other approaches while still essentially provides needed size information.

First, it is necessary to determine GMD (geometric mean diameter or d_g) of the lognormal PSD, which will provide the same active surface area as measured by the EAD. GMD is equal to CMD (count median diameter) for the lognormal distribution, and has the following relationship with the diameter of average of the distribution weighted by d^p, $d_{\bar{p}}$, by the Hatch-Choate equation [58]

$$\frac{d_{\bar{P}}}{d_g} = \exp\left[\frac{p}{2}\ln^2\sigma_g\right] \qquad \text{(Equation 2-7)}$$

Where σ_g is geometric standard deviation of the lognormal distribution.

Then for p=1.13, the GMD can be expressed as

$$GMD = \frac{\left[\frac{\sum_i n_i d_i^{1.13}}{N}\right]^{\frac{1}{1.13}}}{\exp\left[\frac{1.13}{2}\ln^2\sigma_g\right]} = \frac{\left(\frac{1}{c}\right)^{1.13}}{\exp\left[\frac{1.13}{2}\ln^2\sigma_g\right]} \cdot \left(\frac{EAD\,response}{CPC\,response}\right)^{\frac{1}{1.13}}$$

(Equation 2-8)

This is a function of EAD/CPC ratio once the geometric standard deviation of the lognormal distribution is determined.

To further understand the relationship between GMD and diameter of average surface area, typical nucleation and accumulation modes are assumed to have lognormal distribution. We found average σ_g =1.4 for nucleation mode and σ_g =1.7 for accumulation

mode from our measurement. These values are consistent with other values in the literature. Zheng et al. used σ_g =1.3 for nucleation mode and σ_g =1.9 for accumulation mode [59]. Harris and Maricq reported σ_g of 1.7 and 1.8 for diesel vehicles and engines respectively [60]. Xue also reported similar GSD ranging from 1.6 to 1.9 for accumulation mode from diverse light duty vehicles [61]. p values of 1, 1.13 and 2 were used to cover the range of power depending on measurement principle, regime (continuum, transition and free molecular), type of surface area (geometric vs active surface) and other things (e.g. particle wall loss) for aerosol surface instruments.

The relationship between GMD and diameter of average surface area is shown in Figure 2-1. There is a linear relationship as expected. The narrower distribution (shown in dotted lines for σ_g =1.4 mimicking GSD of nucleation mode) is the more sensitive to the change in geometric mean diameter. There was very little difference for the relationship between p=1 and 1.13 when GSD is large (σ_g =1.7 mimicking GSD of accumulation mode). We assumed σ_g =1.7 and p=1.13 for the rest of the analysis.

The Hatch-Choate equation has been often used to estimate PM metrics related to various moments of the size distribution. Maynard estimated particle surface area from particle number measurement by a CPC and particle mass measurement by a photometer, such as the Dustrak (TSI, St. Paul) to extract particle surface area concentration from existing PM and PN data set in health effect studies [62]. On the other hand, Woo et al. measured particle mass, surface area, and number concentrations using mass concentration monitor (MCM, TSI), EAD, and a CPC respectively and re-constructed lognormal

distribution [63]. They suggested the integral measurement has high temporal resolution compared to other methods.

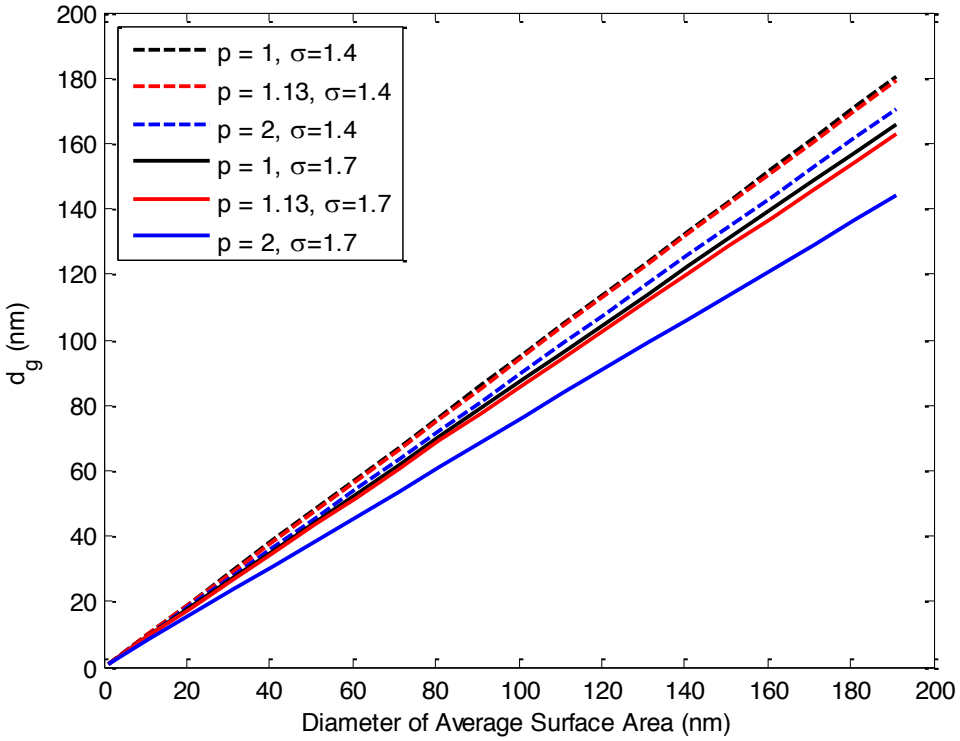

Figure 2-1: Relationship between GMD and diameter of average surface area for σ =1.4 and 1.7 when p=1, 1.13 and 2.

It is also noteworthy that a similar attempt was made by Fierz et al. using a uniquely designed diffusion charger [64]. They made a miniature diffusion size classifier combing a diffusion charger with a diffusion battery. Small particles are detected at the diffusion stage and the rest of particles are detected at the filter stage. With the ratio of currents from the two stages they could determine average size as well as total particle number.

It should be noted the cutoff diameters of the two instruments (CPC and EAD) need to be matched as close as possible for the best result. If the difference of cutoff diameters between the two instruments are too big, then GMD determination will be incorrect.

2.2 Experimental Setup

Ambient air measurement data were collected to validate the concept instead of mobile measurement, because particle size distributions on-road change more rapidly than what standard particle sizing instrument (namely SMPS) can measure. However, the monitoring devices (CPC and EAD) is fast enough (1Hz) to be applicable for on-road measurement once the concept is validated. Table 2-1summarizes size range and time resolution of instruments used in this study.

Table 2-1: PM instruments in the mobile platform.

Instrument	**Model No.**	**Size range (nm)**	**Concentration range.**	**Time resolution**
TSI CPC	3772	10 - 3000	0 – 1.0 x 10^4 particles/cm^3	1 Hz
TSI EAD	3070A	10 - 1000	0.01 – 2500 mm/cm^3	3.75 Hz
TSI SMPS	3081	8 - 346	100-1,000,000 particles/cm^3	2 min

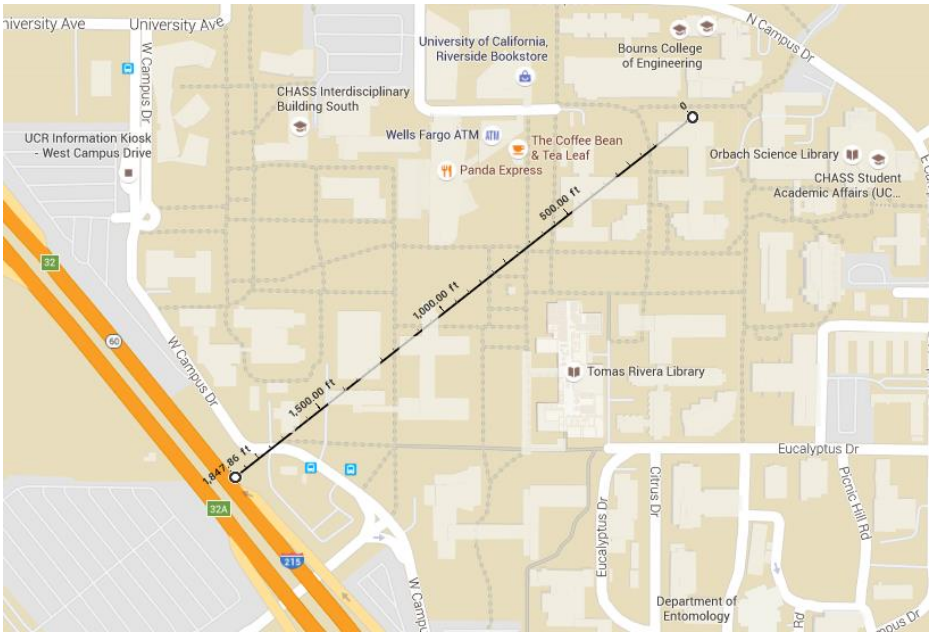

Figure 2-2: Map of the sampling location.

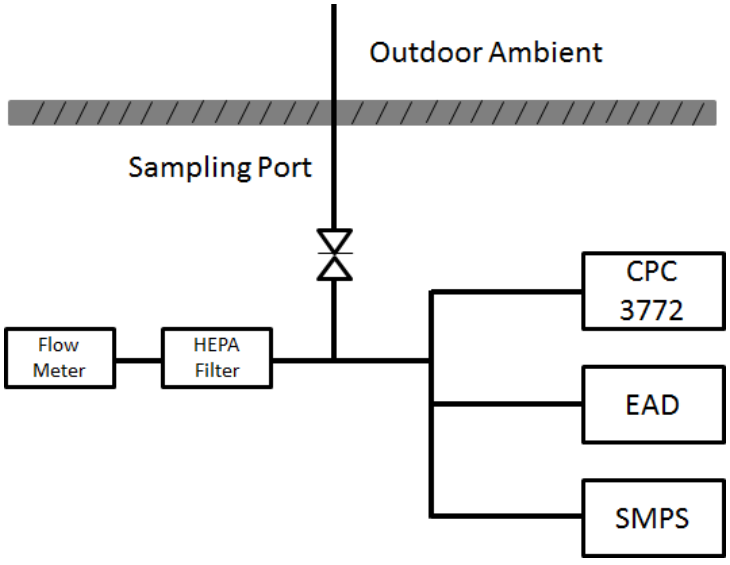

Figure 2-3: Schematic diagram of instrument installation at the mobile platform. Note enlarged picture of sample probe.

Ambient outdoor air was sampled using a 3/8" copper tubing on a third floor of a building on campus at the University of California Riverside as shown in Figure 2-2. The extrusion of the copper tubing was perpendicular to the building outside wall with the opening approximately one meter away. The sampling line was connected to a needle valve to control the flow before the T-connection as shown in Figure 2-3. The purpose of connecting a HEPA filter to a flow meter is to dilute the sample flow (~1 lpm) with particle free air (~5 lpm) to prevent saturation of a CPC. The dilution ratio was set to 6 by adjusting the needle valve while measuring the flow rates before the HEPA filter. The diluted sample flow was distributed to three instruments. A condensation particle counter (CPC) (TSI model 3772) were used to measure particle concentration. CPC 3772 has a cutoff diameter 10 nm and a maximum range of 10^4 particles/cm^3. An electrical aerosol detector (EAD) (TSI, model 3070A) was used to measure active aerosol surface area. Both CPC and EAD sampling rates were set to 1 Hz to have fast and same sampling time resolution. The scanning mobility particle sizer (SMPS) consists of a classifier (TSI, model 3080) with a long column differential mobility analyzer (TSI, model 3081) and an ultrafine CPC (TSI, model 3776). The ultrafine CPC used butanol as a working fluid and has a lower detection limit of 2.5 nm. The SMPS provides total count and particle size distribution. The SMPS has 64 channels and particle size range was set from 8 nm to 346 nm. Each size distribution scan takes approximately two minutes. There was a repeat of three continuous scans every ten minutes (i.e. three continuous scans for ~6 minutes and wait for ~4min then repeat). The aerosol neutralizer used x-ray to bring the aerosol to a bipolar charge distribution.

2.3 Results and Discussions

The particle size spectra in Figure 2-4 showed dynamic changes of particle size distributions due to transport and photochemistry. Particle size distributions measured by SMPS were used to check consistency of the EAD, CPC measurement, and EAD/CPC ratio. Total particle concentration and active particle surface area calculated from SMPS particle size distributions were compared with CPC and EAD measurement.

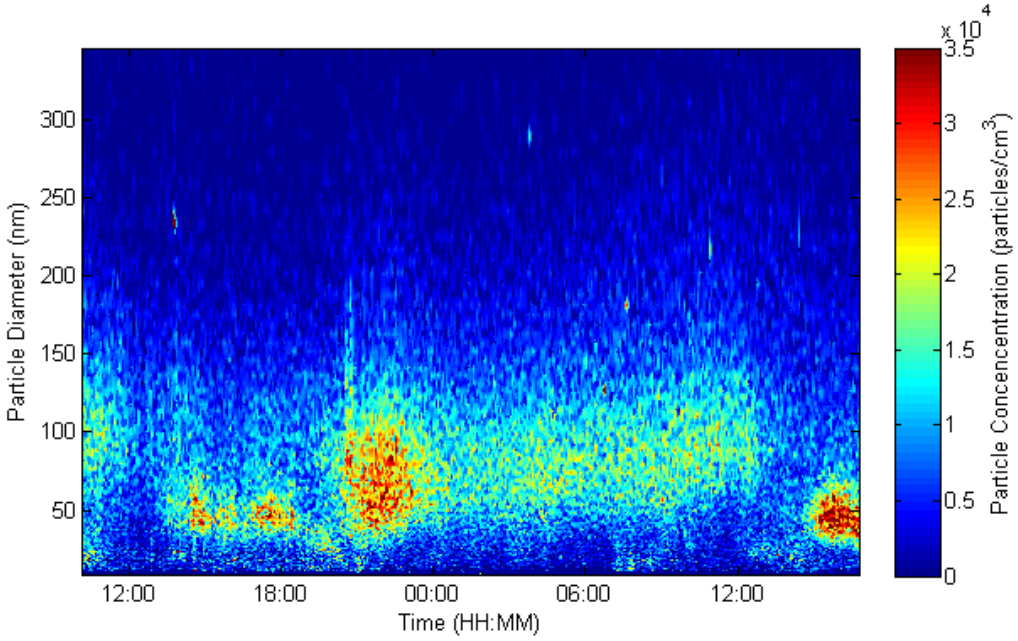

Figure 2-4: Ambient particle size spectra from measurement site.

The total particle concentrations showed good agreement in Figure 2-5a between CPC and SMPS. It should be noted that CPC data showed higher time resolution as expected with particle concentrations ranged between 5×10^3 to 2.0×10^4 particles/cm^3. Particle concentrations decreased as a thermal boundary layer increased until little past 12:00. Particle concentrations increased and remained constant in the afternoon (~12:00 to

~19:00) likely due to competition between new particle formation and removal processes. Particle concentrations increased as a thermal boundary layer decreased in the evening (~19:00 to ~22:00). Particle concentrations decreased due to the change of wind direction from ~22:00 to ~00:00. EAD response converted from particle size distributions using Equation 2-3 compared well with measured EAD response as shown in Figure 2-5b. The actual EAD measurement showed higher time resolution and sensitivity to higher concentrations. The surface area concentrations converted from SMPS were slightly lower than the EAD measured values. This is probably because of the narrower size range of SMPS compared to CPC and EAD.

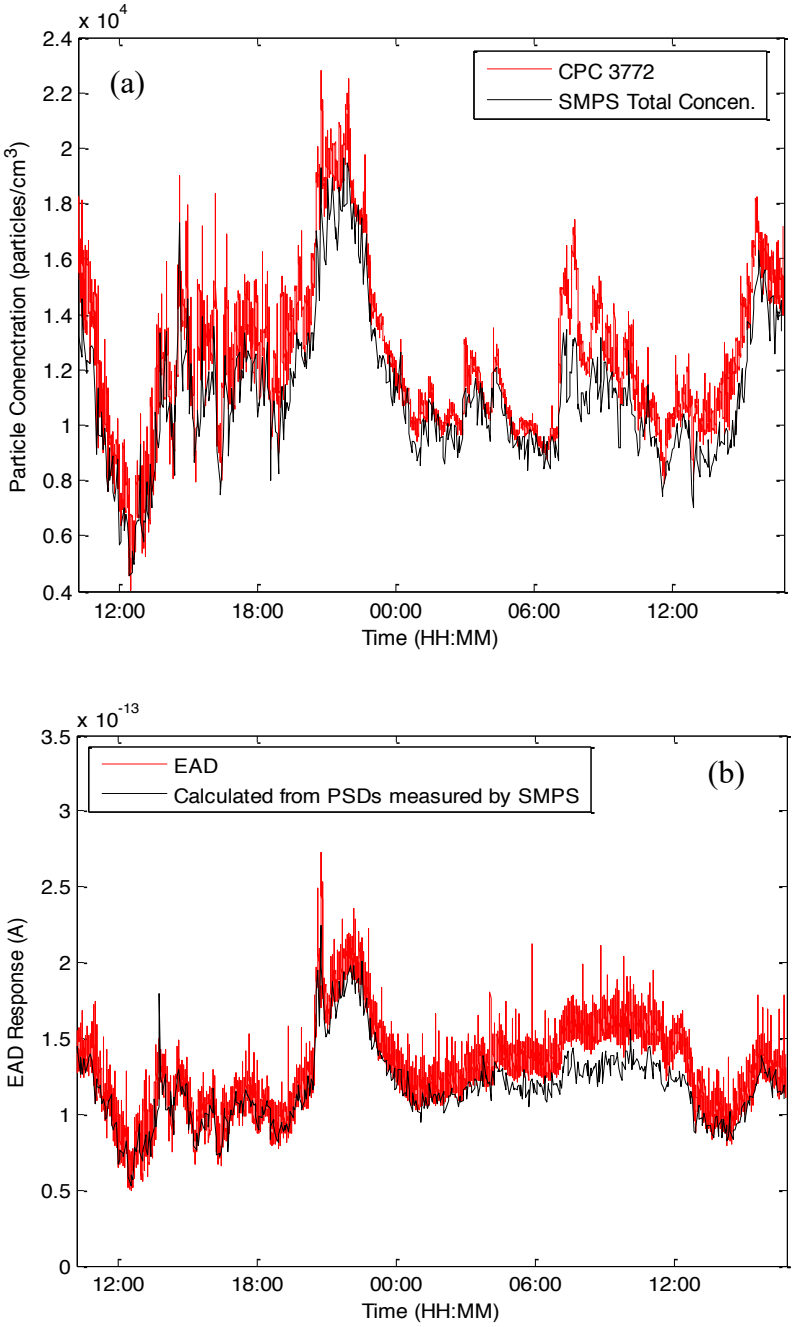

Figure 2-5: (a) Comparison between SMPS and CPC measurements. (b) Comparison between calculated EAD responses from PSDs measured by SMPS and EAD measurements.

SMPS measured particle size distributions are normalized by the total count of the size distribution and presented in the order of GMD of the equivalent unimodal lognormal distribution in Figure 2-6. The size distributions were chosen to have constant increment of ~5 nm with respect to GMD. As the GMD of the equivalent unimodal lognormal distribution increased, nucleation mode gradually decreased or disappeared. For accumulation mode, the GMD of the accumulation mode increased and an additional mode appeared at ~150-200nm.

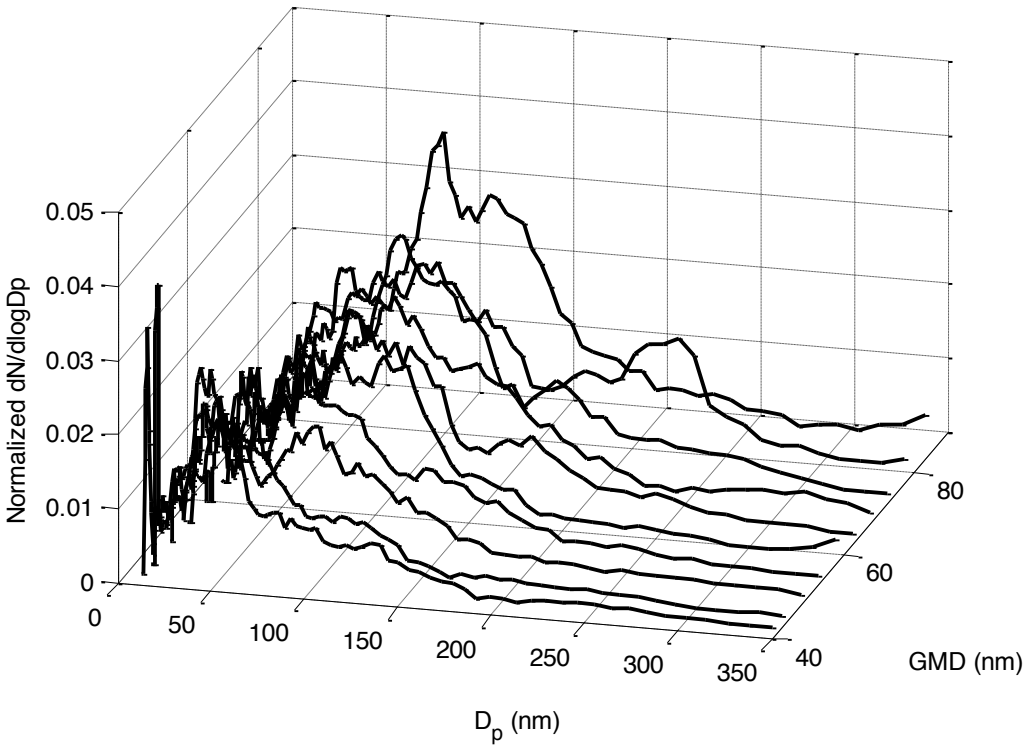

Figure 2-6: Normalized ambient particle size distributions presented as a function of GMD.

As a final check to our proposed monitoring metrics of PN, PS, and PS/PN, GMD (or d_g) was calculated from the particle size distributions measured by SMPS and compared with GMD obtained from EAD/CPC ratio using Equation 2-8. GMD by the particle size distribution was referred as GMD_{PSD} and GMD by the CPC and EAD measurements was referred as $GMD_{PS/PN}$. GMD_{PSD} ranged from 42 to 85 nm and $GMD_{PS/PN}$ ranged from 35 to 115 nm. Wider range of $GMD_{PS/PN}$ is attributed to higher time resolution. In general, the comparison in Figure 2-7a shows a good agreement and correlation (ρ=0.88) between two GMDs. Figure 2-7b shows comparison using 60s moving average, which shows improvement in correlation (ρ=0.90).

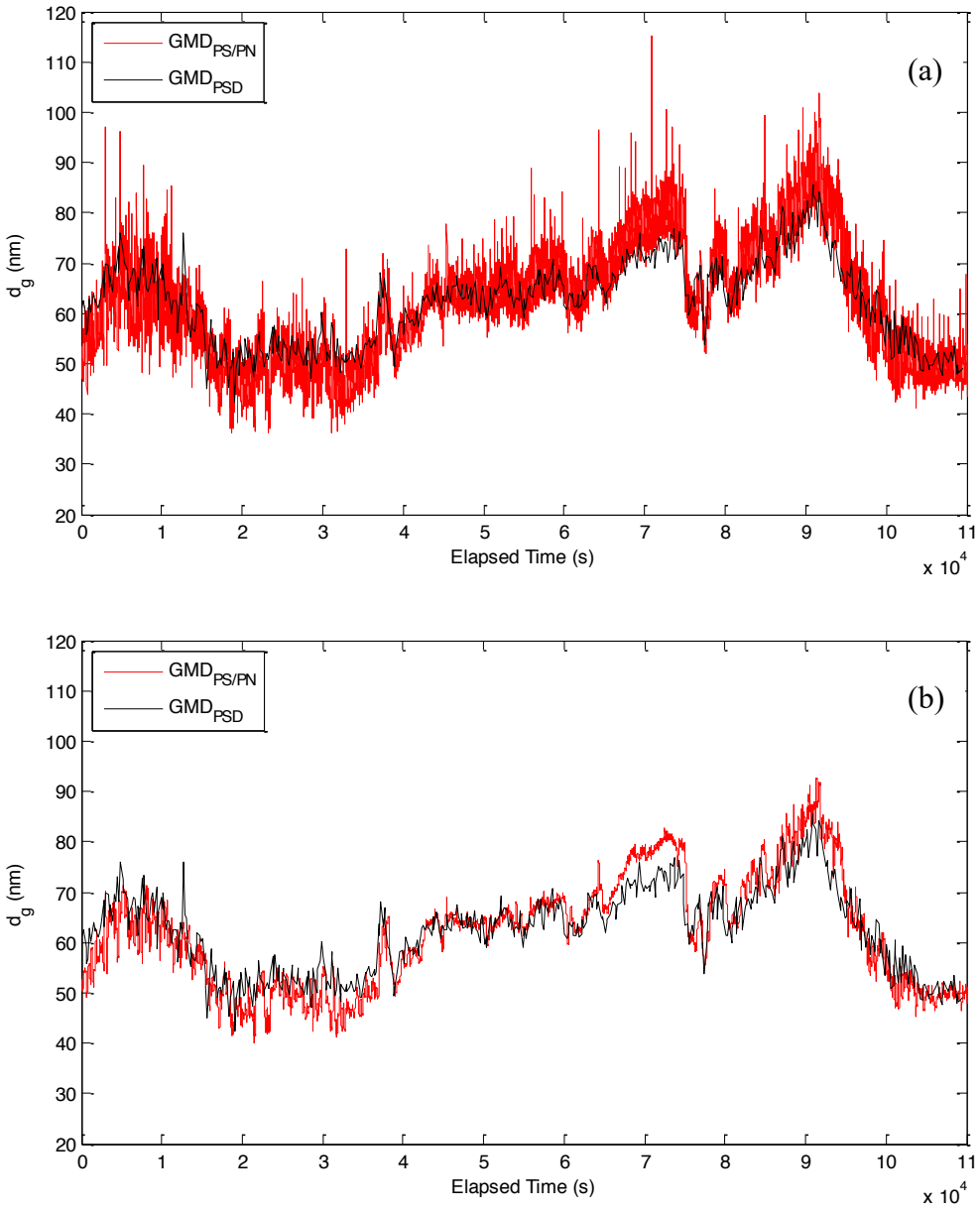

Figure 2-7: Comparison of GMDs between from the measurement of EAD and CPC (for GMDPS/PN) and measurement of particle size distribution (for GMDPSD). (a) real time (r^2=0.77, ρ=0.88) (b) 60s moving average (r^2=0.82, ρ=0.90).

Figure 2-5, Figure 2-6, and Figure 2-7 confirmed the validity of EAD and CPC measurement, and the proposed metrics. This suggests a particle surface instrument along with a particle counting instrument can be an excellent particle concentration monitoring device with which three important single valued metrics (PN, PS, and particle size in terms of GMD) can be obtained. The PN/PS ratio can be used to obtain an equivalent unimodal lognormal particle size distribution.

2.4 Conclusion

This study aims to test feasibility of multiple and simultaneous deployment of mobile monitoring systems with two particle instruments, a particle counter (e.g. CPC) and a particle surface instrument (e.g. EAD), to obtain spatially and temporally resolved particle concentrations on major highways. Spatiotemporally resolved particle concentrations are beneficial to better assess public's exposure to dynamically varying particle emissions near source (e.g. on-road and near road). Obtaining and analyzing real time PSDs over a wide region on a routine basis is costly and not practical. In addition, it is impossible (or extremely difficult) to visually present PSDs over a wide region. We propose to use particle number and surface area instrument to monitor particle number (PN), particle surface area (PS), and particle size (in terms of a GMD of an equivalent lognormal distribution). Three single valued metrics are convenient to present in contour forms.

We validated the concept through ambient particle measurement and by having an additional PSD measurement using a SMPS. The EAD and CPC response calculated and integrated from the SMPS data correlated well with the measured EAD and CPC response,

respectively. In addition, the ratios of PS and PN (or EAD/CPC) was used to calculate the GMD of a lognormal PSD which has an equivalent total particle surface area. The GMDs calculated from SMPS data and EAD/CPC ratio measurement agreed well and they provide size information which is important to understand particle transport. Attention should be paid to have similar cut-off diameters and ranges for both instruments to get consistent and desired results.

3 Monitoring nanoparticles on major highways in Southern California: A Lagrangian approach using a mobile monitoring system

Many prior studies employed electric vehicles (EV) as a mobile platform [19, 22]. The EV has an advantage of zero emissions, but has disadvantages of short mileage of about 100 miles on highway per charge, lack of charge stations, high cost, and less availability. On the other hand, conventional port fuel injection (PFI) gasoline vehicles have very low particle emissions, a longer range of 400 miles on highway per fuel tank, and abundance of gas stations. However, the PFI vehicles were not widely adopted as a mobile platform due to the concern of self-pollution. Nguyen and Jung conducted a computation fluid dynamics simulation for the scenario of a conventional PFI gasoline vehicle being used as a mobile platform for particle monitoring [65]. They used experimental data from a Federal Test Procedure (FTP) test, which is a transient cycle, as an input to account for dynamic nature of vehicle emissions. They found out that the chance of self-pollution for particles is very low, and even in the worst case the effects of exhaust particles emissions from the PFI mobile platform is negligible by choosing a proper sampling location [65].

3.1 Methods

3.1.1 Mobile platform and sampling system

This is a continuation of the preliminary analysis and the detailed experimental setup was thoroughly described in Grady's thesis [66]. In summary, a port fuel injection vehicle (Ford Focus) was used a mobile platform for this study. The sampling inlet was located at the front passenger window and used 3/8" outer diameter copper tubing for

transfer line. The platform consisted particle counters (CPC 3007), surface area measurement (EAD 3070A), particle size distribution (NanoScan SMPS 3910, OPS 3330), GPS logger (San Jose Navigation FV-M8). All instruments were powered by two deep cycle marine batteries (US 200 XC2). All instruments were measuring at rate of 1 Hz except for NanoScan SMPS and OPS, which were measuring at 60s per scan.

3.1.2 Driving route

SR-91 (route 1) and I-710 (route 2) were selected due to their vehicle compositions. A section from UCR to Yorba Linda of the SR-91 was selected because of its high concentration of light-duty daily commuter vehicles. The second route was the I-710, which contained high concentration of heavy-duty truck entering and leaving the Port of Long Beach. Figure 3-1 shows the tested routes. A more thorough description can be found in Grady's study [66].

(a)

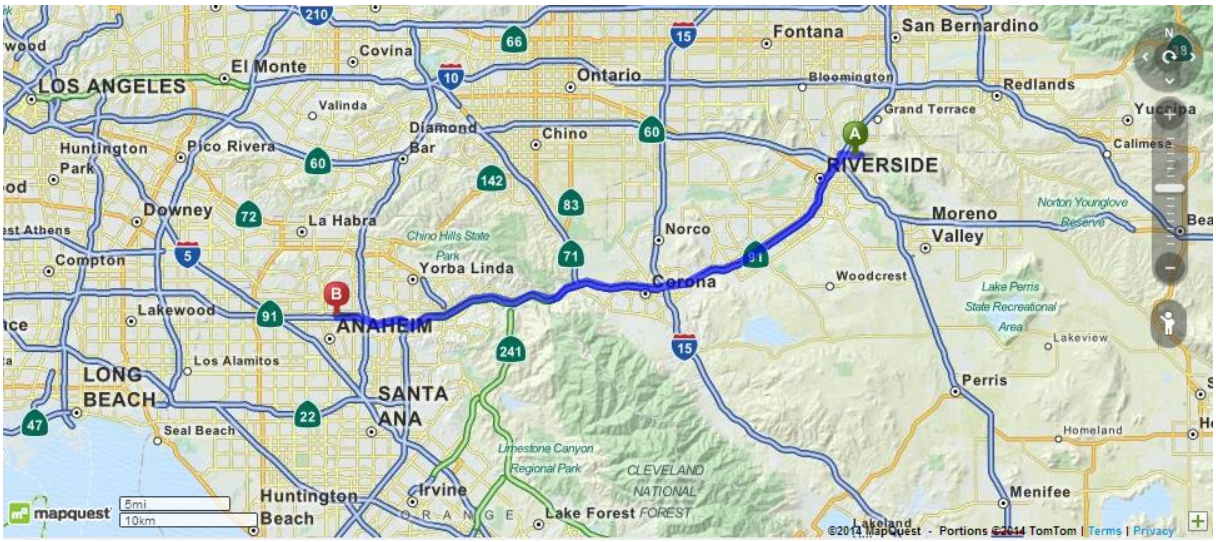

(b)

Figure 3-1: Maps of driving routes. (a) Route 1 is from Riverside to Anaheim including the section of Yorba Linda Creep to represent morning commute traffic of light duty vehicles with some mix of heavy duty vehicles. (b) Traffic from heavy duty vehicle is represented in Route 2 (I-710), which leads to the Port of Long Beach.

3.2 Results and Discussions

3.2.1 Particle size distribution on highways

The on-board GPS at the mobile platform recorded locations and time. With that information, the vehicle speed could be calculated and corresponding traffic conditions could be deduced. This section describes relationship between particle size spectra and traffic conditions deduced from the GPS data of the mobile platform.

The NanoScan SMPS measured a particle size distribution every minute while the mobile platform moving in route 1 and 2. Figure 3-2ab show particle size spectra in contour for route 1 in west and eastbound. Variations in elevation is also given in Figure 3-2c. Note that the mobile platform measured somewhat average particle emissions upstream of the sampling location. The westbound in route 1 is morning commute traffic from Inland Empire to Orange County, while eastbound is well flowing traffic until 70 miles distance where there is a stop-and-go type congestion. There was a burst of nucleation mode particles near 1 and 7 mile distance as shown in Figure 3-2a. While the first nucleation mode particles in 1 mile distance matches with the strong acceleration shown in Figure 3-2d, the second nucleation mode in 7 mile distance does not match with the speed chart in Figure 3-2d as there is no acceleration near 7 mile distance. Interestingly, the return traffic in the eastbound showed stop-and-go type congestion near 70 mile distance. It is speculated that it is possible that there was a systematic (i.e. long lasting) congestion in the eastbound near 70 mile distance during the morning commute time and the nucleation mode particles measured in the westbound near 7 mile distance might have come from the eastbound traffic. There were frequent peaks for the accumulation mode between 15 and

23 mile distance in westbound. The congestion in this location is called Yorba Linda creep. The peaks matched well with accelerations during the congestion meaning the measurement reflects road way particle concentrations near or upstream of the mobile platform. Particle size spectra in eastbound showed a major peak near 60 mile distance in the nucleation mode. Again, it was interesting to see that there was no reason to have this peak in the westbound looking at the vehicle speed in Figure 3e. The nucleation mode was likely due to the stop-and-go traffic in the westbound. Note that the mobile platform measured the particle size distribution next to the HOV lane and the sampling probe stuck out to the right window. Therefore, the sampling location was relatively close to the traffic in the opposite direction although the sampling location was determined such that it can take somewhat averaged particle concentrations from the vehicles moving in the same direction.

(a)

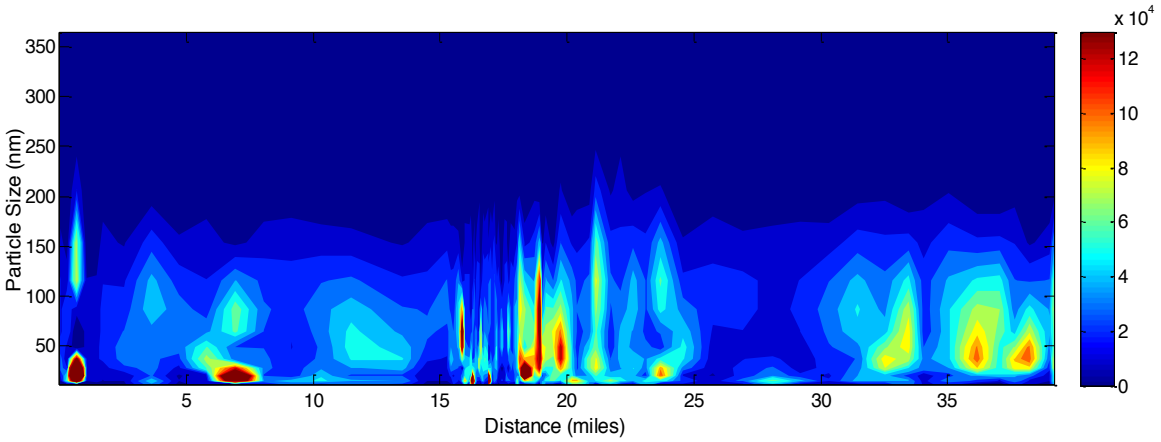
x 10^4
Particle Size (nm)
350
300
250
200
150
100
50
5
10
15
20
25
30
35
Distance (miles)
12
10
8
6
4
2
0

(b)

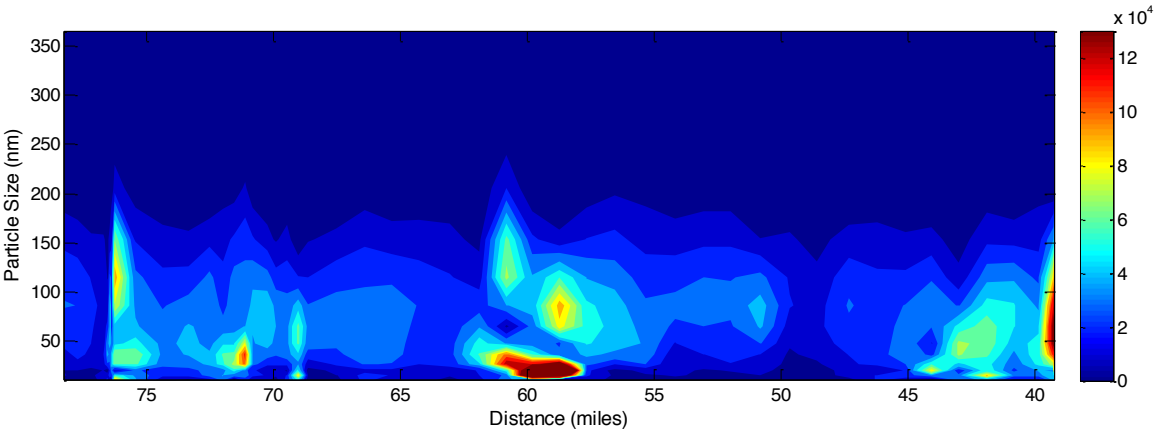
x 10^4
Particle Size (nm)
350
300
250
200
150
100
50
75
70
65
60
55
50
45
40
Distance (miles)
12
10
8
6
4
2
0

(c)

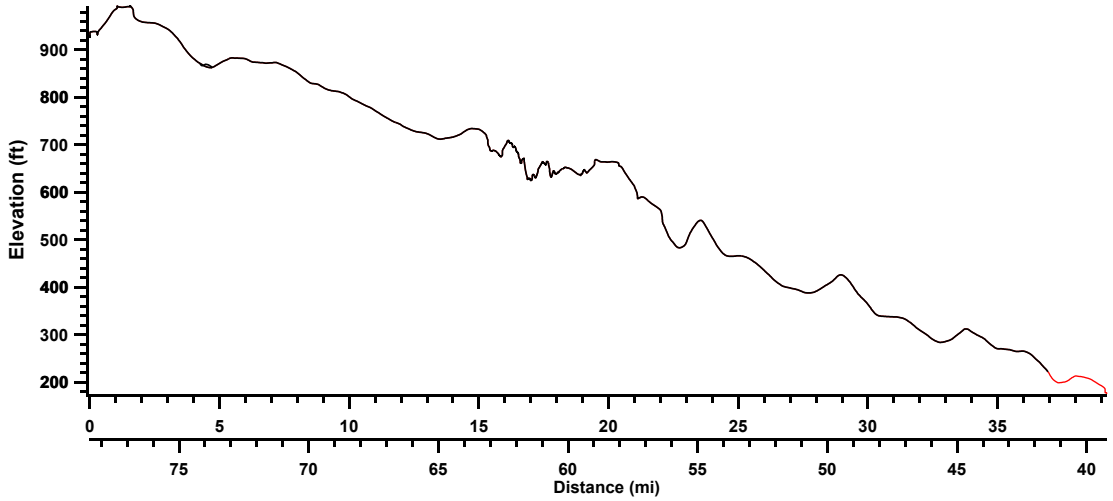
Elevation (ft)
900
800
700
600
500
400
300
200
0
5
10
15
20
25
30
35
75
70
65
60
55
50
45
40
Distance (mi)

(d)

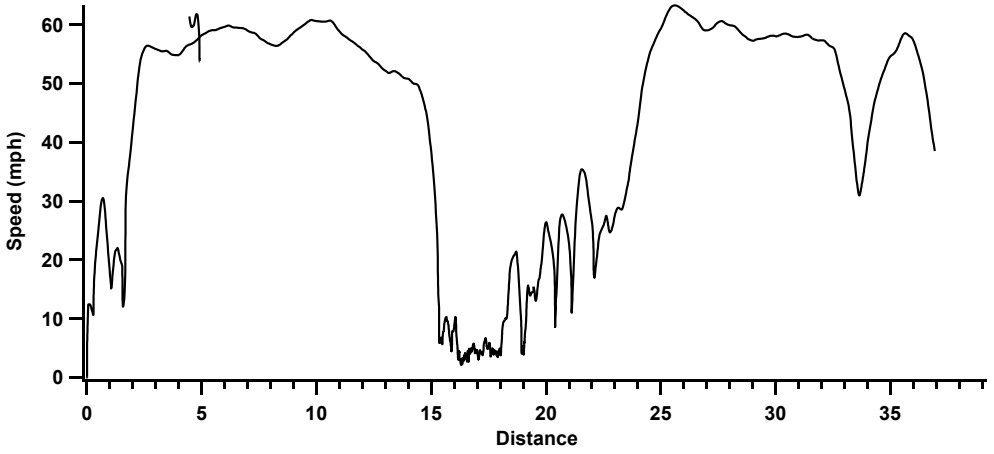
Speed (mph)
0
10
20
30
40
50
60
0
5
10
15
20
25
30
35
Distance

(e)

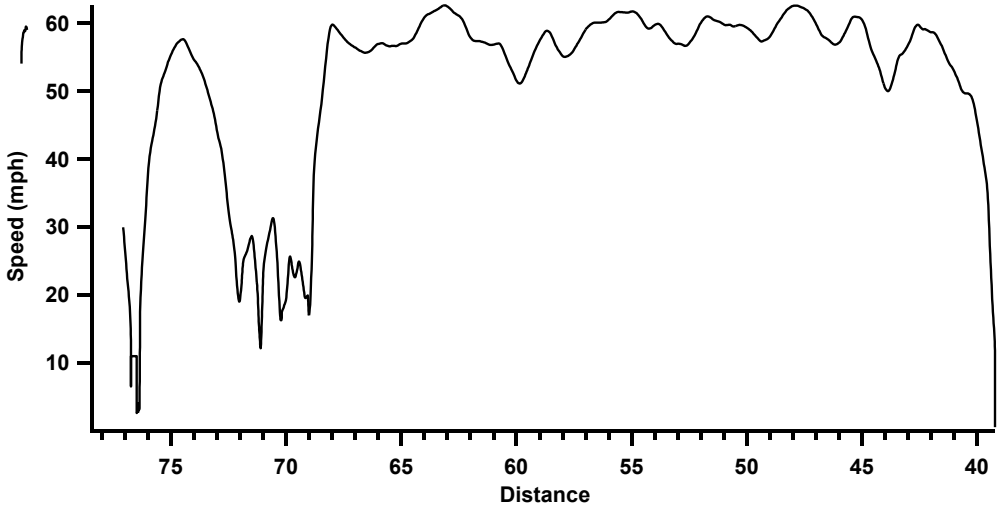
Speed (mph)
10
20
30
40
50
60
75
70
65
60
55
50
45
40
Distance

(f)

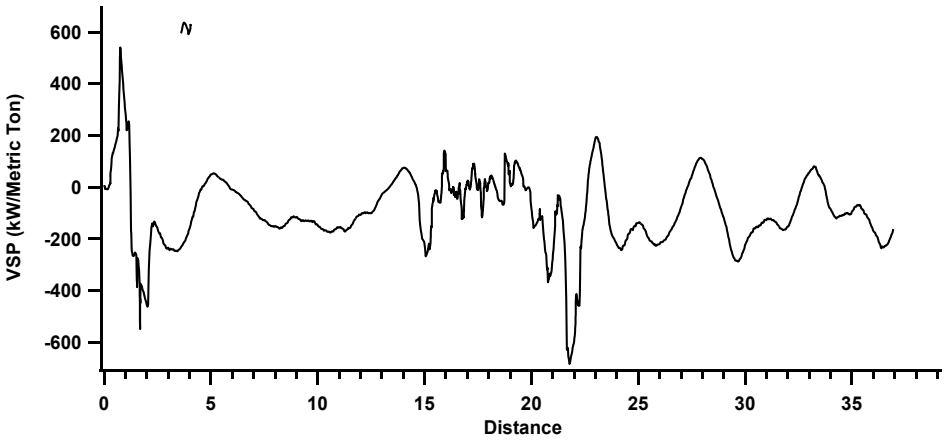
VSP (kW/Metric Ton)
-600
-400
-200
0
200
400
600
0
5
10
15
20
25
30
35
Distance

(g)

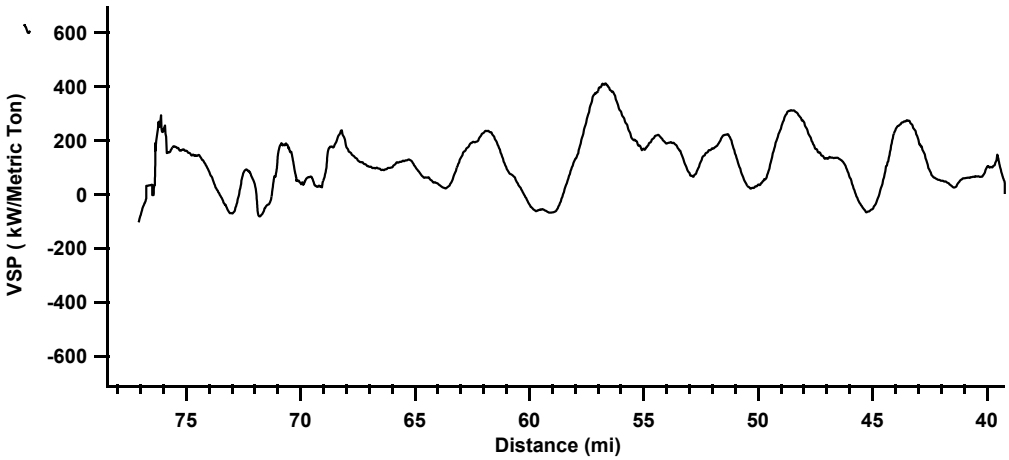

Figure 3-2: (a) Particle size spectra of route 1 westbound, (b) Particle size spectra of route 1 east bound, (c) Elevation variation of route 1, (d) Speed of the mobile platform (Westbound), (e) Speed of the mobile platform (Eastbound), (f) VSP (Vehicle Specific Power) of the mobile platform (Westbound), (g) VSP (Vehicle Specific Power) of the mobile platform (Eastbound).

The VSP is an instantaneous power per unit mass of the vehicle. It is the power necessary to overcome the rolling resistance, aerodynamic drag, and to increase the kinetic and potential energy of the vehicle (Jiménez-Palacios et al. 1999). VSP is defined in the following formula

$$VSP = \frac{Power}{Mass} = \frac{\frac{d}{dt}(KE+PE)+F_{rolling}\cdot v+F_{aerodynamic}\cdot v}{m} \quad \text{(Equation 3-1)}$$

For light-duty vehicle and light-duty trucks, Equation 3-1 can be simplified to (Equation 3-2 3-2 below when input parameters are in miles per hour for vehicle speed and miles per hour per second for acceleration [67].

$$VSP \approx 0.22 \cdot v \cdot a + 4.39 \cdot grade \cdot v + 0.0954 \cdot v + 0.0000272 \cdot (v + v_w)^2 \cdot v$$

(Equation 3-2)

The input parameters are vehicle speed (v), head wind speed (v_w), vehicle acceleration (a), and road grade ($grade$). The on-board GPS recorded the date, time, vehicle's longitude and latitude coordinates, speed, and altitude. The vehicle acceleration was determined by dividing the speed difference with each time increments. With the longitude and latitude coordinates, the vehicle traveled distance was calculated by using the Haversine formula. Road grade is the slope of the road, which is expressed as percentages. Using the calculated distance and recorded altitude, the road grade was determined by the ratio of altitude over distance. The wind data during the test was calm on SR 91, so the head wind speed was assumed to be negligible. After calculating the input parameters, the resultant VSP was determined in which the unit is in kW per metric ton.

VSP was calculated to better correlate peaks in particle size spectra with the traffic conditions. It should be noted that VSP was calculated for the mobile platform. Therefore, it does not necessarily represent VSPs of other vehicles upstream. However, the VSP of the mobile platform at least can show the trend of the VSP for the group of vehicles flowing together. In general, steep slope in VSP vs distance curve (Figure 3-2f) agreed well with high concentrations of nucleation and accumulation mode (Figure 3-2a) particles for the westbound trip. Slopes in VSP vs distance chart (Figure 3-2g) were more gradual and peak concentrations were lower during the eastbound trip.

TSI OPS measures particles larger than 300 nm. OPS spectra in the range from 0.3 μm to 10 μm for route 1 and 2 indicated no significant concentrations larger than 1 μm. In additions, Figure 3-3 shows total particle concentration measured by the OPS. Our study did not measure refractive indices of sample particles simultaneously. We either used default refractive index provided by the manufacturer or Urban refractive index from Levoni et al. (1.353+0.0182j) [68]. In either case, there were not any significant particle concentrations that match with the change in traffic conditions in comparison to the NanoScan SMPS data. We attribute this to the different origin/formation process of the particles. Particles measured by OPS may not strongly relate to the vehicle emission and traffic conditions.

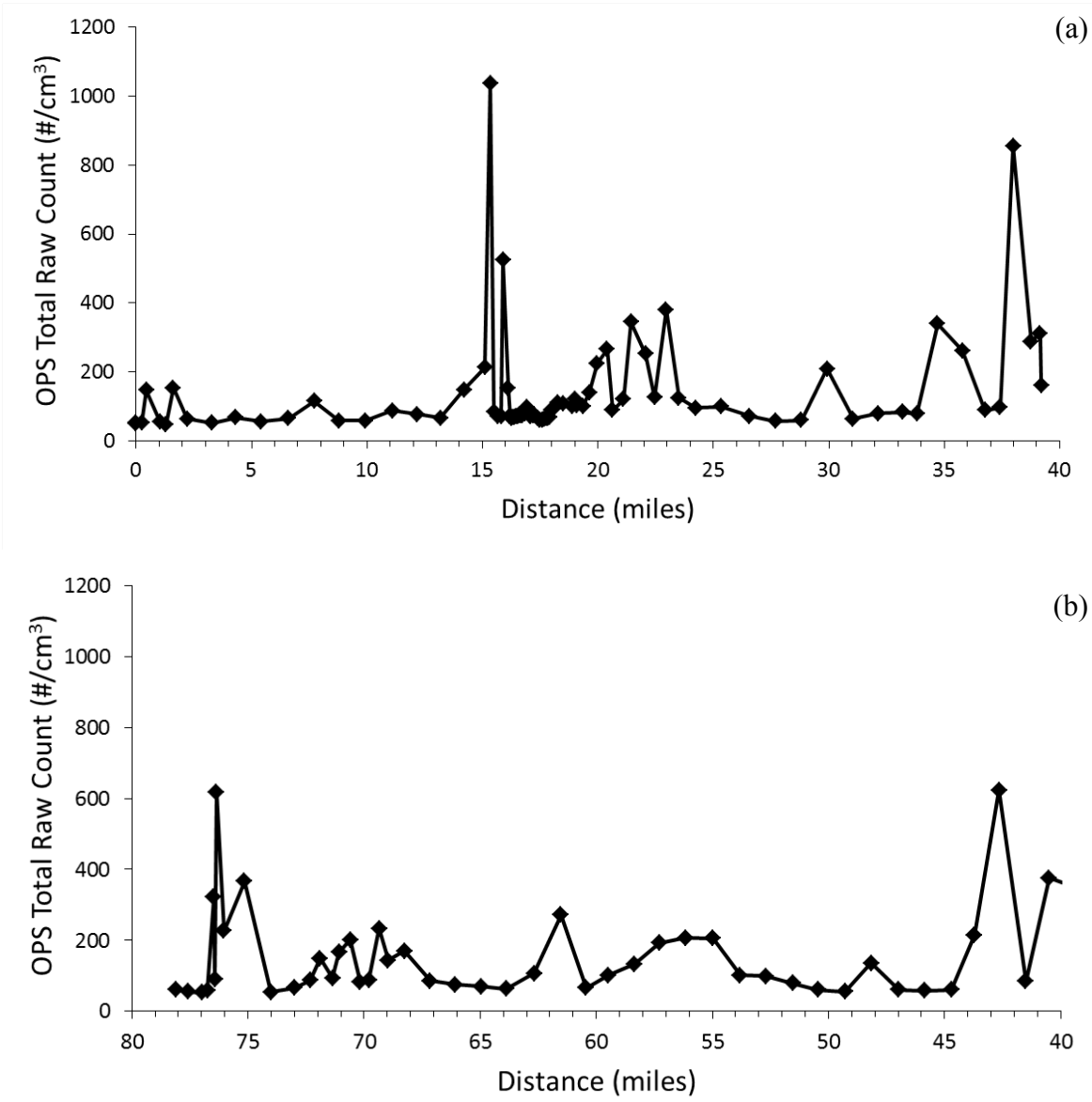
(a)
OPS Total Raw Count (#/cm3)
1200
1000
800
600
400
200
0
0
5
10
15
20
25
30
35
40
Distance (miles)
(b)
OPS Total Raw Count (#/cm3)
1200
1000
800
600
400
200
0
80
75
70
65
60
55
50
45
40
Distance (miles)

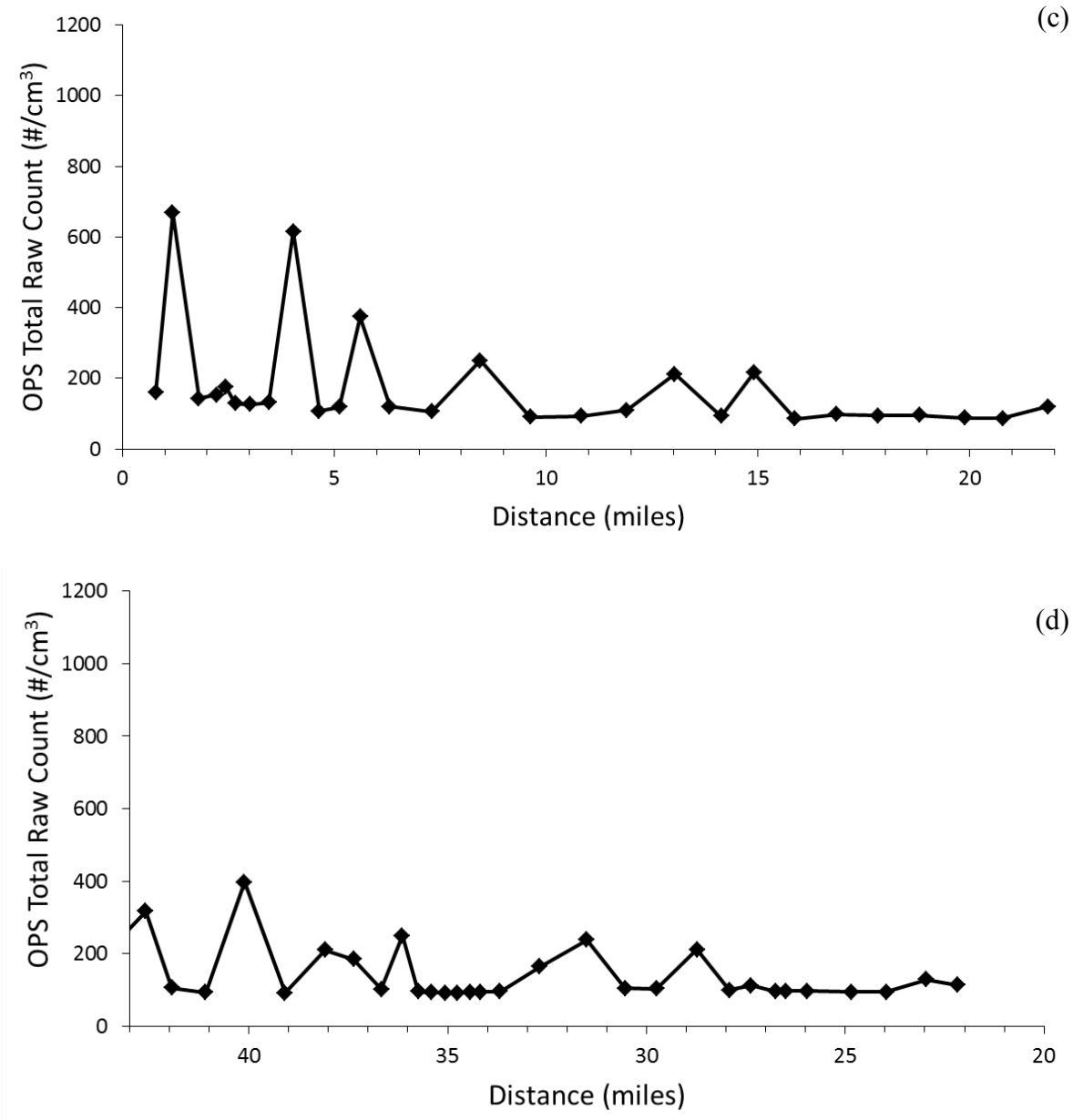

Figure 3-3: (a) Total Raw Count from OPS data for Route 1 westbound, (b) Total Raw Count from OPS data for Route 1 eastbound, (c) Total Raw Count from OPS data for Route 2 southbound, (d) Total Raw Count from OPS data for Route 2 northbound

3.1.2 Use of Meteorological and traffic information for interpretation of particle size distributions

Figure 3-4ab show particle size spectra from NanoScan measurements for rout 2 as a function of distance for south and northbound. Figures 5cde show variations in elevation of the route 2 and speed of the mobile platform for south and eastbound, respectively. Figure 3-4fg show VSP for south and northbound. The route 2 is on highway 710 which is known for its high fraction of heavy duty diesel truck going in and out of the Port of Long Beach. High concentrations of accumulation mode particles were observed by previous studies on this highway [69]. Interestingly, particle size spectra in southbound showed much lower accumulation mode particle concentrations than expected. Peak concentrations were noticeable at around 1, 14, and 20 miles distance for nucleation mode particles. Peak concentrations at 1 and 4 miles distance matched with acceleration shown in Figure 3-4d, but it is questionable why there were no peaks during other acceleration events such as 7 and 15 miles distance. Peaks for accumulation mode particles were at low concentrations and appeared around 11, 14, 16 and 18 miles distance. VSP chart, Figure 3-4f, showed the highest VSP event was around 20 miles distance. Northbound particle size spectra (Figure 3-4b) showed high concentrations of both nucleation and accumulation mode particles. Peak concentrations for nucleation mode particles were around 27, 30, 36-38, 38-41, and 43 miles distance. Interestingly all of these events matched well with strong acceleration events shown in Figure 3-4e. Peak concentrations for accumulation mode particles were present around 36 and 41 miles distance.

(a)

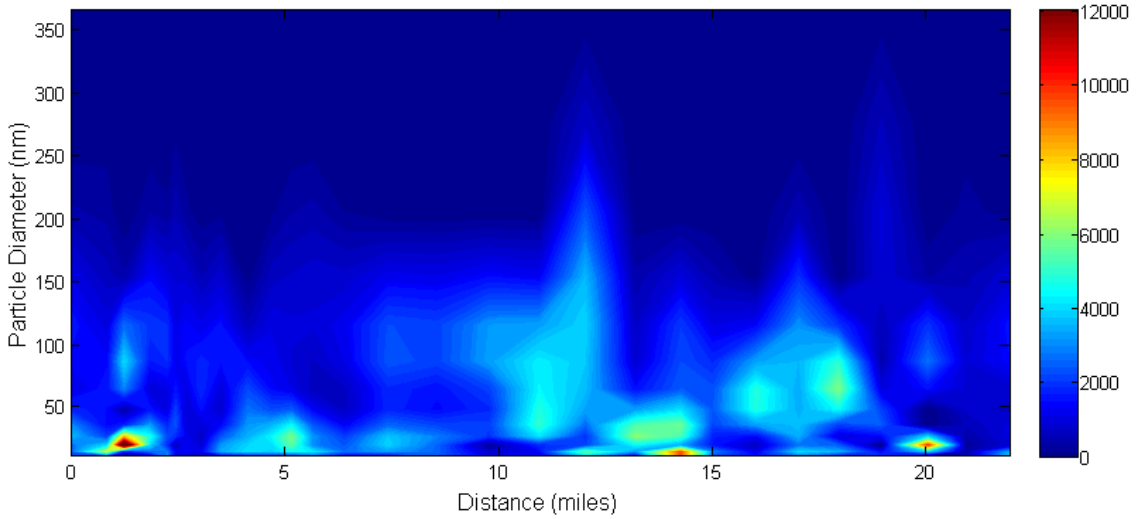
Particle Diameter (nm)
350
300
250
200
150
100
50
0
5
10
15
20
Distance (miles)
12000
10000
8000
6000
4000
2000
0

(b)

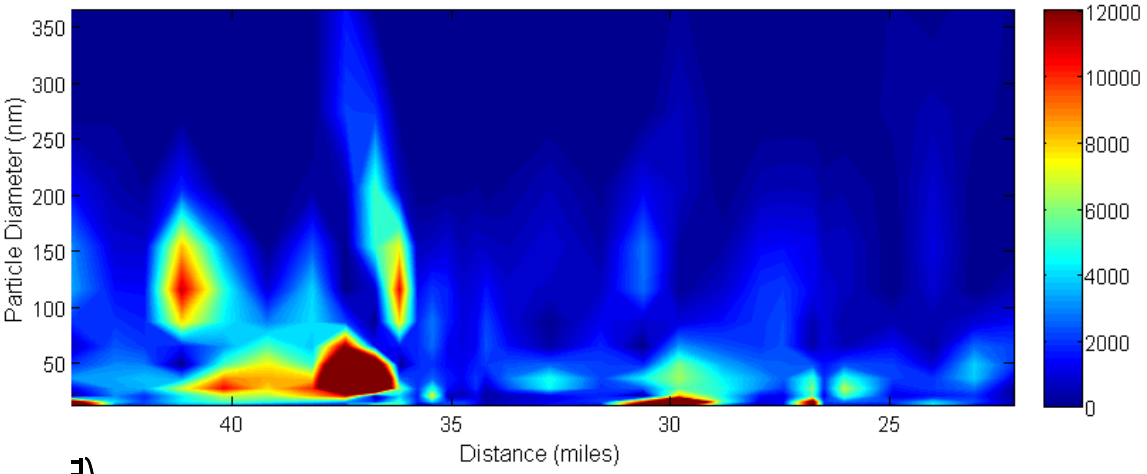
Particle Diameter (nm)
350
300
250
200
150
100
50
40
35
30
25
Distance (miles)
12000
10000
8000
6000
4000
2000
0

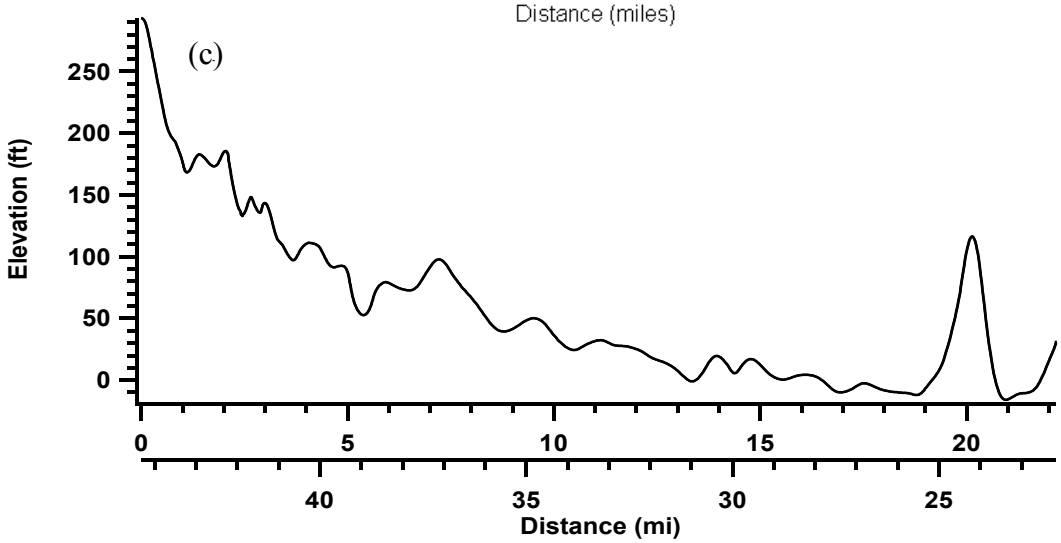
(c)
Elevation (ft)
250
200
150
100
50
0
0
5
10
15
20
40
35
30
25
Distance (mi)

(d)

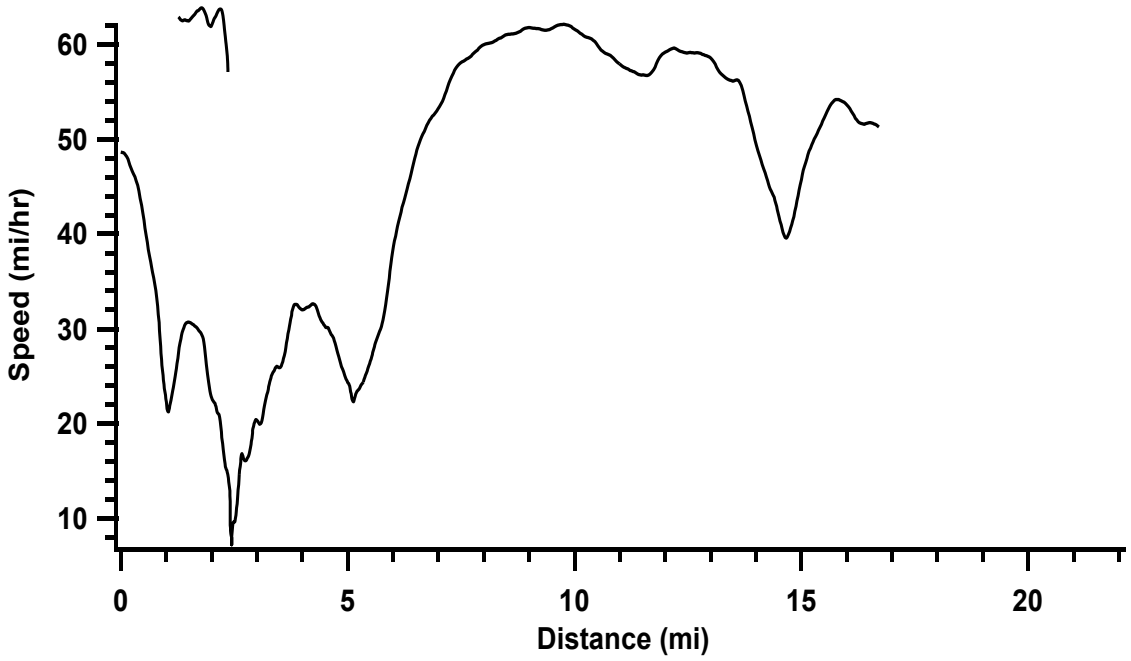
Speed (mi/hr)
60
50
40
30
20
10
0
5
10
15
20
Distance (mi)

(e)

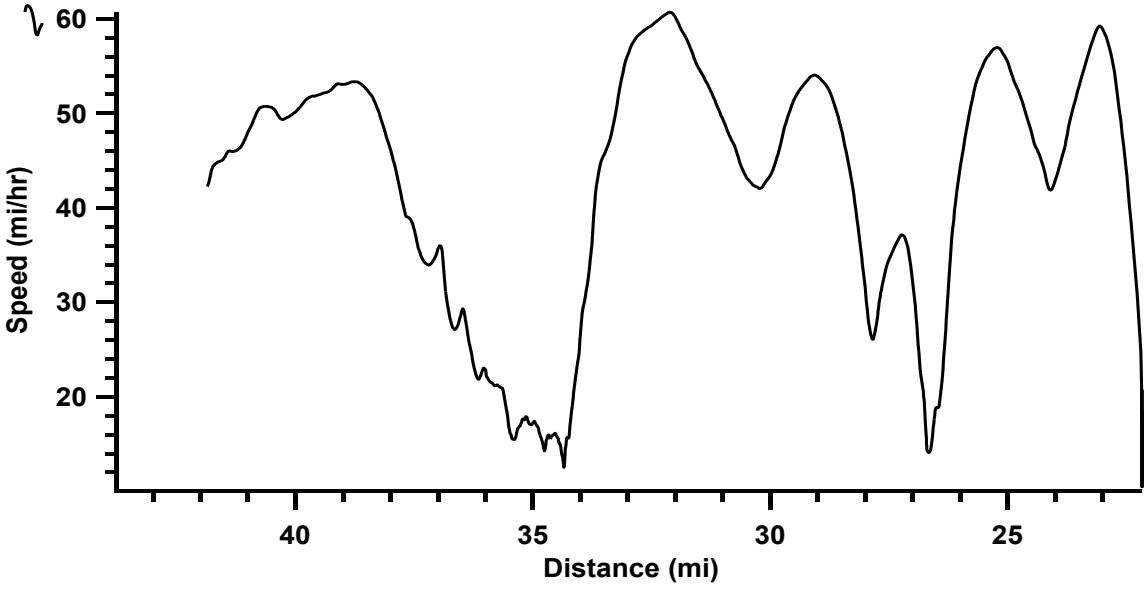
Speed (mi/hr)
60
50
40
30
20
40
35
30
25
Distance (mi)

(f)

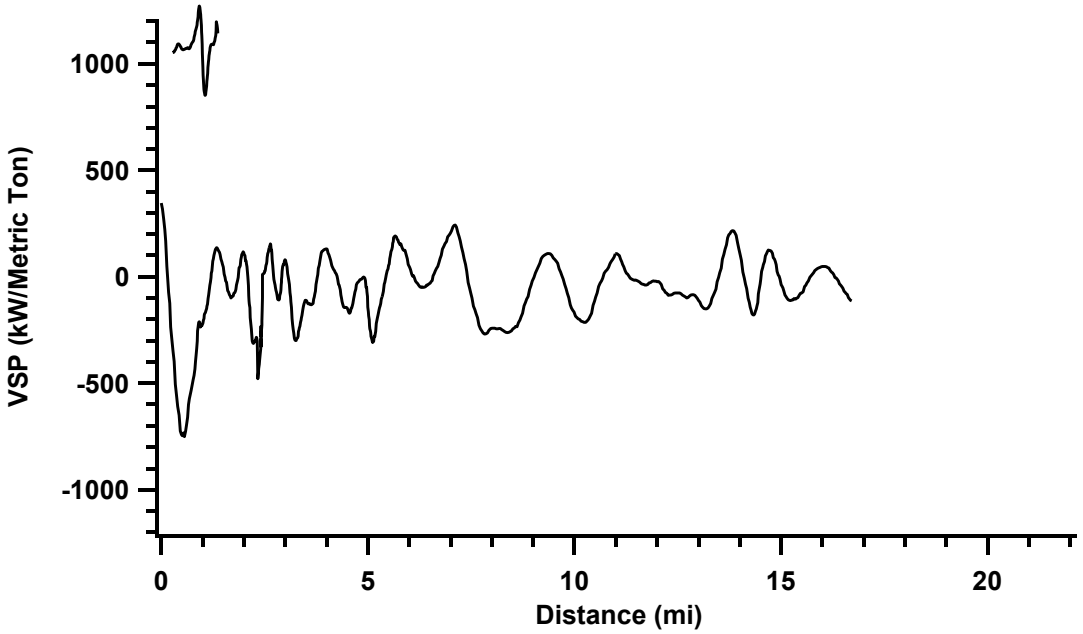

(g)

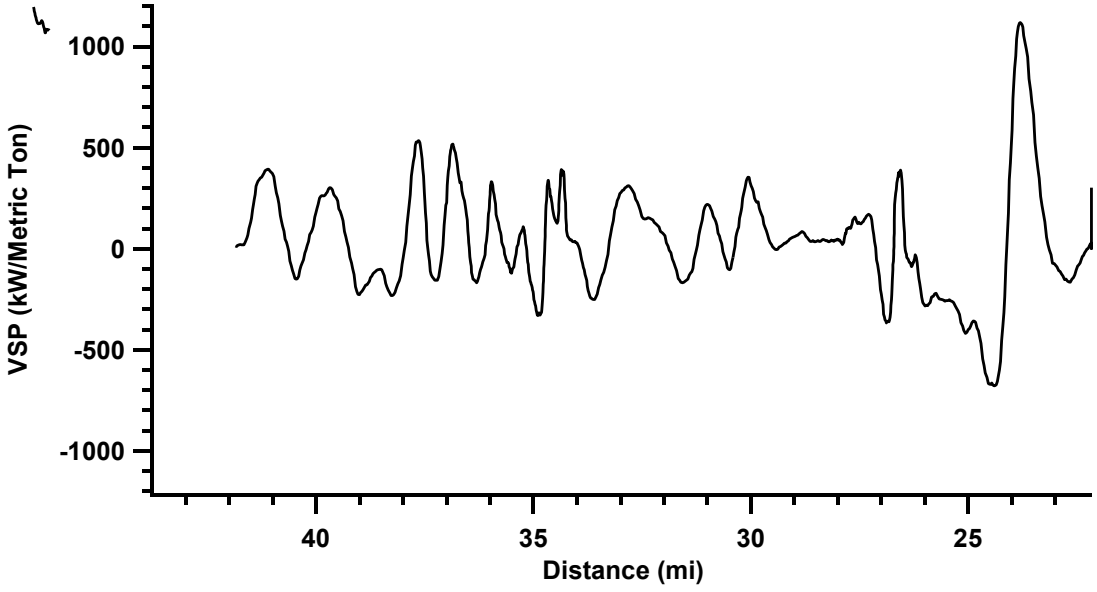

Figure 3-4: (a) Particle size spectra of route 2 southbound, (b) Particle size spectra of route 2 north bound

Although the mobile monitoring is extremely useful, an alternative way was tested to monitor vehicle emissions without mobile monitoring systems. This is a qualitative approach for further study. As route 1 data showed a close relationship between traffic conditions which is obtained from a single vehicle, which served as a mobile monitoring platform, and particle emissions, it was determined to use traffic information obtained from traffic monitoring sensors to predict average vehicle speed following Barth et al. study [70]. California has some traffic stations that report every 1 minute and some that report every 5 minutes, so it was determined to get every 5 minute data from CAL DOT. For every 5 minutes of travel, a station very near the location where the mobile platform was found, and the data for that time was looked up at that station. They had the average occupancy and the average speed. The traffic sensors are activated whenever there is a vehicle above them. The average occupancy is obtained by ratio of the time activated to total time. The average vehicle speed obtained by the traffic information is shown in Figure 3-5a and Figure 3-5b. This captures major traffic events, such as congested versus well-flowing traffic. It shows a good agreement with that measured by the mobile platform shown in Figure 3-4de. This gives a possibility of using traffic information to monitor air quality near and on highway. Particle emissions at different vehicle speed can be obtained using an emission model such as MOVES (Motor Vehicle Emission Simulator) and local air quality can be predicted using a dispersion model combining with meteorological input from monitoring stations. The mobile platforms can be used as a mean to provide a real time calibration for prediction and also provide a safety net on monitoring particle exposure due to higher time and spatial resolution, which cannot be compensated by other means.

(a)

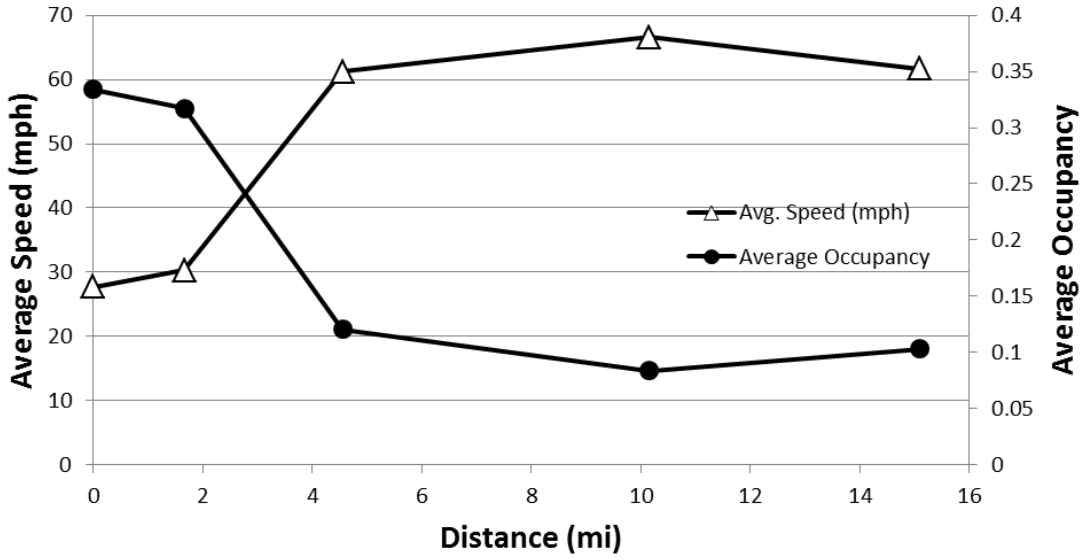

(b)

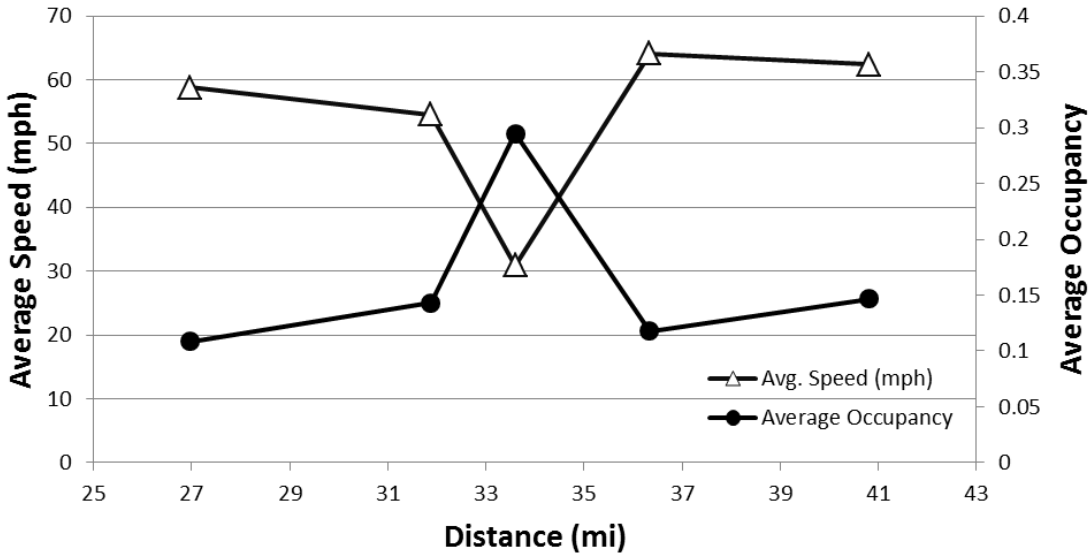

Figure 3-5: (a) Average vehicle speed and (b) average occupancy

3.2.2 Nanoparticle monitoring using CPC and EAD

Although particle size distributions are very useful information to understand transport and health effect of particles, it is not a single valued metric. Therefore, it is costly and difficult to measure and report spatially and temporally resolved particle size distributions over wide area. A single valued metric such as particle concentration and/or particle surface area are ideal to understand temporal and spatial variations of particle emissions on and near road. However, single metrics themselves do not provide information on particle transport. This study aims to show the ratio of particle surface area and concentration contain information related to particle size distribution. As studied in Chapter 2, the alternative method was applied to stationary monitoring location. This is to further investigate the metric in highly transient environment, such as on-road measurements.

Particle concentrations from the NanoScan SMPS were obtained by integrating particle number size distributions. Particle concentrations on the route 1 varied from 1.5×10^3 to 2.5×10^5 particles/cm^3, which is comparable to [71, 72]. It should be noted that the maximum concentration CPC 3007 can measure is 1.0×10^5 particles/cm^3. Therefore, the CPC must have been saturated when concentrations exceeded its limitation. It is recommended to use a wide range CPC, such as CPC 3022 in future studies that was used in other studies [22,73, 74]. On the other hand, total particle concentrations measured by the NanoScan SMPS are less likely to be saturated as the concentration was measured after the particle size was resolved. Second by second data from the CPC showed dynamic nature of the particles on the road. Particle concentrations measured by the CPC and

NanoScan SMPS agreed very well. However, the data from NanoScan SMPS showed less spikes than those from CPC due to the difference in instrument time resolution. EAD response was calculated from the particle size distribution measured by the NanoScan SMPS and compared to actual EAD measurement data. Particles entered the EAD are charged by ions generated by corona discharge in a counter jet mixing chamber.

(a)

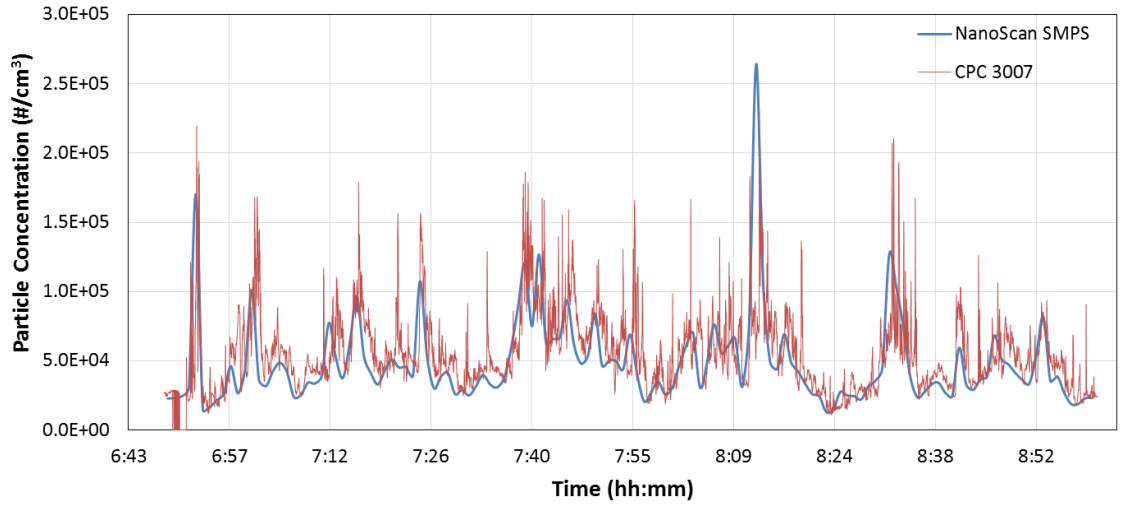

(b)

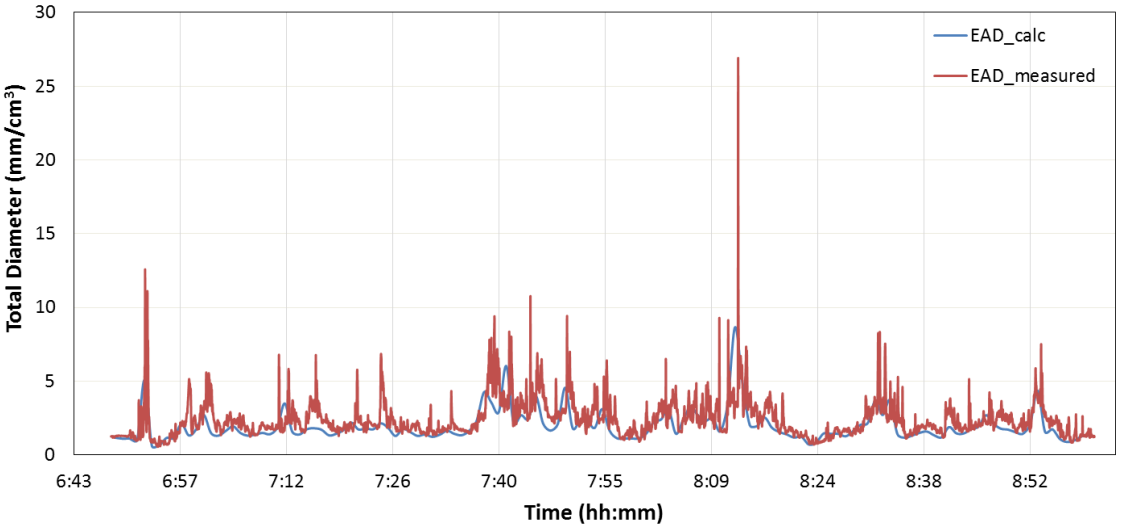

Figure 3-6: (a) Comparison between NanoScan SMPS and CPC measurements. (b) Comparison between calculated EAD response and EAD measurements

While particle number (PN) and particle surface (PS) concentrations give information on concentrations in two important metrics, they do not provide direct information on particle size or the shape of particle size distribution. We suggest the ratio of EAD/CPC (or χ_{PSA}) contains such information. As both particle concentrations and EAD response calculated from the size distributions measured by the NanoScan SMPS agree well with CPC and EAD measurements, we determined to use particle size spectra in Figure 3-7 to extract (on infer) physical meaning of EAD/CPC or EAD response per particle or average mean particle surface area.

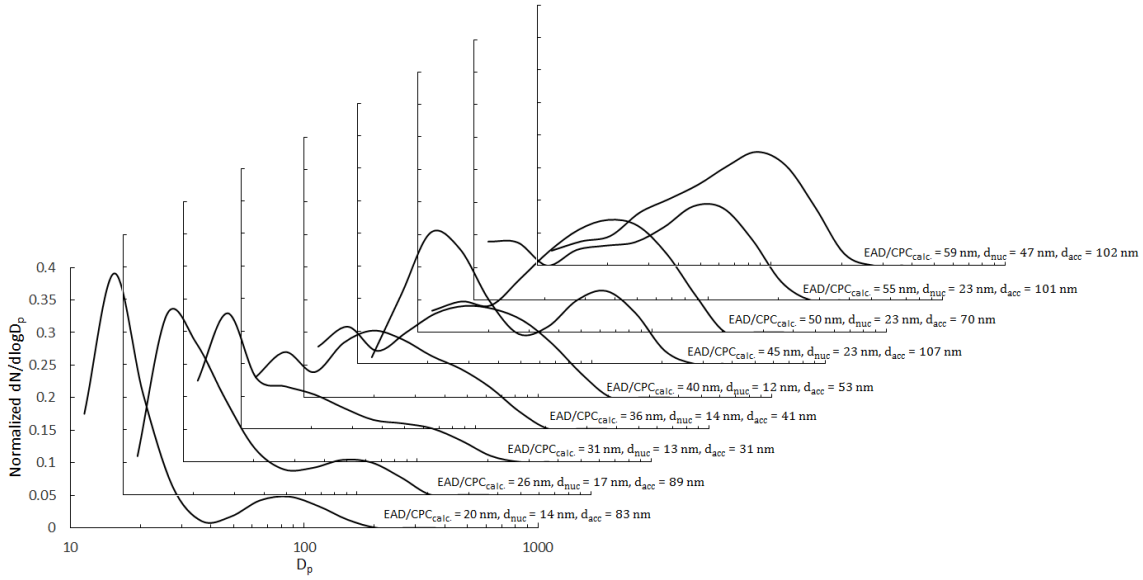

Figure 3-7: Particle size spectra with EAD/CPC ratio

The EAD/CPC ratio was chosen to have a constant increment as close as possible (~5 nm) in Figure 3-7. The particle count in each bin is normalized by the total count of the sample run. As the ratio increases, the profile shows a transition from nucleation to accumulation mode. From Figure 3-7, the exception that the profile does not follow the

trend is when the ratio is 45 nm. It is also interesting to see a trimodal mode distribution some cases like EAD/CPC equals 31 nm and 36 nm. Trimodal distribution may be either measurement artifact or result of aging (or coagulation) of particles by different vehicle exhaust sources on the highway. Furthermore, bimodal fit program was used on all SMPS samples for route 1, which provides information regarding geometric mean diameter (GMD) and standard deviation (σ). The nucleation mode diameter ranges from 3 nm to 45 nm with a mean diameter of 24 nm. The accumulation mode has a range from 30 nm to 135 nm with a mean diameter of 82 nm. It is noted that some distributions may have a trimodal profile. Thus, the bimodal fit program did not always fit the distribution very well.

To better understand physical meaning of particle size distribution shape factor, χ_{PSA}, lognormal particle size distributions were used. Figure 3-8 shows relationship between particle size distribution shape factor (or EAD/CPC ratio) for lognormal distribution with geometric standard deviations of 1.3 and 1.9 for nucleation and accumulation mode, respectively. The EAD/CPC ratio of the lognormal distribution of the accumulation mode turned out to be nearly equivalent (with a slope of 1.09) to the geometric mean diameter of the lognormal distribution of the accumulation mode. This relationship makes the use of EAD/CPC ratio extremely useful for ambient particle monitoring as a single value metric which can assess the shape of equivalent particle size distribution.

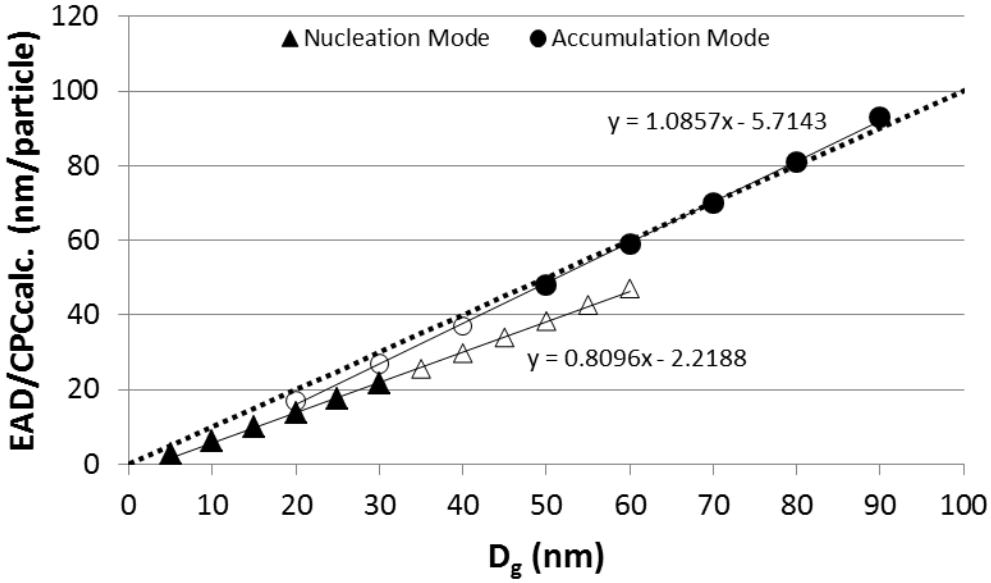

Figure 3-8: Standard deviations for nucleation and accumulation mode are 1.3 and 1.9 respectively.

3.2.3 Future and current implications

A further analysis was done to understand the implication of the EAD/CPC metrics obtained from route 1 test. EAD/CPC ratio both measured and calculated from the size distributions ranged from 19 to 73 nm. Two dotted lines were drawn based on model accumulation and nucleation mode particle size distributions to give an idea of equivalent particle size distributions. Interestingly on the highway, the frequency of seeing unimodal distribution solely by nucleation or accumulation mode was not very often. As a result, most of the EAD/CPC ratio fell between these two guide lines drawn by modal distributions. The metrics PN, PS, and PS/PN (with EAD/CPC) can also applicable to monitor ambient particle concentrations in other locations such as background stationary monitoring stations.

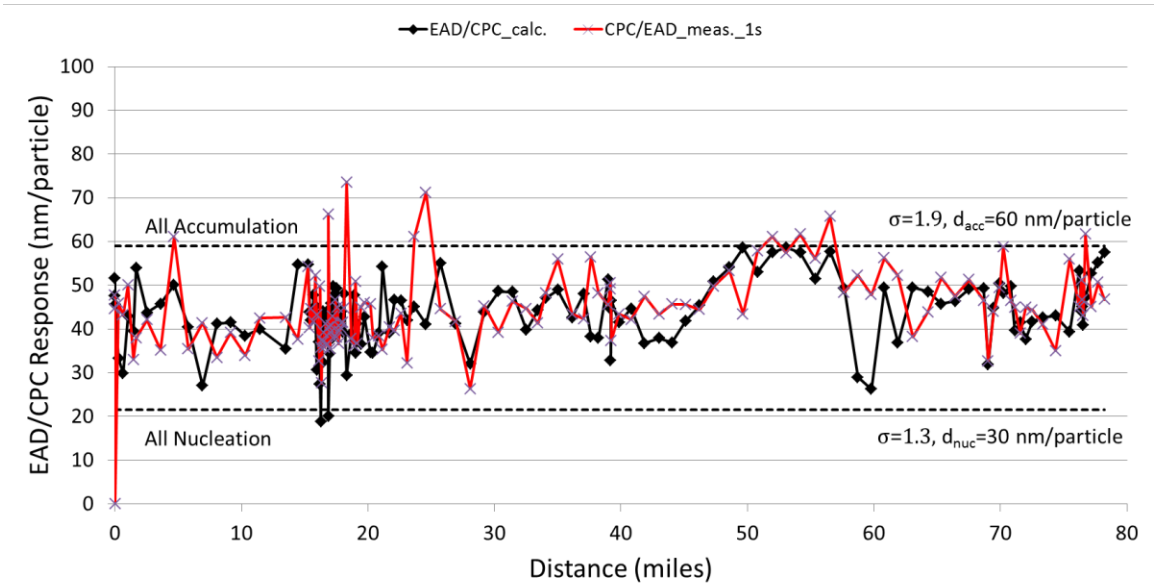

Figure 3-9: EAD/CPC responses of Route 1. Note CPC/EAD ratio by measurement was shown per mile for convenience. There are much higher resolutions (in terms of distance) data.

3.3 Conclusion

It is known that people are exposed to particle emissions significantly on and near roadways. This study aimed to test feasibility of multiple and simultaneous deployment of mobile monitoring systems with two particle instruments: particle counter (e.g. CPC) and particle surface instrument (e.g. EAD). The spatially and temporally resolved particle emissions on major highways were monitored using these instruments.

This study has shown dynamic nature of particulate matter emission on highways using mobile measurements. The study has found the PM emissions are strongly dependent on traffic conditions. Nanoparticles as well as carbonaceous soot particles were more abundant during congested traffic when frequent acceleration of the vehicles was

necessary. On the other hand, particles larger than 300 nm, which was measured by the OPS, showed no correlation with traffic conditions, implicating different particles formation process. There was a good agreement on traffic conditions determined by existing traffic sensor network on roadways and by the GPS of the mobile platform, while the latter showed much higher time resolution.

In addition, we examined the ratio of PS and PN (or EAD/CPC) as an indicator for the shape of particle size distribution using concurrent measurement of particle size distributions by NanoScan SMPS. The metric of EAD/CPC ratios provided a good perspective of the particle size distribution. The EAD/CPC ratio of the lognormal distribution of the accumulation mode turned out to be nearly equivalent (with a slope of 1.09) to the geometric mean diameter of the lognormal distribution of the accumulation mode. This relationship makes the use of EAD/CPC ratio extremely useful for ambient particle monitoring as a single value metric which can assess the shape of equivalent particle size distribution. We propose to use PN and PS measurement to monitor particle emissions on roadway with high temporal and spatial resolution. Attention should be paid to the cut off diameters and range of both instruments to get consistent and desired results.

4 Evaluation of Partial Flow Dilution Systems for Very Low PM Mass Measurements

4.1 Introduction

The purpose of this study is to compare the PFDs ability to provide reproducible measurements at very low PM emission levels using commercially available PFDs and to provide a comparison against a CVS tunnel. This program focuses on evaluating the capabilities of commercial PFDs to meet LEV III/Tier 3 PM emission measurement requirements and is designed to address a number of open questions about the application of PFDs for LDV exhaust emissions testing including: 1) whether PFDs show equivalency to full flow (CVS) exhaust sampling for two distinct driving cycles; 2) what the noise sources for PFD versus CVS sampling are; 3) what is needed to "pre-condition" these sampling systems (PFD/CVS tunnel); 4) how sensitive the PFD performance is to exhaust flow measurement; 5) what the relative performance attributes and issues for individual PFD units are; 6) what improvements can provide more efficient and accurate partial flow system performance in light-duty chassis dynamometer testing at Tier 3 PM standard levels.

For this study, a series of tests were conducted with three different PFDs and exhaust flow meters (EFMs) with and without vehicle exhaust. Initially tests were conducted to evaluate the accuracy, response, and proportionality of both the EFMs and PFDs. This included a laboratory test that evaluated the EFMs over a range of different flow rates, a laboratory test that evaluated the sampling delays for an EFM and PFD for vehicle exhaust, and a test that evaluated the performance of the individual EFMs in

monitoring vehicle exhaust flow. The main PFD comparison was conducted with a GDI vehicle over different combinations of FTP and US06 tests.

4.2 Experimental Setup and Analysis

4.2.1 Test Setup

4.2.1.1 Vehicles

The test vehicle was a 2016 Hyundai Sonata gasoline direct injection (GDI) vehicle with a PM emission rate of ~2 mg/mi for the FTP and ~5 mg/mi for the US06 cycle. It has a 2.4 L engine with a mileage of 14,700 miles and is certified to the California LEV III SULEV 30 PC Certification standard. This vehicle had a PM emission rate that was sufficiently high enough to provide filter mass levels that were readily measurable, but not too high to create filter plugging or contamination issues. This vehicle was inspected to ensure that it was in sound mechanical and operational conditions upon arrival using a standard checklist.

4.2.1.2 Test Fuel

Commercially available retail E10 California fuel was used for testing. One batch of fuel was used for the main PFD comparison tests in this study. A fuel change procedure with multiple drains and fills and preconditioning driving was performed on the vehicle prior to beginning the testing for this study.

4.2.1.3 Test Cycle

The FTP and US06 cycles were the two cycles used in this study, because they are used in the certification procedure for LDVs. The FTP was performed as a standard 3-bag test with cold start, hot stabilized, and hot start phases. Prior to the FTP tests, the vehicle

was preconditioned over an LA04 prep cycle followed by a cold soak of between 12 to 36 hours.

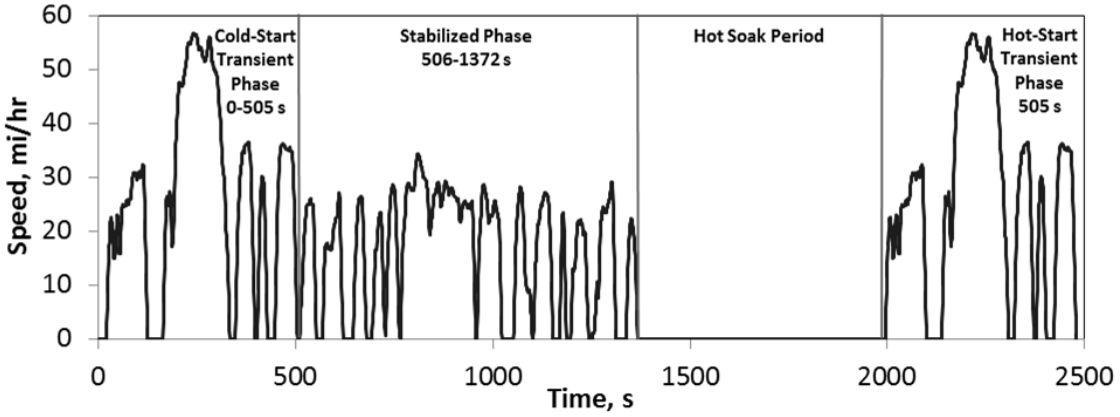

Figure 4-1: FTP 3-bag test schedule [75]

The US06 test is a more aggressive testing cycle that is included as part of the certification testing procedure. The US06 tests were conducted immediately after the corresponding FTP test and the FTP bag analysis. A US06 preconditioning cycle was conducted right after the FTP test and immediately before the US06 emissions test. Both speed traces are shown in Figure 4-1and Figure 4-2.

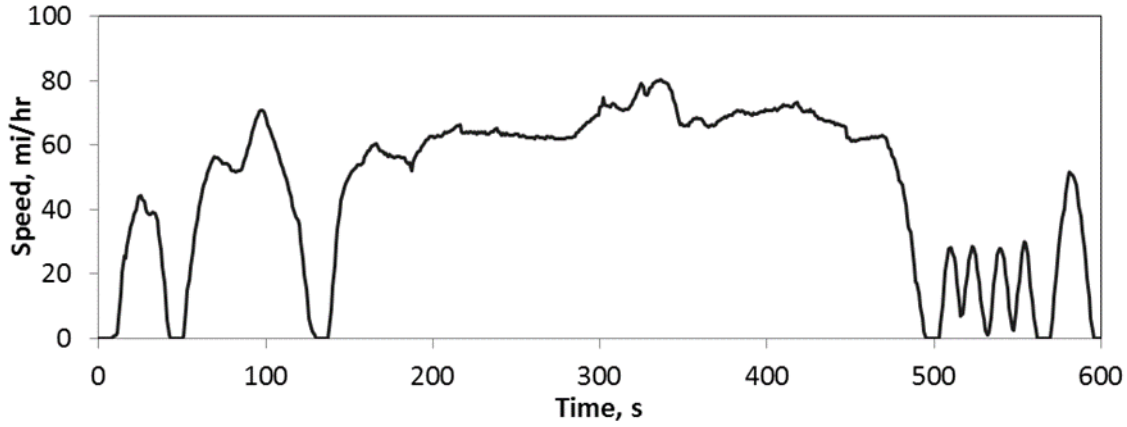

Figure 4-2: US06 test schedule [75].

4.2.2 PM Sampling and Measurement

The two PM sample approaches utilized in this study were a CVS PM and PFD PM sampler. Each of these systems are unique in their measurement of PM. The CVS method utilizes the full vehicle exhaust and PM is collected on filters under fixed constant flow conditions. The PFDs sample a small fraction of the exhaust (typically around 1-2%) that is extracted in a manner proportional to the exhaust flow. Proportionality and accuracy in the exhaust flow measurement are factors for the PFDs that could affect the comparison between the CVS method and the PFD method. This can create some biases between the PFD and CVS methods. This section describes the configuration details of the PM sampling approaches for both sampling systems. The overall experimental setup is shown schematically in Figure 4-3. For the FTP testing, the PFD could be setup to collect a cumulative filter over all three bags of the FTP or to sample PM separately for each of the individual phase, and it was decided to utilize the composite (or cumulative) method.

4.2.2.1 Full flow dilution (CVS)

For the CVS method, probes for both composite and by phase PM sampling were utilized. A multi-filter sampler that simultaneously collected PM on three different gravimetric filter samplers from the dilute CVS was utilized to evaluate different parameter changes in parallel. This design maximized the number of parallel measurements to minimize the confounding factors of test-to-test vehicle/driver variability. This sampler is designed to meet 40 CFR 1065 and 1066 requirements and utilized a single heated sampling probe, a particle impactor, a heated control chamber for the various filter holders, a residence chamber designed to provide a residence time of 2.5 seconds for each of the

FFVs, compliant filter holders with filter cassettes, solenoid bypass valves, and four National Institute of Standards (NIST) traceable mass flow controllers (MFCs). The system is controlled via a LabVIEW program and was integrated into CE-CERT's driver's aid system for automatic flow control, logging, and monitoring.

The heated chamber contained several PM samplers designated Probe A, B, and C. The PM samplers were designed for varying FFVs while maintaining similar residence times. These probes all collected from a standard a 1" OD (0.87" ID) tube that extended into the CVS. A description of the PM samplers that were collected from each probe is provided below:

Probe A – CVS Probe A (CVS_A) collected a cumulative PM filter over the entire duration of the 3-bag FTP tests. The flow rate for probe A for a 3 bag FTP was 100 cm/s for the bag 2 segment with flow rates that were 43% and 57% of that value for bags 1 and 3, respectively.

Probe B – CVS Probe B (CVS_B) was connected to a flow splitter with 3 legs. This probe collected filters for the individual bags for the 3 bag FTPs. The flow for this probe was set at 100 cm/sec, with an exception of one set of three FTP tests that was run at a second higher FFV of 130 cm/s. Note that this was the same nominal FFV that was used for bag sampling for Probe A.

Probe C – CVS Probe C (CVS_C or EC/OC) collected a cumulative PM filter over the entire duration of the 3-bag FTP. The filter media used with this probe was a quartz filter that was utilized for organic carbon (OC) and elemental carbon (EC) characterization using thermal optical analysis (TOA) off-line analysis methods. This measurement is

typically referred to as the EC/OC measurement using the TOA analysis method. All EC/OC analysis were performed by an outside certified laboratory. EC/OC samples were collected for a subset of tests. CVS_C was set at a nominal flow of 100 cm/sec for bag 2, and used the same flow weighting values as Probe A for bag 1 and 3.

4.2.2.2 Partial flow dilution (PFD)

The three main PFD systems used for this testing were AVL, Horiba, and Sierra systems. These were commercially available PFDs that were on the market at the time of this project. These systems are designed to use a range of different EFMs in conjunction with their proportional PM samplers. The PFDs were all set up to sample from the raw exhaust at a point before it enters the dilution tunnel, as indicated in the test configuration graphic provided in Figure 4-3. The flow proportionality was maintained by integrating the PFDs with a selected EFM that showed good performance in preliminary testing. PM filter weighing utilized the same practices as for the CVS system described earlier, with the flow rates for bags 1 and 3 being 43% and 57%, respectively, of the nominal bag 2 flow rate.

The partial flow systems were originally designed to operate at a maximum of 100 cm/sec FFV. During of this study, the PFDs were also tested at a higher FFV of 130 cm/sec. Although the PFDs were not designed for these higher FFVs, it was expected they would perform satisfactory at the higher flow.

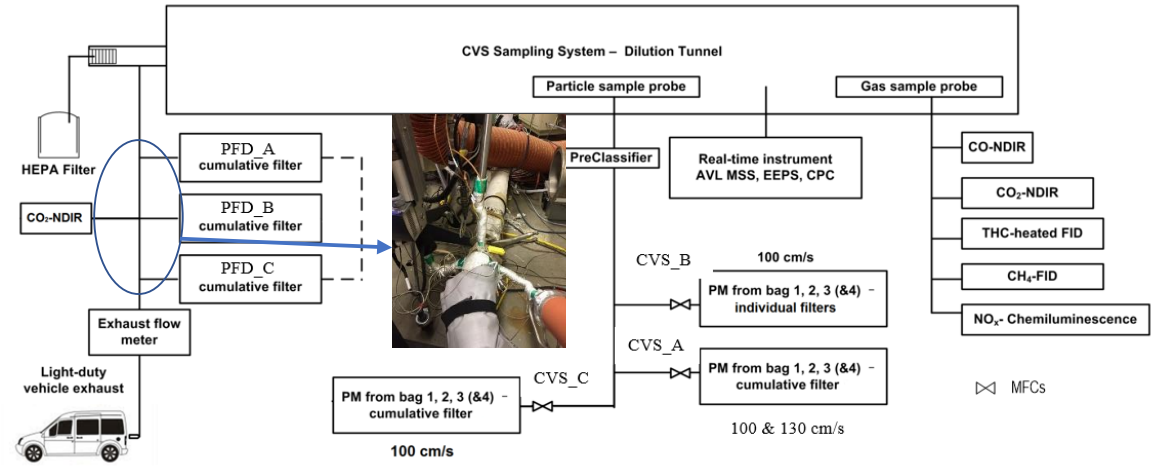

Figure 4-3: Schematic Diagram of Sampling Configuration for Emission Measurements

4.2.2.3 Exhaust Flow Measurement (EFM)

Three exhaust flow measurement principles were evaluated in this project: ultrasonic, venturi, and a differential pressure annubar. AVL at the time of testing recommended the Sick Carflow150 (2.5") EFM system (ultrasonic), Horiba offers their own EFM called the EXFM-ONE (ultrasonic), and Sierra offers a venturi meter called the ExhaustTrak. These EFMs are denoted EFM A, EFM B, and EFM C, respectively. Each of the PFD manufacturers prefers using their own EFM, but they all agreed that testing with only one EFM would be preferred over all three EFMs being installed at once. Towards the later part of the testing, AVL introduced their new EFM, which is a differential pressure annubar type. AVL offered an integrated EFM, which uses differential pressure for its flow principles. The Sick, Horiba, and Sierra EFMs were used for the main part of this research, while the AVL EFM was used at the end of the study. The EFMS were placed

in the raw exhaust prior to the sampling point for the PFDs and prior to the CVS, as shown in Figure 4-3.

4.2.2.4 Dilution Factor (DF)

Dilution is used to prevent water condensation for the gravimetric PM sampling method and it provides a basis for consistent sampling between laboratories [76, 77, 78]. For the CVS, the dilution factor is the ratio of total average CVS flow divided by the total average exhaust flow. For the PFD, it is the total volume through the filter divided by the extraction flow volume. The CFR requires a minimum dilution of 7 to 1 on a per bag basis. For the CVS, the phase with the lowest DF was bag 1 and for the PFD it was bag 2. The reason for the different DF minimum phases is a result of the different weighting methods (FFV vs. extraction ratio).

For the CVS, the phase with the lowest DF was bag 1 and for the PFD it was bag 2. The reason for the different DF minimum phases is a result of the different weighting methods (FFV vs extraction ratio).

CVS: The CVS flow rate was with a constant displacement pump system utilizing a heat exchanger prior to flow control. Typically, flow control is set by pre-configured targets designated by the manufacturer. Since a minimum phase of DF equal to 7 was desired, flow control was determined by selecting a rotational frequency of the CVS that produced the appropriate DR, as per the carbon balance method as discussed below. The DF over the given test interval, was determined using the following Equation 4-1 (CFR Eq. 1066.610-2) defined by 40 CFR 1065/1066.

$$DF = \frac{1}{\left(1+\frac{\alpha}{2}+3.76\cdot\left(1+\frac{\alpha}{4}-\frac{\beta}{2}\right)\right)\cdot(x_{CO2}+x_{NMHC}+x_{CH4}+x_{CO})}$$

(Equation 4-1)

where: $x_{CO2}, x_{NMHC}, x_{CH4}$ and x_{CO} represent the averaged wet corrected concentration of CO_2, NMHC, CH_4 and CO measured in the sample over the test interval. In this study, α and β were set to be 1.92 and 0.03, respectively, because commercial E10 gasoline fuel was utilized, Table 1 of 40 CFR 1065.655.

PFD: The DF for the PFDs was nominally set to 7 to 1 by varying the sample extracted from the exhaust as determined by Equation 4-3. The resulting DFs for bags 1 and 3, at the desired PM filter weightings, were higher than for bag 2, therefore bag-2 represented the lowest DF allowed by 1066.

The DF of the PFDs was determined by using the flow-based method calculation 40 CFR Part 1066.110(b)(2)(iii) for the PFDs.

$$DF = \frac{V_{PMstd}}{V_{exhstd}} \qquad \text{(Equation 4-2)}$$

Where V_{PMstd} is the total dilute exhaust volume sampled through the filter (denoted as G_{tot} for the PFD) over the test interval at standard reference conditions (20˚C and 101.325 kPa), in m^3. This flow volume is the accumulated volume sampled through the filter. V_{exhstd} is the total exhaust volume sampled (denoted as G_p from the PFD as the probe flow) from the vehicle at standard reference conditions, in m^3. The exhaust volume sampled is the sample probe flow rate total volume that is in proportion to the exhaust flow. If we put DF in terms of the PFD measurements it becomes:

$$DF\_Q = \frac{G_{tot}}{G_p} \quad \text{(Equation 4-3)}$$

where the G_{tot} and G_p are the total diluted exhaust flow (filter flow) and proportional sampled exhaust flow extracted from the raw exhaust. These measurements are directly taken from the PFD and are independent of the CVS measurement system. Setting up the PFD DF control was done by changing the scripts and test run files inside the PFD software.

4.2.2.5 PM mass emissions

PM sampling was conducted in compliance with the procedures in 40 CFR 1066 and associated references in 40 CFR Part 1065. Cumulative PM samples were collected over each FTP with flow-weighting MFCs. Total PM mass samples for both the CVS and PFDs were collected using Whatman 47 mm polytetrafluoroethylene (PTFE) filters. They were weighed with a 1065-compliant microbalance in a conditioned room meeting 1065 requirements. Buoyancy corrections for barometric pressure differences were also made for the PM filter weights, as stated in 40 CFR Part 1065. The tunnel blank values used were based on actual measurements and exceeded the CFR limits of 5 µg. The background corrections for the CVS probes A and B were 11 µg. The background corrected values for PFD A, B, and C from the average of six tunnel blank tests, they were 3, 5, and 4 µg, respectively. The tunnel blank tests were taken over a span of four months.

4.2.3 Experimental Design

A series of three different tests were utilized to evaluate different components of the PFD sampling systems. This included EFM comparison tests, a test to evaluate the sampling proportionality of the three individual PFDs, and then a side-by-side comparison

of the three PFDs where vehicle exhaust was sampled in parallel by the PFDs over a series of emission tests. This section describes the details of each of these tests.

4.2.3.1 EFM calibration

The purpose of the main EFM comparison test was to evaluate the accuracy, response, and proportionality of each EFM while operating with one PFD, which in this case was PFD A. The goal behind this test was to characterize the performance of each EFM under typical testing conditions with an in-use GDI vehicle. The factors that could impact EFM operation include cold start operation, and steady state vs. transient operation. The EFM performance was evaluated based on raw and dilute CO_2 measurements. The raw measurements utilized CO_2 concentrations measured directly from the raw exhaust and the exhaust flow from the EFM as reported by the PFD to determine CO_2 mass emissions. Both the bag and modal CVS dilute CO_2 concentrations along with the CVS total flow were used to determine the dilute CO_2 mass emissions. The experimental setup for this test is illustrated in Figure 4-3, where the sampling in the raw exhaust included the CO_2 measurements, PFD A, and then each of the EFMs tested individually in sequence. Triplicate tests over the LA4 cycle were performed for each EFM. A single LA4 was run to precondition the vehicle prior to running the triplicate LA4s. The LA4s were separated by an approximately 10 minute soak between tests. More details of the experimental setup for each of these tests are provided in Table 4-1.

Some additional tests were also performed to evaluate the calibrations of the EFMs as well as the EFM measurement noise for measuring vehicle exhaust under steady state conditions. These tests are discussed in greater detail in the Supporting Information. The

15+ point calibration check was performed by an outside laboratory on each of the EFMs, covering the following test points of 0, 2, 4, 6, 8, 10, 20, 30, 40, 50, 60, 70, 80, 90, 100 scfm, and a few other flow rates for some tests. The EFMs all showed good correlations over the full flow rate range examined in this calibration. The slopes of the regression lines varied from 0.9818 to 1.0027 and all the R^2 were greater than or equal to 0.9999. Some larger differences were seen at lower flow rates, where the EFMs showed differences that ranged from -5% to 30%. The steady state vehicle exhaust tests covered speeds from idle to 60 mph (representing exhaust flows from 4 to 60 lpm). For the steady state tests, EFM_A and EFM_B showed similar single standard deviations (1σ) over all the points, with the EFM_B average 1σ (0.37 scfm) being slightly lower than that for EFM_A (0.54 scfm). For EFM_D, the average 1σ was slightly less at 0.75, while EMF_C showed the highest average 1σ of 1.00, and for exhaust flows below 30 scfm it was 1.35.

4.2.3.2 PFD sampling proportionality test

PFD sample flow delays and inaccuracies can vary between PFD systems due to varying line lengths, response times, and design differences. PFD sample flow is not directly measured by a PFD, but is typically calculated from the difference of the total flow over the filter and the dilution flow. As the PFDs receive current signals for the flow measurements from EFM, the sample flow rates are adjusted according to the set extraction ratio. The purpose of this test was to evaluate PFD delays and possible accuracy differences between the PFD units while utilizing a common EFM over transient driving conditions. This allowed for an evaluation of PFD performance in terms of proportionality and flow rates to determine if the PFD systems were operating as designed before conducting the

main side-by-side PFD test. One EFM, in this case EFM B, was used in conjunction with each of the PFDs to measure the exhaust flow and provide the signal for PFD proportional sampling for LA04 driving cycle. The inlet sampling port of the PFD was connected to a LFE (laminar flow element) with a HEPA filter instead of the exhaust transfer line. Therefore, the PFDs were sampling particle free test-cell air instead of exhaust while following the LA04 test cycle. The LFE is a NIST traceable, high quality, fast responding flow meter with a valid certification. The LFE has a maximum sampling flow rate of 21 SLPM, and for the LA04 driving cycle, measured LFE flow was above this maximum value less than 1% of the time. For this test, the PFDs were configured to have an FFV of 100 cm/sec and a DF of 7 at an extraction ratio of 1.48%. Similarly, the CVS was also operated at DF of 7. PM filters were not collected for either the CVS or the PFD. Referring to Figure 1, the experimental setup for this test for the raw exhaust sampling included the LFE, EFM A, and then each of the PFDs tested individually in sequence. The raw exhaust CO_2 measurements were not performed during this test. More details of the experimental setup for each of these tests are provided in Table 4-1.

Table 4-1: Test vehicles and PFD settings

	Test #	Vehicle Specification	Prep. Cycle	Test Cycle	EFM	Phase	PFD_A		PFD_B		PFD_C	
							FFV (cm/s)	r (%)	FFV (cm/s)	r (%)	FFV (cm/s)	r (%)
EFM Comparison	1-3	2016 Hyundai Sonata GDI	LA4	LA4	EFM_A	1	100	0.926	100	0.926	100	0.926
						2	100	2.16	100	2.16	100	2.16
	1-3	2016 Hyundai Sonata GDI	LA4	LA4	EFM_B	1	100	0.926	100	0.926	100	0.926
						2	100	2.16	100	2.16	100	2.16
	1-3	2016 Hyundai Sonata GDI	LA4	LA4	EFM_C	1	100	0.926	100	0.926	100	0.926
						2	100	2.16	100	2.16	100	2.16
PFD Proportionality	1	2016 Hyundai Sonata GDI	LA4	LA4	EFM_B	1	100	1.48				
						2	100	1.48				
	1	2016 Hyundai Sonata GDI	LA4	LA4	EFM_B	1			100	1.48		
						2			100	1.48		
	1	2016 Hyundai Sonata GDI	LA4	LA4	EFM_B	1					100	1.48
						2					100	1.48
PFD Side-by-side Comparison	1-6	2016 Hyundai Sonata GDI	LA4	3-bag FTP	EFM_A	1	100	0.926	100	0.926	100	0.926
						2	100	2.16	100	2.16	100	2.16
						3	100	1.22	100	1.22	100	1.22
	7-9	2016 Hyundai Sonata GDI	LA4	3- bag FTP	EFM_A	1	130	1.18	130	1.18	100	0.926
						2	130	2.74	130	2.74	100	2.16
						3	130	1.56	130	1.56	100	1.22
	1-6	2016 Hyundai Sonata GDI	FTP, US06	US06	EFM_A		100	0.669	100	0.669	100	0.669

4.2.3.3 PFD side by side comparisons

Finally, simultaneous measurements were conducted with each of the PFD systems sampling in parallel using one selected EFM. A schematic layout of the test setup is provided in Figure 4-3, where EFM A was used. Table 4-1 describes the PFD configuration parameters and testing cycles, which included nine repeats of the FTP and six repeats of the US06 test cycle. This provided sufficiently robust comparisons under certification conditions, under cold start conditions, and under more aggressive driving conditions. Six FTPs were conducted at a FFV of 100 cm/s and three additional FTP tests were conducted at a FFV of 130 cm/s. Although PFD_A and B were operated at the 130 cm/s FFV, PFD_C was not able to operate at a this higher FFV with the sampling tube diameter of 0.25 inch OD, and was configured to 100 cm/s instead. The six US06s were all conducted at an FFV

of 100 cm/s. Prior to these official tests, preliminary tests were conducted to ensure the PFDs were working according to specifications and to set up the appropriate dilution conditions for the testing. Performance checks included leak checks, calibrations, and that the exhaust flow rate signals for the EFM and the PFDs matched.

4.3 Results and Discussions

4.3.1 PFD and EFM performance checks

4.3.1.1 EFM Comparisons

The relative differences between the raw exhaust CO_2 emissions rates and the dilute CVS CO_2 emission rates from the bag measurements for the EFM comparison tests conducted over the LA4s are shown in Table 4-2 for the bag 1 and bag 2 averages for each of EFMs. The breakdown of the CO_2 emission rates and percentage differences between the EFM, CVS bag, and CVS modal CO_2 emission rates are provided in Supplemental Section. Overall, the EFM and CVS emission rates were in relatively good agreement with a range from -1.2 to 2.0% for bag-1 and from -0.5 to 5.0% for bag-2. The differences between the EFM and CVS CO_2 emissions rates were 2.0% or less for all EFM/test configurations, except for the bag 2 comparisons for EFM A and B. It should be noted that the stability of the extraction ratios for the different EFMs was also evaluated during these tests. These results are presented in the Supporting Information. EFM_A and EFM_B had relatively similar performances, but only one could be selected for the rest of this study. Coupling the low percentage CO_2 emission rates differences together with the low variability for EFM_A, it was decided to use EFM_A for the PFD comparison tests.

Table 4-2: Average percent differences between raw exhaust EFM/PFD and dilute bag CVS CO_2 emission rates

EFM	Bag 1	Bag 2
A	-1.2% ± 0.3%	3.5% ± 0.1%
B	2.0% ± 0.9%	5.3% ± 0.6%
C	1.7% ± 0.5%	-0.5% ± 0.8%

4.3.2 PFD Sampling Proportionality Test

The purpose of this test was to evaluate the accuracy and proportionality of the PFD calculated sample flow system. Errors in the sample flow calculation (related to factors such as flow delays and flow accuracy) can lead to proportionality differences between the PFD units while utilizing a common EFM. Comparisons were performed over a hot start LA4, with a single test for each PFD. A correlation analysis was performed to evaluate the comparisons between the PFD and LFE sample flows. A summary of the sample flow correlations is provided in Table 4-3. The correlation shows slopes of 1.0034, 1.0358, and 0.9711 for PFD_A, PFD_B, and PFD_C, respectively, and R^2 values of 0.995, 0.992, and 0.985 for PFD_A, PFD_B, and PFD_C, respectively. When the regression is forced through zero, the slopes change slightly to 1.011, 1.006, and 0.9496, respectively, with similar R^2 values. There were a few outlier points in the correlations, which are shown in detail in the supplemental material. The outlier points occurred during the phase transition between Phase 1 and Phase 2 of the LA4 505 seconds into the cycle. For these outlier points, the LFE reported typical values, while the PFD flow values were low. This also may be caused by delays in the PFD flow control response to the cycle phase change signal

from the data acquisition system. Similar correlation R^2 values were also found between the LFE sample flow and exhaust flows reported by the PFD, which are shown in further detail in the supplemental section. This is to confirm the accuracy of the proportionality and response relative to the exhaust flow.

Table 4-3: Correlation results between the PFD and LFE sample flow rates for the PFD proportionality tests

Sample	LA4	EFM	PFD			Correlation			
			FFV	DF	Unit	SEE	R^2	Slope	Int.
1	hot 2-Bag	B	100	7	A	0.30	0.995	1.003	0.067
1	hot 2-Bag	B	100	7	B	0.38	0.992	1.036	-0.26
1	hot 2-Bag	B	100	7	C	0.53	0.985	0.971	-0.20

These results are comparable to those seen in the previous E-66 project. In that study, a number of PFD systems, including AVL-SPC, Cummins-AEI, Horiba-MLDT, Sensor-MPS, and a Sierra-BG3, were evaluated using a heavy-duty engine on an engine dynamometer. The PFDs achieved sampling proportional to the exhaust flow with a response time of 200 ms or faster, which was sufficient to run the PFDs in real time under transient engine operation [10]. This was considerably improved from an earlier 2002 study conducted at the Southwest Research Institute (SwRI) where the PFD response times were found to be too slow to provide for adequate sampling under transient engine operating conditions [35]. Foote et al. tested two PFDs with gasoline vehicles and also found both units were able to meet the proportionality requirements for traditional powertrains, although they did find issues in proportionality for hybrid electric vehicle (HEV) powertrains that have zero flow conditions as part of their operation [34].

4.3.3 Side-by-Side PFD emission test results

4.3.3.1 PFD performance for the side-by-side emission tests

Table 4-4 shows the relative percent difference for PFDs B and C compared to PFD_A for the exhaust flow, sample flow, and total flow. The extraction ratio (r) and filter flow rate (Gtotal) had the lowest relative error, with differences being typically around 0.1% and differences for all tests being less than 0.5%. The exhaust flow (Gext) and sample flow (Gprobe) differences for PFD_B and PFD C relative to PFD_A varied between -1.1% to 1.8%. Note Gext is determined by each PFD by interpreting output signal of the EFM, which in this case was EFM_A. It is assumed that the exhaust flow (Gext) differences may be a result of input signal processing errors by the PFDs or slight differences in calibration. While the biases for the exhaust flow and sample flow among PFDs are important to characterize, biases in these parameters will only have an impact on the PM emission rate if they impact the extraction ratio. It is assumed that the bias of Gext is due to systematic input signal processing error which leads to another systematic bias of Gprobe. If our speculation is correct then these systematic biases for Gext and Gprobe will cancel out when determining extraction ratio (r) and final PM emission rate. In the comparisons here, the differences between the PFDs for exhaust flow and sample flow are generally biased in the same direction for PFD_B and PFD_C relative to PFD_A. For example, both the exhaust flow and sample flow rates are biased high by 1.1% for PFD_C relative to PFD_A. Table 4-4 shows that extraction ratio difference ranged from 0.0 to 0.4 % independent from the systematic bias of Gext and Gprobe, which confirms our assumption. Overall, the

results of this test suggest that there should not be a bias in PM emission rates between the different PFDs due to sampling proportionality considerations.

Table 4-4: Comparison of PFD measurements to PFD A by test and phase (FFV = 100, n = 6)

Test	PFD	%r	%Gexh	%Gprobe	%Gtotal
FTP Ph1	A	-	-	-	-
FTP Ph1	B	0.1%	0.0%	0.2%	0.01%
FTP Ph1	C	0.1%	**0.7%**	**0.8%**	-0.01%
FTP Ph2	A	-	-	-	-
FTP Ph2	B	0.1%	**0.2%**	0.3%	0.01%
FTP Ph2	C	0.0%	**1.1%**	**1.1%**	-0.01%
FTP Ph3	A	-	-	-	-
FTP Ph3	B	0.1%	1.7%	**1.8%**	0.02%
FTP Ph3	C	0.0%	**-1.1%**	**-1.1%**	-0.01%
US06	A	-	-	-	-
US06	B	0.0%	-0.5%	-0.4%	0.0%
US06	C	0.4%	-0.1%	0.3%	0.0%

%r is the percent difference for the extraction ratio, %Gexh is the percent difference for the average exhaust flow, %Gprobe is the percent differences for the average sample flow rate by probe, and %Gtotal is the percent difference for the average filter flow or total dilute plus sample flow. Gexh was measured by one system and reported by each of the PFD suppliers where Gprobe and Gtotal were measured separately for each of the three systems. All comparisons were based on PFD A.

The correlation between the exhaust flow and the sample flow was also evaluated for each of the PFDs. The correlation results between the PFD sample flow and the exhaust flow are presented in Table 4-5 for the cumulative data for the FTP tests separated by FFV. The comparisons show high correlations between the sample and exhaust flow, with all three PFDs having R^2 values > 0.99 for both the FTP and US06 with a 95% confidence interval (95% CI) of 0.002. For this correlation, the standard error estimate (SEE), which is measure of the data spread between the exhaust and sample flows, divided by the average exhaust flow (Gext_mean) and the correlation intercept (b) divided by the maximum

sample flow (Gp_max) represent different measures of the quality of the PFD proportionality. The quality of the PFD proportionalities (as represented by SEE/Gexh_mean and b/Gp_max) were very similar for all tests and all FFVs utilized. All PFDs showed an average SEE/Gexh_mean and b/Bp_max of 0.04% and 0.03%, respectively, for the 100 cm/s FFV tests. The FTP tests with an FFV of 130 cm/s had similar SEE/Gexh_mean and b/Bp_max values.

Table 4-5: Comparison of PFD measurements to PFD A by test and phase (FFV = 100, n = 6)

Test	Statistic	PFD A		PFD B		PFD C		Overall	
		ave	95% CI	ave	95% CI	ave	95% CI	ave	95% CI
FFV_100 n = 6	R2	0.998	0.002	0.999	0.001	0.998	0.003	0.998	0.002
	SEE	0.010	0.014	0.006	0.003	0.005	0.028	0.007	0.014
	SEE/Gexh_mean	0.04%	0.04%	0.03%	0.05%	0.01%	0.06%	0.03%	0.05%
	SEE/Gexh_max	0.01%	0.01%	0.01%	0.01%	0.00%	0.01%	0.01%	0.01%
	b	0.0003	0.0017	0.0002	0.0009	0.0007	0.0036	0.0004	0.0017
	b/Gp_max	0.02%	0.10%	0.03%	0.12%	0.04%	0.21%	0.03%	0.11%
FFV_130 n=3 [1]	R2	0.998	0.001	0.997	0.004	0.998	0.002	0.998	0.002
	SEE	0.010	0.007	0.012	0.013	0.000	0.000	0.007	0.014
	SEE/Gexh_mean	0.06%	0.08%	0.08%	0.13%	0.00%	0.00%	0.05%	0.09%
	SEE/Gexh_max	0.01%	0.03%	0.02%	0.04%	0.00%	0.00%	0.01%	0.03%
	b	0.0001	0.0005	0.0006	0.0011	0.0000	0.0008	0.0002	0.0008
	b/Gp_max	0.01%	0.04%	0.05%	0.10%	0.00%	0.09%	0.02%	0.07%

[1] Standard error estimate (SEE) is a measure of data spread about the correlation between exhaust flow and sample flow, Gexh_mean is the average exhaust flow, Gexh_max is the maximum exhaust flow, b is the intercept for the correlation between sample flow and exhaust flow, and Gp_max is the maximum sample flow.
[2] Averages (ave) and 95% confidence intervals (95% CI) are based on averages of FTP Ph 1, Ph2, Ph3, and US06 test cycles. Overall ave and 95% CI is based on the average results of PFD A, B, and C listed in Table 4-5.
[3] Data includes the U06 outlier test discussed later in the report (note all the US06 tests were valid from a PFD operational perspective so the outlier was a result of other influences).

Although all PFDs were operating consistently and with highly correlated proportionality flow, there was some data that showed a poor correlation at high exhaust flow rates for PFD_C for the US06 cycle. The observation did not impact the overall proportionality statistics or its performance so this may just be an observation for future

consideration. Deeper analysis shows that at 50 slpm sample flows, the pressure at the filter face reduced from 98 kPa to 67 kPa, which resulted in a change in FFV from 100 cm/sec to 132 cm/sec. One observation is that at sample flows of 50 slpm the low filter face pressure could be a result of a high pressure drop from a 0.15 inch ID sample probe. The FTP tests did not show the same issue due to the lower peak sample flow rates.

4.3.3.2 PM emission rates for PFD side-by-side tests

The PFD and CVS PM mass emission rates are presented in Figure 4-4 for each FTP test and in Figure 4-5 for each US06 test. The PM emission rates presented are based on current 40 CFR Part 1066 calculations for PFDs and CVSs for sample weighting onto a single filter. Also included were correction factors for tunnel blanks, CVS flow corrections, and raw sample flow corrections. Additionally, the CVS flow (Vmix) was corrected for raw exhaust removed prior to the CVS by the PFDs. In general, the combined flow corrections represented more than 5%, but less than 10% of the Vmix.

The PM emission rates show significant test-to-test variability for both the FTP and US06 tests. The FTP emissions varied from 1.15 mg/mi to 1.84 mg/mi for CVS_A, with all PM samplers generally showing similar trends for a given test. The US06 PM emission rates for CVS_A varied from 1.64 to 0.40 mg/mi for tests #2 through #6, but showed a much higher emission rate of 4.35 mg/mi for test #1.

For the US06 test sequence, the first test was an outlier both in terms of the observed PM mass emission rates as well as in comparing the bias between the CVS and the three PFDs, which impacted the overall mean t-tests analysis. The first US06 test value was more than two times higher than the average of the other test points and was three times higher

than the standard deviation of tests two through six (i.e., a statistical outlier from the mean). High PM emissions for the first US06 test after the vehicle has not been tested or ran over a long span of time have been seen in other studies [79]. Xue et al. reported greater sensitivity of gravimetric method to more aggressive US06 cycle than FTP cycle [48]. It is speculated the PM mass on this first test may have been influenced by PM desorption from the tailpipe and transfer line. The fact that CVS PM showed the highest PM emission among all of the PM samplers suggests that there was desorption from the CVS wall as well. Since the first US06 test affected the mean significantly, is a statistical outlier, and may have been impacted by contamination. The first US06 data point was omitted from the analysis in this section.

The average FTP and US06 PM emission rates for each of the individual samplers for the different tests are presented in Figure 4-6, where the error bars represent one standard deviation. The average FTP PM emission rate varied for different samplers from 1.21 mg/mi to 1.49 mg/mi at FFV = 100 cm/s, from 1.02 to 1.29 mg/mi at FFV = 130 cm/s, and from 1.34 to 1.63 mg/mi for the US06 tests. Note PFD_C did not operate at the higher FFVs, so its data may not be as comparable to the other PFDs at FFV=130 cm/s. The error bars between the FTP and US06 tests were similar.

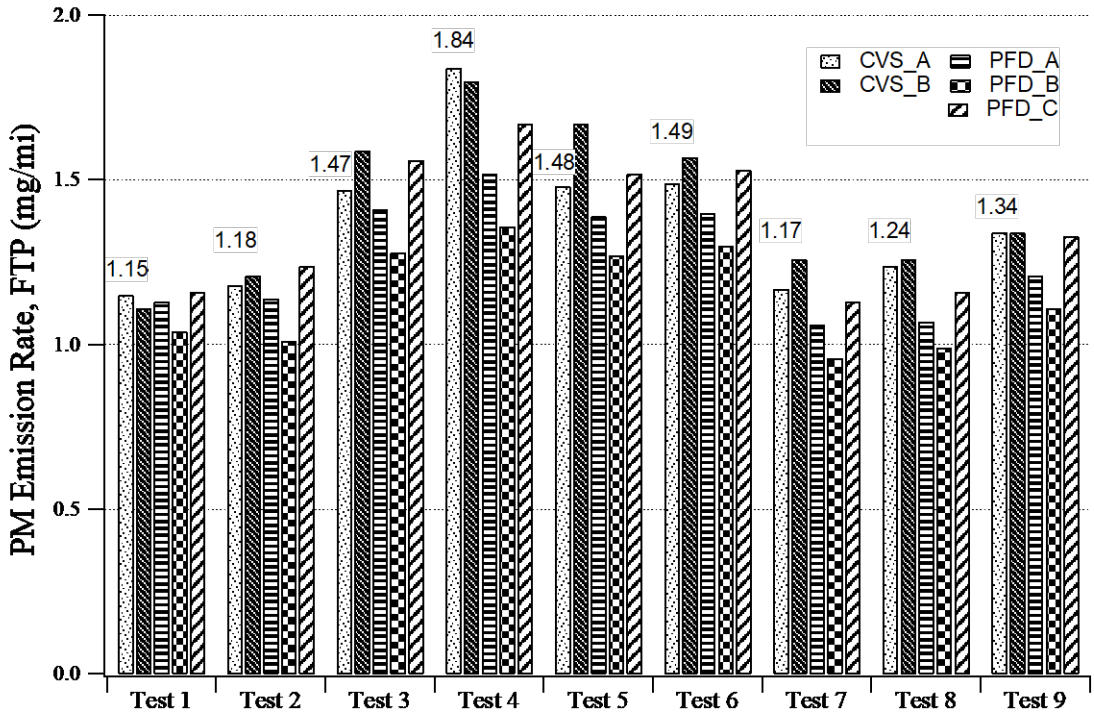

Figure 4-4: PM Emission Rates for PFD and CVS Measurements over the FTP

[1] CVS_A is the CVS combined flow weighted PM sampler and CVS_B is the by phase PM sampler. The CVS flow weighting was performed by varying the FFV. The FFV for CVS_B was 100 cm/s, and the FFV for CVS_A was nominally 100 cm/s for bag 2 with appropriate flow weighing for the other bags. All the PFD samplers utilized a single filter with sample flow weighting (i.e., the sample fraction was varied by phase). PFD A and PFD B utilized nominal FFVs of 100 cm/s for the first six FTPs and 130 cm/s for the final three FTPs. PFD_C was operated at 100 FFV for all tests because the system could not maintain flow stability at 130 FFV.

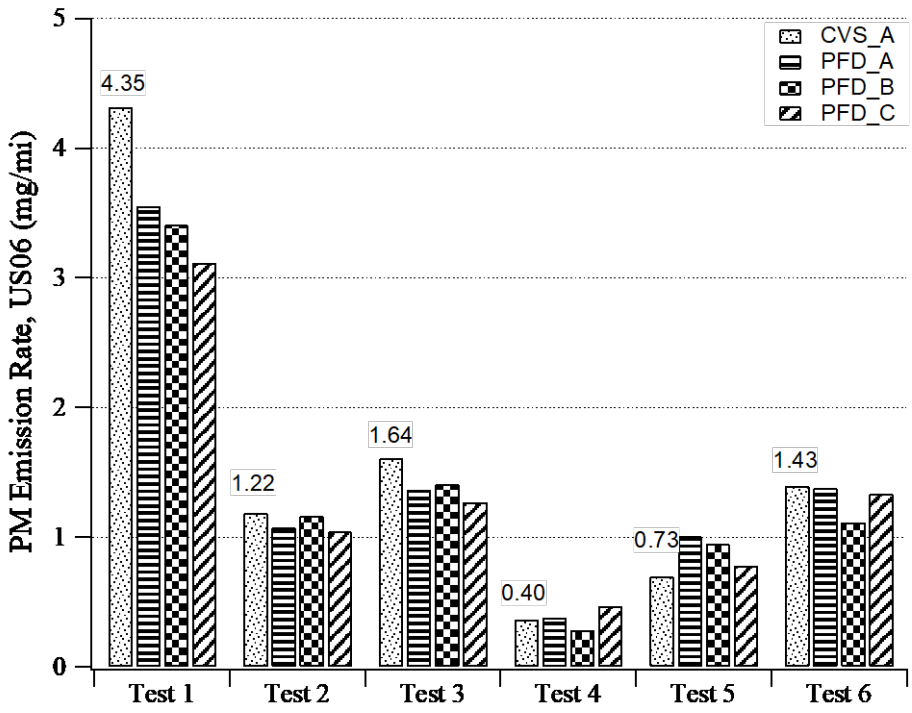

Figure 4-5: PM Emission Rates for PFD and CVS Measurements over the US06

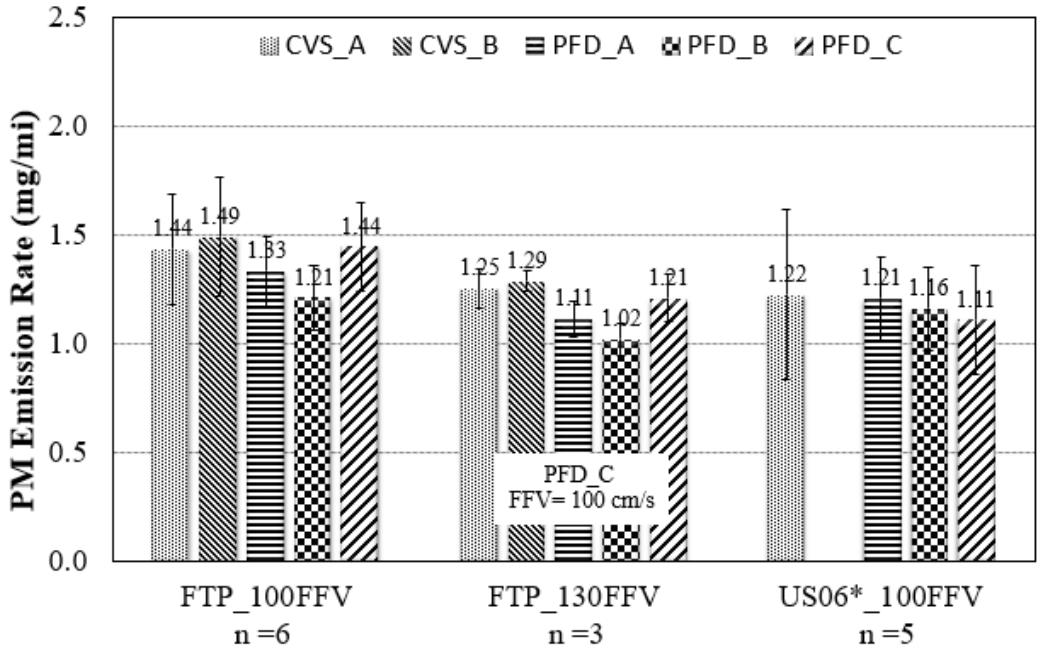

Figure 4-6: Average PM Emission Rates for PFDs and CVS Measurements

CVS_A is the CVS combined flow weighted PM sampler and CVS_B is the by phase PM sampler. The CVS flow weighting was performed by varying FFV for each phase of the FTP phases. All the PFD samplers utilized a single filter with sample flow weighting (i.e.: the sample fraction was varied by phase). PFD_C was operated at 100 FFV for all tests because the system had an issue with flow stability at 130 FFV.

4.3.3.3 T-test and f-test statistics for PFD side-by-side tests

The average, relative percentage difference, and paired two tailed t-test statistics for the different PM samplers for the PFD side-by-side tests for both the FTP and US06 tests are presented in Table 4-6, where CVS_A was used as the basis for all the comparisons. The two CVS PM probes (A and B) both agreed well for the FFV = 100 cm/s (within 3.8%) and FFV = 130 cm/s tests (within 2.9%), where the t-test p-values (0.2 and 0.4) indicate the means are not statistically different (Table 4-6). The lack of differences in

averages for the CVS PM measurements suggests the single filter combined method is in good agreement with the individual filter method by phase [15].

The PFD probes showed a mixed comparison relative to the CVS_A probe. PFD_A showed a relative difference of around -7% at FFV = 100 and -11 % at FFV = 130 for the FTP tests and –0.7% for the US06 tests, see Table 6. When all the tests were pooled together, the relative difference was -8.4%. The paired two tailed t-test suggests the means were statistically or marginally statistically different with all the data pooled together (p-values = 0.005), for FFV = 130 (p-value = 0.02), and for FFV = 100 cm/s (p-value = 0.069, or marginally statistically significant), but not for the US06 tests (p-value = 0.94). PFD_B also showed statistically different means (p-values: < 0.02) for all the FTP tests (p-value = 0.000), but not the US06 (p-value = 0.52). For PFD_B, the relative differences were -15.6%, -18.6%, and -6.2% for the FTP_100, FTP_130, and US06 tests, respectively. PFD_C showed the lowest relative error compared with CVS_A for the FTP tests, with the percent difference varying from ±0.6% (FFV = 100 cm/s and all data pooled together). As for the US06 tests, PFD_C showed a -6.7% compared to CVS_A. In all cases, the differences between CVS_A and PFD_C were not statistically different. All the US06 tests showed a negative bias, but the t-test suggests the mean differences were not statistically significant. The F-test results show no statistically significance (all p-values > 0.24) between any of the PFDs and the CVS_A probe, suggesting there was no difference in the testing variability between the different PM measurements

Table 4-6: PFDs Comparison for all test cycles at FFV = 100 cm/s and FFV=130 cm/s.

Description	Sample	FFV	CVS_A	CVS_B	PFD_A	PFD_B	PFD_C
FTP - ave (mg/mi)	4	100	1.44	1.49	1.33	1.21	1.44
FTP - % dif	4	100	--	3.8%	-7.2%	-15.6%	0.6%
FTP p-value	4	100	--	0.188	**0.069**	**0.008**	0.818
FTP - ave (mg/mi)	3	130	1.25	1.29	1.11	1.02	1.21
FTP - % dif	3	130	--	2.9%	-11.2%	-18.6%	-3.4%
FTP p-value	3	130	--	0.353	**0.016**	**0.003**	0.160
FTP - ave (mg/mi)	9	varies	1.37	1.42	1.26	1.15	1.37
FTP - % dif	9	varies	--	3.5%	-8.4%	-16.5%	-0.6%
FTP p-value	9	varies	--	0.088	**0.005**	**0.000**	0.759
US06 - ave (mg/mi)	5	100	1.05	--	1.04	0.99	0.98
US06 - % diff	5	100	--	--	-0.7%	-6.2%	-6.7%
US06 P-Values	5	100	--	--	0.94	0.52	0.44

[1] p-values calculated from paired two tail t-test.

Additional analyses were also performed to evaluate differences between the PFDs themselves. All the PFD's showed low p-values (<0.05) for the pair t-tests between each of the other PFDs. This suggests the means were statistically different between each of the PFDs. Overall, the spread between the different PFDs was on the order of 16%. The F-tests also showed there were statistically significant differences in testing variability between each of the PFDs.

4.3.3.4 Bias and contamination discussion

The average FTP CVS versus PFD percent difference was -8.5% with all the PFDs averaged together, although differences of up to 18.6% were seen for some PFD/test combinations. In a previous study, Xue et al. [48] found that, in general, there were no statistically significant PM emissions differences for 4-bag FTP or US06 tests for a lower PM source vehicle with a FTP PM emission rate of ~0.1 mg/mi. For a higher PM source vehicle, with an FTP emission rate of ~2.0 mg/mi, mean emissions showed a low relative

error rate of between -2.7% and -5.9% between a PFD (DF=5 FFV=150) and a CVS system. Foote et al. compared two PFDs with CVS PM emission measurements for two gasoline vehicles with a range of PM emissions from 0.1 to 10.0 mg/mi [34]. The correlations between the CVS and the two PFD PM emissions had slopes of 1.03 and 0.74, respectively, indicating good measurement accuracy for one of the PFD systems while the other PFD showed a negative bias relative to the CVS. PM mass emission rate comparisons for PFDs as part of the E-66 showed more mixed results depending on the PM emission level [43]. At PM levels comparable to 10% of the 2007 PM standard for on-highway heavy-duty engines, some PFDs showed PM emissions that were not statistically different from those measured by the CVS system, while other systems showed results that ranged from 50 to 75% lower to as much as 3 times higher. At higher PM levels comparable to 80% of the 2007 PM standard for on-highway heavy-duty engines results were more varied, with some PFD/test condition combinations providing PM emissions within 10-20% of the CVS, but many other PFD test condition combinations showing differences with the CVS ranging from 30% to up to 2.5 times higher. some PFDs showed PM emissions that were not statistically different from those measured by the CVS system, while other systems showed results that ranged from 50 to 75% lower to as much as 3 times higher.

The differences between the CVS and PFD PM mass emissions could be due to attributed to several factors. Differences in tunnel blank values between the CVS and PFDs suggest that there could be some background contamination from the transfer line and CVS tunnel that could be influencing the CVS PM emission rate. This could have a significant

impact at the low PM mass levels and filter weights seen in this study. As discussed above, the background corrections for the CVS probes A and B were 11 µg, compared 3 to 5 µg for the PFDs. Further details regarding the tunnel blank tests are in the supplemental material. For comparison, if a 13 µg was assumed for the tunnel blank of CVS tunnel, this would change the overall FTP comparison from -8.5% to -0.2%. The potential impacts of tunnel contamination were investigated more extensively in a separate study that will be presented in future paper. It is also possible the dynamics of the proportional sampling in measuring transient emissions could be more complicated for PM than for the simpler EFM and PFD proportionality experiments discussed in section 4.3.1. Although PFD CO_2 emission rates were found to be within 5% of the CVS CO_2 for all tests discussed in section 4.3.1.1, larger differences might be seen for more transient pollutant emissions such as PM. Additionally, this test was only conducted for PFD_A. In the E-66 study, it was found that when the residence time, dilution ratio, and dilution air temperature of a PFD were better matched with that of the CVS that differences in PM emission results could be reduced significantly, suggesting that PM differences could be related to multiple different operating parameters. Overall, additional tests will be needed to better evaluate the sources of error contributing to the differences between the CVS and PFD PM mass emission rates.

4.4 Summary and Conclusions

As progressively more stringent PM standards are being put in place for LDVs, there has been an increased emphasis on evaluating and improving the accuracy of PM measurements at low concentrations. The purpose of this study is to compare commercially available PFDs, both unit-to-unit and against a CVS tunnel, particularly with regards to

their ability to provide reproducible measurements at very low PM emission levels. This program focused on evaluating the capabilities of commercial PFDs to meet LEV III/Tier 3 PM emission measurement requirements. The comparisons included an EFM comparison and calibration check, a PFD sample proportionality evaluation, and a side-by-side comparison of PFDs for FTP and US06 emission tests.

Separate evaluations were done for the EFMs and PFDs. An evaluation of CO_2 emissions determined from EFM calculations and the CVS showed that differences between the EFM and CVS CO_2 emissions rates were 2.0% or less for all EFM/test configurations, except for the bag 2 comparisons for EFM A and B. Proportionality checks for all the PFDs showed very good control of proportionality, easily meeting the CFR 1066 and 1065 requirements for all tests performed. The biases in the PFD setup were generally within 0.1% for configured parameters, with the highest difference being 0.4%. Differences in exhaust flow and sample flow were larger at around 1%, but the biases were generally in the same direction so that it did not have a significant impact on the extraction ratio, which would be the main contribution to bias in the PM emission rates.

The side-by-side PFD emission test comparisons showed different results depending on the PFD and the test cycle. PFDs and CVS emission rates had relative PM emission rate differences between -16.5% to -0.6%. The average PM emission rate difference of all PFDs in comparison to the CVS was -8.5% for all nine FTP tests, which is a slight improvement from Foote study [34]. The means were statistically different for two of the PFDs based on the paired 2-tailed t-test, but not for the third PFD. As for the US06 tests, the PFDs and the CVS had difference in the ranged of -6.7% to -0.7%, and

were not statistically different. The differences between the CVS and PFDs could be due to a number of different factors, including potential tunnel contamination, the dynamics of the proportional sampling in measuring transient emissions, or other differences in operating parameters, such as residence time, dilution ratio, and dilution air temperature. The study also found that tunnel blanks had a significant impact on the PFD comparison. An estimated CVS tunnel blanks of 11 µg was used in this study, which exceeded the 5 µg limit allowed by CFR 1066. If 13 µg tunnel blank for the CVS tunnel was assume instead, it would change the overall FTP comparison from -8.5% to -0.2%. One of the advantages of using PFDs at LEV III of 1 mg/mile is that they have the potential to reduce adsorption of artifacts, which can be significant at that emission level.

5 Appendix

5.1 EFM Calibration

EFM accuracy over the range of operation may be subject to relatively large uncertainties. Prior to the main testing, a calibration check test was done to evaluate the accuracy of all three EFM's over the range of flows expected for the selected test vehicles under the controlled laboratory conditions. For this test, each of the three proposed EFMs were sent to an accredited flow calibration laboratory for accuracy and linearity verification. The laboratory utilized for this testing was Dick Munn's Co. of Los Alamitos, CA. Each EFM had a minimum of 15-point calibration using ambient air at 20oC. The calibration was planned for the following test points of 0, 2, 4, 6, 8, 10, 20, 30, 40, 50, 60, 70, 80, 90, 100 SCFM, with the 100 SCFM was selected based on the anticipation that this would be representative of flow that would be seen for the US06 cycle. Additional calibrations were also run at a few other flow rates, with the highest calibration flow rate being 300 SCFM. It should be noted that some tests were also performed on the chassis dynamometer to evaluate the stability of the EFMs under steady state emissions, and to use a carbon balance method to compare the performance of different EFMs with a CVS system. The PFD and EFM CO2 mass emissions compared to the CVS CO_2 emissions were within 2.0% for the LA4 bag-1 and within 5.0% for bag-2. These results are discussed in greater detail in the supplemental material.

The results of regression analyses for the calibration check by the certification laboratory are provided in Table S1. From the calibration check by the certification laboratory and regression analysis, the EFMs all showed good correlations over the steady

state flow rate range examined with this calibration. The slopes of the regression lines were 0.98, 0.99, and 1.00, respectively, for EFM_A, EFM_B, and EFM_C and all the R2 values were equal to 1.00. EFMs A, B, and C showed higher relative errors at exhaust flows below 5 scfm (low flow operation) ranging from -5% to 30%. This suggests low flow operation (for the tested EFMs) may result in a positive bias for EFM_A and B with a mixed bias for EFM_C. EFM_A and EFM_B showed similar single standard deviations (1σ) over all the points with the average 1σ for EFM_B (0.37 scfm) being slightly lower than EFM_A (0.54 scfm). EFM_C showed the highest 1σ of 1.0 scfm, and for flows below 30 scfm the 1σ was 1.35 scfm, with EFM_D having a lower slightly lower 1σ at 0.75 on average. The higher standard deviation may be a result of the measurement principle differences, where C and D both used pressure for their measurement and EFM A and B used the speed of sound.

Table S1. Calibration Table for all three EFMs

Target	Std	EFM A			Std	EFM_B			Std	EFM_C		
	Actual	Indicated	Actual Error	Relative Error	Actual	Indicated	Actual Error	Relative Error	Actual	Indicated	Actual Error	Relative Error
SCFM	SCFM	SCFM	SCFM	(%)	SCFM	SCFM	SCFM	(%)	SCFM	SCFM	SCFM	(%)
0	0.000	0.000	0.000	0.000	0.000	0.000	0.000	0.000		0.000	0.000	0.000
1	1.00	1.21	0.210	21.0	1.00	1.30	0.300	30.0	0.998	0.953	-0.0450	-4.51
2	2.00	2.06	0.060	3.00	2.00	2.22	0.220	11.0	2.00	1.91	-0.0950	-4.75
3									3.00	3.14	0.145	4.84
4	4.00	3.95	-0.050	-1.25	4.00	4.52	0.520	13.0	4.01	4.56	0.550	13.7
5	5.00	4.92	-0.080	-1.60	5.00	5.30	0.300	6.00				
6	6.00	5.97	-0.030	-0.500	6.00	5.98	-0.0200	-0.333	6.00	6.36	0.359	5.99
7	7.00	6.92	-0.080	-1.14	7.00	7.04	0.0400	0.571				
8	8.00	7.68	-0.320	-4.00	8.00	8.05	0.0500	0.625	8.01	8.30	0.288	3.60
9	9.00	8.82	-0.180	-2.00	9.00	9.11	0.110	1.22				
10	10.0	9.78	-0.220	-2.20	10.0	10.1	0.120	1.20		10.5	0.453	4.53
20	20.0	19.6	-0.360	-1.80	20.0	19.9	-0.150	-0.750	20.0	20.1	0.144	0.721
30	30.0				30.0	29.7	-0.270	-0.900	30.0	29.6	-0.376	-1.25
40	40.2	39.5	-0.72	-1.79								
46									46.0	45.3	-0.717	-1.56
50					50.0	49.6	-0.450	-0.900				
60	60.2	59.1	-1.08	-1.79	60.0	59.6	-0.400	-0.667				
74									74.0	73.8	-0.231	-0.312
80	79.7	78.1	-1.56	-1.96	80.1	79.3	-0.850	-1.06				
90	90.3	88.8	-1.50	-1.66	89.8	89.0	-0.820	-0.913				
100	100	98.7	-1.34	-1.34	100	99.3	-0.880	-0.878	100	97.8	-2.47	-2.46
115									116	115	-0.957	-0.826
165									164	167	2.47	1.50
170	171	169	-2.70	-1.58								
230									229	228	-0.734	-0.320
295									294	295	1.89	0.643
300	301	295	-5.72	-1.90	299	297	-2.00	-0.670				

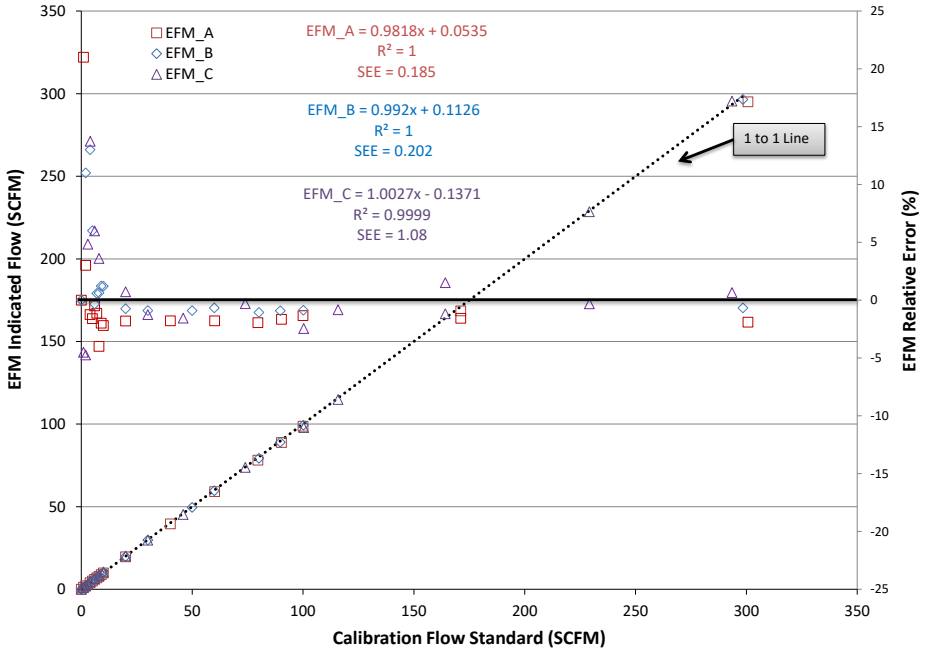

Figure S1. Steady state EFM flow correlation and relative error from 0 to 350 SCFM.

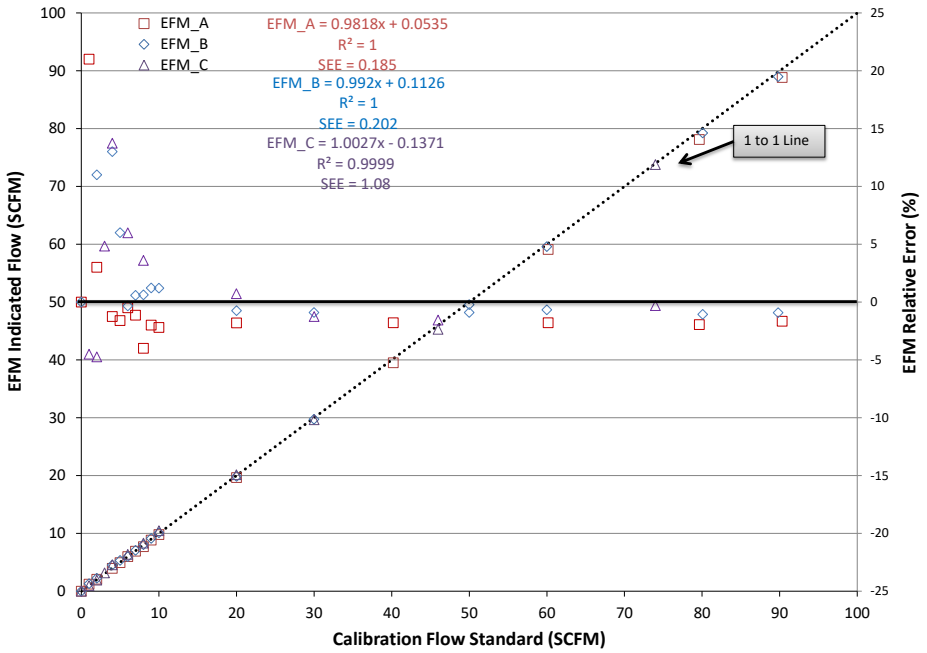

Figure S2. Steady state EFM flow correlation and relative error from 0 to 100 SCFM.

5.2 Vehicle steady state tests

Real-time EFM measurement noise can impact the performance of the PFD which depends on fast and accurate proportional control of an EFM. Figure S3 shows how this noise can affect the measurement during an emission test. Given the importance of measurement noise, UCR designed an additional test with a test vehicle's exhaust under steady state cruise conditions. The goal of these tests was to quantify the standard deviation of each EFM under low flow conditions, which is similar PFD comparison tests. The exhaust flow was measured at various steady state vehicle speeds ranging from engine-off, idle, and up to 60 mph with each EFM connected between the vehicle and the CVS. For speeds above 30 miles per hour, the cruise control was used to minimize driver influence on exhaust flow, while for speeds below 30 miles per hour the cruise control was not available so the vehicle speed was manually maintained by the driver. Data was collected for approximately two minutes at each speed. The noise was calculated by using a single standard deviation (1σ) for 30 samples. Only the last 30 seconds of exhaust flow data was used in the flow analysis unless the vehicle speed was unstable where the average was taken (just before the end of the test period).

Early results showed EFM_C had the higher noise than the other two EFMs. The purpose of this study was to consider PFDs under "best possible conditions". The EFM_C system upgraded their EFM with a small capillary tube to minimize pressure fluctuations in the measurement of the differential pressure. The as received system is referred to as the "noCap" flow system and the modified system (with the installed capillaries) is referred to as the "w/Cap" system for the remainder of this report.

The single standard deviation (noise) results are presented in Table S2 and the real-time data in Figure S3 shows results for each test. Figure S3 also shows the real-time results for EFM_D, which was a new EFM available on the market and was added to the study for EFM and PFD comparisons. The results are presented at each of the vehicle speeds (from engine off to 60 mph). At idle the nominal exhaust flow was 4 scfm and at 60 mph the nominal exhaust flow was 27 scfm. A few points in Table S2 are grayed out because of the variability in maintaining good vehicle speed control. It is suggested these measured standard deviations are not a result of the EFM performance, but due to the driver performance.

EFM_A and EFM_B showed similar single standard deviation (1σ) over all the points with EFM_B (0.37 scfm) average 1σ being slightly lower than EFM_A (0.54 scfm), see Table S2. EMF_C showed the highest 1σ where on average it was 1.00, and for flows below 30 scfm the 1σ was 1.35 scfm with EFM_D just slightly less at 0.75 on average. The higher standard deviation may be a result of the measurement principle difference where C and D both use pressure for their measurement where EFM A and B use sound. Note due to the real vehicle exhaust test, the 1σ reported here may be higher than that found at a certification flow laboratory, but these data are more representative of emissions testing and partial flow control interrelationships.

Table S2. Steady State Flow Measurements and Standard Deviation

EFM	Vehicle (mph)	Engine Off	Idle	5	10	20	31	40	50	60	Avg.
	Nominal Flow Rate (SCFM)	0	4	7	8	11	14	15	20	27	
A	Speed Stdev (mph)	0.15	0.14	0.16	0.52	0.44	0.16	0.24	0.17	0.21	0.18
	Flow Stdev (SCFM)	0.12	0.15	0.16	1.4	2	0.23	0.22	0.26	0.35	0.21
B	Speed Stdev (mph)	0.14	0.13	0.15	0.17	0.26	0.19	0.26	1.2	0.29	0.18
	Flow Stdev (SCFM)	0.02	0.29	0.36	0.45	0.79	0.19	0.22	0.49	0.5	0.30
C w/cap	Speed Stdev (mph)	0.14	0.13	0.18	0.31	0.22	0.18	0.21	0.16	0.18	0.17
	Flow Stdev (SCFM)	**0.71**	**1.0**	**1.1**	1.4	**2.6**	**1.1**	**0.9**	**0.41**	0.21	**1.00**
D	Speed Stdev (mph)	0.12	0.15	0.15	0.17	0.22	0.14	0.11	0.15	0.14	0.15
	Flow Stdev (SCFM)	0.05	**1.7**	**0.70**	**1.3**	**1.1**	**0.73**	**0.64**	**0.43**	0.26	**0.75**

1 The black text are values that are within the average of the other PFDs, the greyed out text is when the vehicle speed wasn't stable and thus the data was not used in the comparison. The red and blue text represents a high outlier and moderate outliners from the rest of the values.

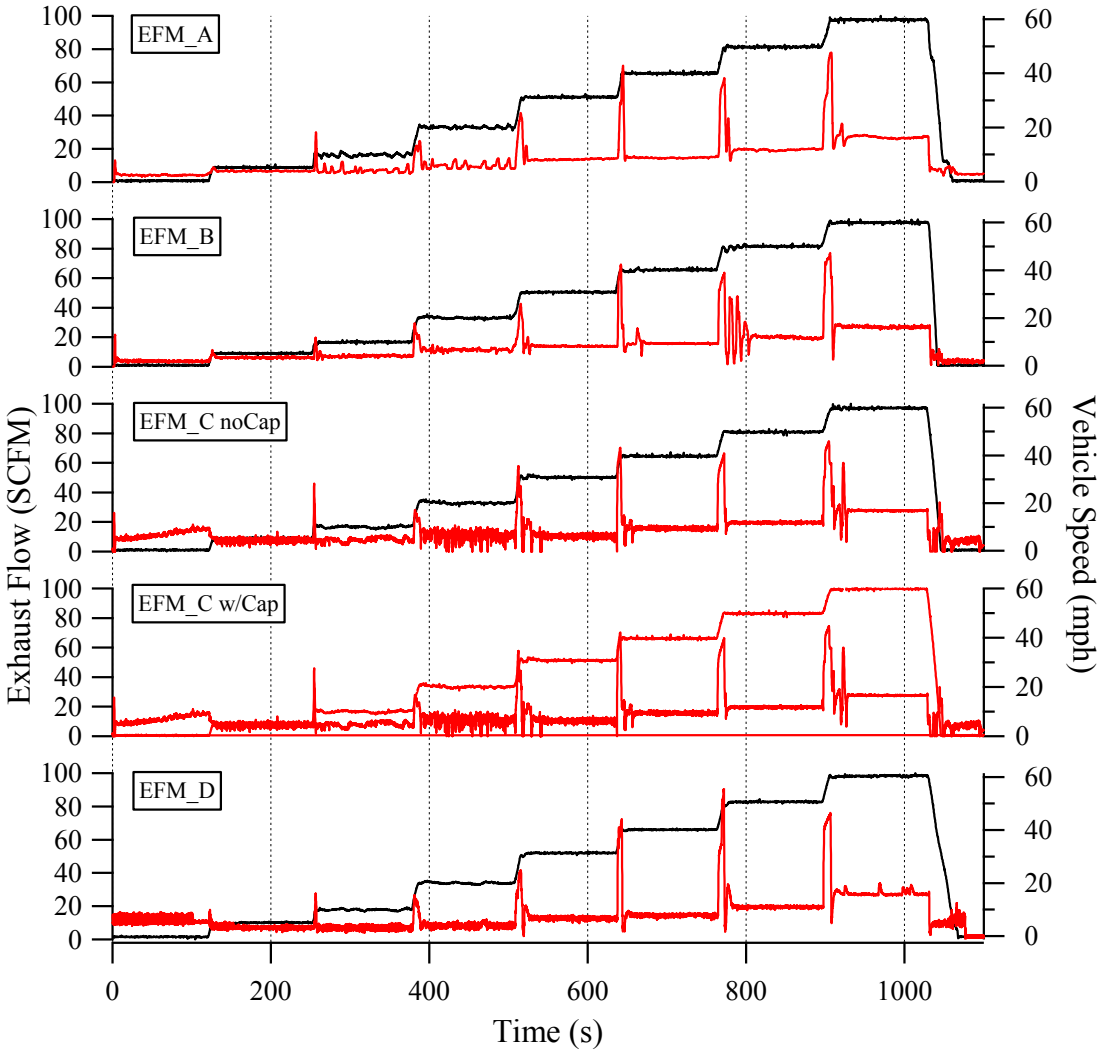

Figure S3. Steady State Test

Table S3. CO2 Mass emission EFM comparisons to the dilute CVS

EFM	Phase 1					
	Raw (g)	Dilute		Raw vs	Raw vs	Dilute M.
		Modal (g)	Bag (g)	Bag	mDilute	Dil Bag
A	953	970	954	0.1%	-1.8%	1.7%
A	957	972	948	1.0%	-1.5%	2.5%
A	942	957	948	0.6%	-1.6%	1.0%
B	928	922	908	2.3%	0.6%	1.6%
B	924	921	889	4.0%	0.3%	3.6%
B	915	909	889	2.9%	0.6%	2.3%
C	937	956	922	1.6%	-2.0%	3.7%
C	958	968	925	3.5%	-1.1%	4.6%
C	947	965	925	2.4%	-1.8%	4.3%

Table S4: CO2 Mass emission EFM comparisons to the dilute CVS

EFM	Phase 2					
	Raw (g)	Dilute		Raw vs	Raw vs	Dilute M.
		Modal (g)	Bag (g)	Bag	mDilute	Dil Bag
A	1208	1171	1172	3.1%	3.1%	0.0%
A	1223	1181	1174	4.2%	3.5%	0.6%
A	1219	1177	1174	3.8%	3.5%	0.3%
B	1141	1088	1086	5.1%	4.9%	0.2%
B	1153	1116	1091	5.7%	3.3%	2.3%
B	1149	1097	1091	5.4%	4.8%	0.5%
C	1174	1207	1167	0.6%	-2.8%	3.5%
C	1174	1210	1164	0.9%	-3.0%	4.0%
C	1150	1201	1164	-1.1%	-4.2%	3.2%

5.3 LFE and PFD Correlation

Correlation plots between the PFD calculated sample flow rates and the LFE measured flow rate are shown in Figure S4-S6 for PFD_A, PFD_B, and PFD_C, respectively. In Figure S7-S9, the LFE is compared to the exhaust flow for an evaluation of the PFD's proportionality. All of the plots represent the data where the flow rate was

less than 21 slpm which is the point where the LFE over ranges. The correlation of the LFE sample flow and the exhaust flow showed an R2 that varied from 0.997, 0.990, and 0.993 for PFD_A, PFD_B, and PFD_C, respectively. In summary the correlation of sample flow and exhaust flow show that PFD systems are accurate, proportional, and responsive.

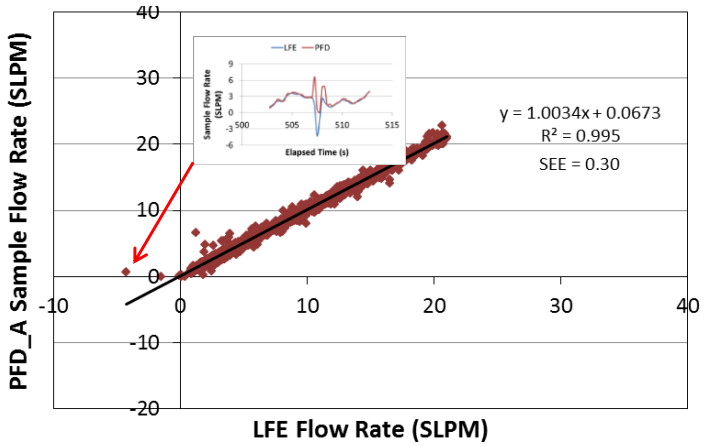

Figure S4. Correlation Plots for LFE and PFD_A Sample Flow Rates below 21 LPM

1 Data is based on 4Hz sampling and based on a single LA4 test cycle (true for the next three cycles) n=5,500.

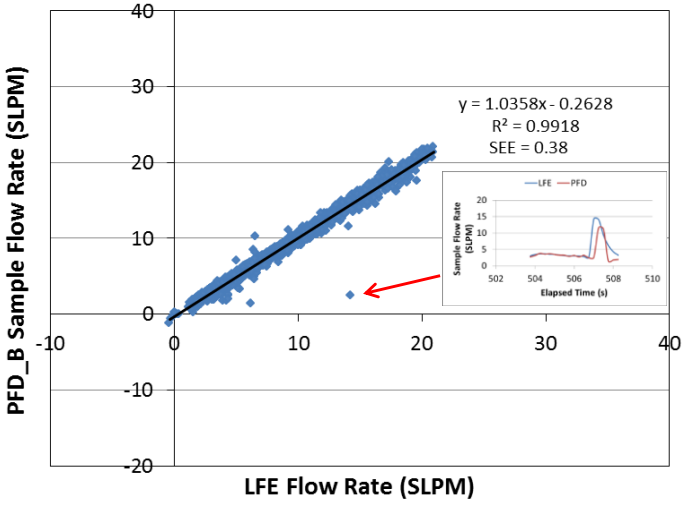

Figure S5. Correlation Plots for LFE and PFD_B Sample Flow Rates below 21 LPM

1 Data is based on 4Hz sampling and based on a single LA4 test cycle n=5,500.

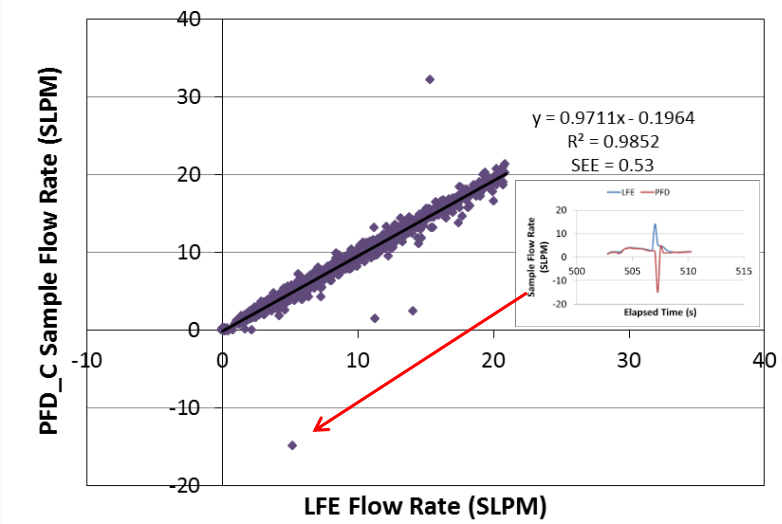

Figure S6. Correlation Plots for LFE and PFD_C Sample Flow Rates below 21 LPM

1 Data is based on 4Hz sampling and based on a single LA4 test cycle n=5,500.

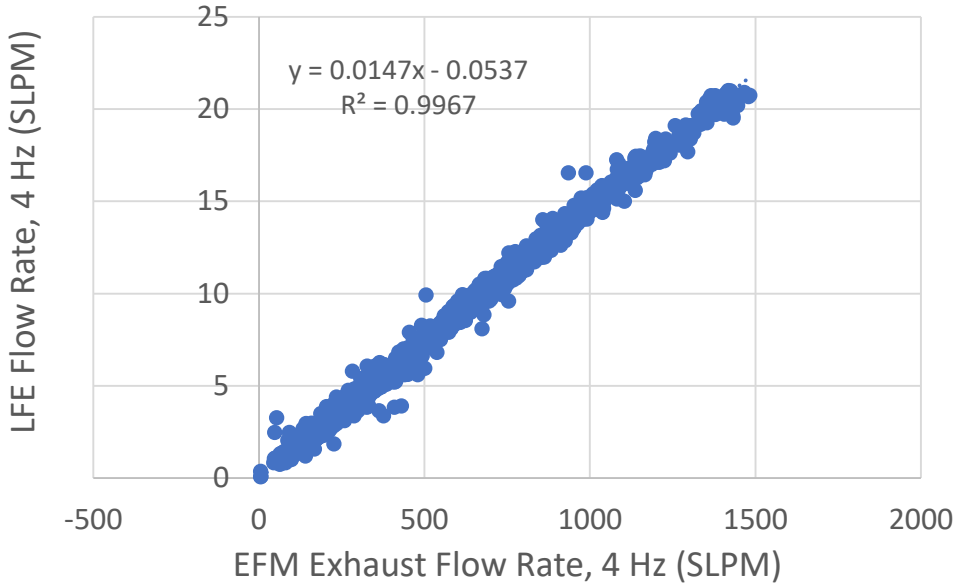

Figure S7. Correlation Plots for LFE sample flow < 21 slpm and PFD_A exhaust flow

1 Data is based on 4Hz sampling, a single LA4 test cycle n=5,497, (data under 0.5 slpm removed, and all PFDs used the same EFM_A.

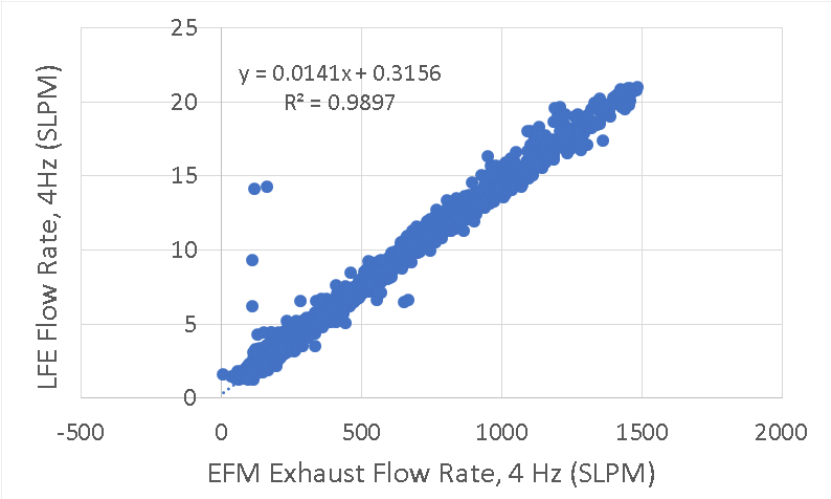

Figure S8. Correlation Plots for LFE sample flow < 21 slpm and PFD_B exhaust flow

1 Data is based on 4Hz sampling, a single LA4 test cycle n=5,497, (data under 0.5 slpm removed, and all PFDs used the same EFM_A.

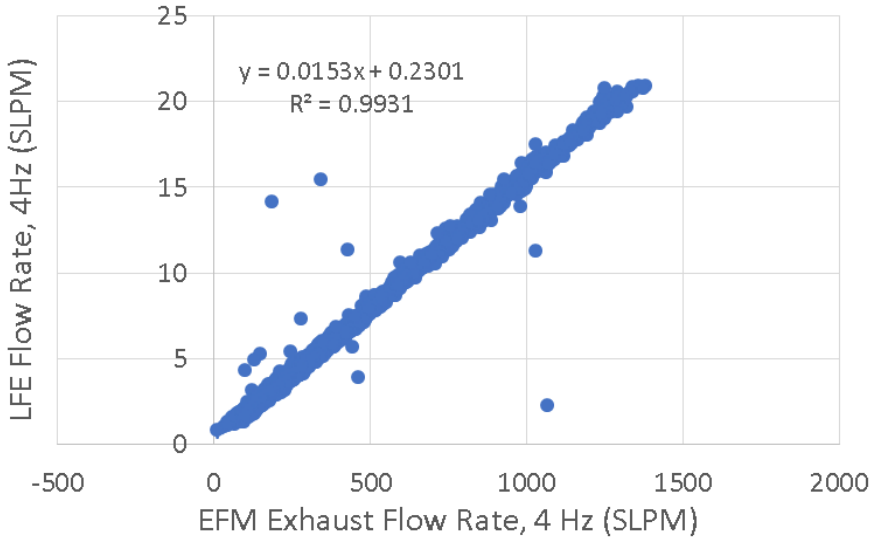

Figure S9. Correlation Plots for LFE sample flow < 21 slpm and PFD_C exhaust flow

1 Data is based on 4Hz sampling, a single LA4 test cycle n=5,497, (data under 0.5 slpm removed, and all PFDs used the same EFM_A

5.4 Extraction ratios for EFM comparisons for the transient vehicle tests

The extraction percentages for each of the EFMs over the LA4 is shown in Figure S10. The noise is denoted by the visible red signal in the figure. EFM_C showed more variability and flow noise than EFM_A or B, which agrees with the measured standard deviation observations from the calibration data and vehicle static tests. In general, EFM_A and B have less or similar noise compared to EFM_C with EFM_A being the lowest of all the EFMs evaluated. It is, however, unclear as to how this would impact the PFDs overall performance. It is also important to note that most of the PM mass is emitted during accelerations from low speed to high speed where exhaust flow is highest and noise contribution is lowest.

Figure S10. Real-time extraction ratio for the LA4 tests conducted with PFD_A and three EFMs

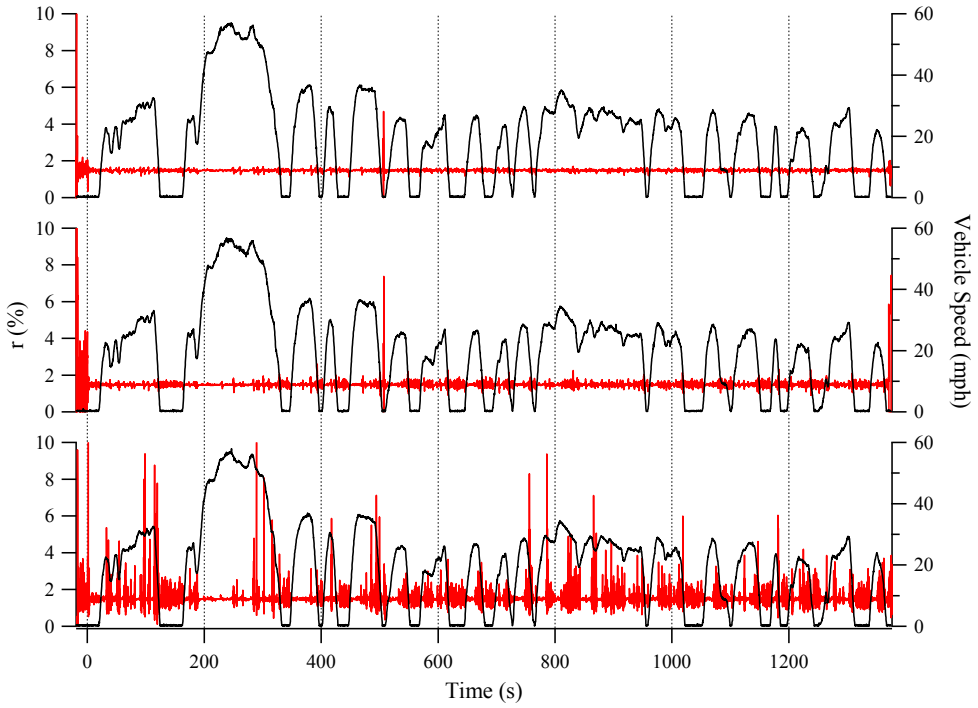

5.5 Tunnel Blanks

Tunnel blanks (TB) were collected during the main testing phases of this study. The tunnel blanks were performed for the two CVS probes (A and B) and the three PFD systems (A, B, and C). The CVS_A probe (the basis of the CVS comparison) showed a high TB during the comparison study and varied TB for the contamination study (varied from 0.016 to 0.003 mg). The CVS_B probe (which sampled by phase thus has 3 to 4 filters) showed a similar trend between the tasks. The PFDs all showed lower tunnel blank values where PFD_A was the lowest overall and PFD_B was the highest. During the contamination testing, the CVS went through a one-hour long NG burner PM removal process where the transfer line and the CVS were maintained at elevated temperatures (transfer line > 250 C and CVS > 50C). Then the CVS was loaded with a high emitting vehicle. The PFD tunnel blanks did not vary much and did not show the same magnitude of PM removal as the CVS

The results presented in this study are based on the testing that occurred after the contamination testing. PFD Comparison tests were to be performed prior to contamination, but due to a software issue with PFD_C, the PFD comparison tests in this study was repeated after the contamination tests. The tunnel blank prior to starting this study repeat was 16 µg. It is believed the tunnel blank would have declined during the testing similar to what was found during before the contamination tests. As such an average CVS TB of 11 µg was utilized, but it is unknown what the best value should be. Note a TB value of 5 creates a bias between CVS Probes A and B, suggesting the 11 is a more reasonable estimate.

Table S5: Tunnel blank results for all PM systems

Date	Task	Test	CVS_A	CVS_B1	CVS_B2	CVS_B3	CVS_B4	PFD_A	PFD_B	PFD_C
9/26/2016	PFD Comparison	1	0.015	0.007	0.001	0.011		0.005	0.006	0.005
8/31/2016	PFD Comparison	2	0.009	0.015	0.009	0.018		0.001	0.010	0.002
10/7/2016	Contamination	1	0.015	0.010	0.014	-0.001	0.008	0.003	0.003	0.003
10/17/2016	Contamination	2	0.005	0.002	-0.001	0.000	-0.002	0.007	0.003	0.003
10/28/2016	Contamination	3	0.003	0.009	0.001	0.004	0.003	-0.001	0.005	0.005
11/23/2016	Contamination	4	0.016	0.006	0.004	0.003	0.002	-0.001	0.005	0.005
11/28 - 12/16	PFD Comparison Repeat	n/a								
Value Used			0.011	0.011	0.011	0.011		0.003	0.005	0.004

References

[1] California Air Resources Board (CARB). The California Almanac of Emissions and Air Quality – 2013 Edition. http://www.arb.ca.gov/aqd/almanac/almanac.htm. Accessed on July 6th, 2016.

[2] U.S. Environmental Protection Agency. National Emissions Inventory (NEI) Air Pollutant Emissions Trends Data. http://www.epa.gov/ttn/chief/trends/index.html. Accessed on July 6th, 2016

[3] Health Effects Institute (HEI). Traffic-Related Air Pollution: A Critical Review of the Literature on Emissions, Exposure, and Health Effects. January 2010

[4] Atkinson, R.; Mills, I.; Walton, H.; Anderson, H. R. Fine particle components and health-a systematic review and meta-analysis of epidemiological time series studies of daily mortality and hospital admission. J. of Exposure Science and Env. Epidemiology. 2014, 1-7

[5] Li, N.; Hao,M.Q.; Phalen, R. F.; Hinds,W.C.; Nel, A. E. Particulate air pollutants and asthmas. A paradigm for the role of oxidative stress in PM-induced adverse health effects. Clin. Immunol. 2003, 109, 250-265.

[6] McCormack, M. C.; Breysse, P. N.; Matsui, E. C.; Hansel, N. N.; Peng, R. D.; Curtin-Brosnan, J.; Williams, D. L.; Wills-Karp, M.; Diette, G. B. Indoor particulate matter increases asthma morbidity in children with non-atopic and atopic asthma. Ann Allergy Asthma Immunol. 2011;106:308-315.

[7] California Air Resources Board (CARB). Estimate of Premature Deaths Associated with Fine Particle Pollution (PM2.5) in California Using a U.S. Environmental Protection Agency Methodology. August 2010.

[8] Dockery, D. W., C. A. Pope, X. Xu, J. D. Spengler, J. H. Ware, M. E. Fay, B. G. Ferris, Jr. and F. E. Speizer. An Association between Air Pollution and Mortality in Six US Cities. New England Journal of Medication,1993, 329: 1753 – 1759

[9] World Health Organization (WHO). Health Effects of Particulate Matter. 2013, Final Report, 20 pages

[10] Health Effects Institute (HEI). Understanding the Health Effects of Ambient Ultrafine Particles. January 2013.

[11] Shah, A. P. et al.. Effect of Inhaled Carbon Ultrafine Particles on Reactive Hyperemia in Healthy Human Subjects. Environmental Health Perspectives, 2008, 116: 375 – 380

[12] U.S. Environmental Protection Agency. National Ambient Air Quality Standards (NAAQS): http://www.epa.gov/air/criteria.html. Accessed on July 20th, 2015

[13] SCAQMD. (2013). Workshop on Draft 2013 SCAQMD Annual Network Plan: South Coast Air Quality Management District.

[14] Barboza, T. (2013). One-fifth of U.S. lives near roads with higher air pollution, LA Times. Retrieved from http://articles.latimes.com/2013/oct/02/science/la-sci-sn-air-pollution-population-traffic-20131002

[15] Violante, F. S., Barbieri, A., Curti, S., Sanguinetti, G., Graziosi, F., & Mattioli, S. (2006). Urban atmospheric pollution: Personal exposure versus fixed monitoring station measurements. Chemosphere, 64(10), 1722-1729.

[16] U. S. Department of Transportation. Summary of Travel Trends – 2009 National Household Travel Survey. Final Report FHWA-PL-ll-022, June 2011, 83 pages

[17] Zhu, Y., A. Eiguren-Fernandez, W. C. Hinds, and A. H. Miguel. In-cabin commuter exposure to ultrafine particles on Los Angeles freeways. Environmental Science Technology, 2007, 41: 2138 – 2145

[18] Durant, J. L., Ash, C. A., Wood, E. C., Herndon, S. C., Jayne, J. T., Knighton, W. B., . . . Kolb, C. E. (2010). Short-term variation in near-highway air pollutant gradients on a winter morning. Atmospheric chemistry and physics (Print), 10(2), 5599-5626.

[19] Fruin, S., Westerdahl, D., Sax, T., Sioutas, C., & Fine, P. M. (2008). Measurements and predictors of on-road ultrafine particle concentrations and associated pollutants in Los Angeles. Atmospheric Environment, 42(2), 207-219.

[20] Massoli, P., Fortner, E. C., Canagaratna, M. R., Williams, L. R., Zhang, Q., Sun, Y., . . . Jayne, J. T. (2012). Pollution Gradients and Chemical Characterization of Particulate Matter from Vehicular Traffic near Major Roadways: Results from the 2009 Queens College Air Quality Study in NYC. Aerosol Science and Technology, 46(11), 1201-1218.

[21] Pirjola, L., Lähde, T., Niemi, J. V., Kousa, A., Rönkkö, T., Karjalainen, P., . . . Hillamo, R. (2012). Spatial and temporal characterization of traffic emissions in urban microenvironments with a mobile laboratory. Atmospheric Environment, 63, 156-167.

[22] Westerdahl, D., Fruin, S., Sax, T., Fine, P. M., & Sioutas, C. (2005). Mobile platform measurements of ultrafine particles and associated pollutant concentrations on freeways and residential streets in Los Angeles. Atmospheric Environment, 39(20), 3597-3610.

[23] Ranjan, M., & Dhaniyala, S. (2009). A novel electrical-mobility-based instrument for total number concentration measurements of ultrafine particles. Journal of Aerosol Science, 40(5), 439-450.

[24] Honicky, R., Brewer, E. A., Paulos, E., & White, R. (2008). N-smarts: networked suite of mobile atmospheric real-time sensors. Paper presented at the Proceedings of the second ACM SIGCOMM workshop on Networked systems for developing regions.

[25] Pallavi Pant, Roy M. Harrison, (2013) "Estimation of the contribution of road traffic emissions to particulate matter concentrations from field measurements: A review", Atmospheric Environment, 77, pp. 78 – 97

[26] Reynolds, A.W., B. M. Broderick. Development of an emissions inventory model for mobile sources. Transportation Research Part D, 5 (2000) 77-101

[27] Environmental Protection Agency, MOVES 2014a User Guide, 201, EPA-420-B-15-095

[28] California Air Resources Board. EMFAC2014 User's Guide. 2014, v1.0.7

[29] Hausberger, S., M. Rexeis, M. Zallinger, R. Luz. Emission Factors from the Model PHEM for the HBEFA Version 3. Graz University of Technology. Institute for Internal Combustion Engines and Thermodynamic (2009) Report Nr. I-20a/2009 Haus-Em 33a/08/679

[30] Abou-Senna, H., Essam Radwan, Kurt Westerlund, C. David Cooper. Using a traffic simulation model (VISSIM) with an emissions model (MOVES) to predict emissions from vehicles on a limited-access highway. Journal of the Air & Waste Management Association, 63(7):819-831, 2013

[31] P. Hao, G. Wu, K. Boriboonsomsin, and M. Barth. Modal Activity-Based Vehicle Energy/Emissions Estimation Using Sparse Mobile Sensor Data. Transportation Research Board Annual Meeting, Washington D.C., January 10-14, 2016Jamriska, L., L. Morawska. A model for determination of motor vehicle emission factors from on-road measurements with a focus on submicrometer particles. The Science of the Total Environment, 264 (2001, 241-255

[32] Ntziachristos, L., Polidori, A., Phuleria, H., Geller, M. D., & Sioutas, C. (2007). Application of a Diffusion Charger for the Measurement of Particle Surface Concentration in Different Environments. Aerosol Science and Technology, 41(6), 571-580.

[33] Frank, B. P., Saltiel, S., Hogrefe, O., Grygas, J., & Garland Lala, G. (2008). Determination of mean particle size using the electrical aerosol detector and the condensation particle counter: Comparison with the scanning mobility particle sizer. Journal of Aerosol Science, 39(1), 19-29.

[34] Foote, E.; Maricq, M. M.; Sherman, M.; Carpenter, D.; Guenther, M.; Peabody, J.; Polster, M.; Szente, J.; Loos, M., "Evaluation of partial flow dilution methodology for light duty particulate mass measurement." SAE Tech. Pap. 2013, 2013-01-1567, doi:10.4271/2013-01-1567.

[35] Khalek, I., Ullman, T., Shimpi, S., Jackson, C., Dharmawardhana, B., Silvis, W., Kreft, N., Harvey, R., Munday, D., Yamagishi, Y., Graze, R., Smitherman, J., Adkins, J., Performance of Partial Flow Sampling Systems Relative to Full Flow CVS for Determination of Particulate Emissions under Steady-State and Transient Diesel Engine Operation. SAE Technical Paper, 2002, 2002-01-1718, doi: 10.4271/2002-01-1718.

[36] Sun, E., McMahon, W., Peterson, D., Wong, J. et al., Evaluation of an Enhanced Constant Volume Sampling System and a Bag Mini Diluter for Near Zero Exhaust Emission Testing. SAE Technical Paper, 2005, 2005-01-0684, doi: 10.4271/2005-01-0684.

[37] Schweizer, T., Stein, H., A new approach to particulate measurement on Transient Test Cycles: Partial flow dilution as alternative to CVS full flow systems. SAE Technical Paper Series, 2000, 2000-01-1134.

[38] Thiel, W., Hornreich, C., Mörsch, O., and Seifert, G., "Problems of Partial Sample Systems for Modal Raw Exhaust Mass Emission Measurement," SAE Technical Paper 2003-01-0779, 2003, doi:10.4271/2003-01-0779.

[39] Mishra, P., Iyer, S., and Klinikowski, D., "Uncertainties in Emissions Measurements in a Partial Flow Sampling System," SAE Technical Paper 2015-26-0096, 2015, doi:10.4271/2015-26-0096.

[40] CFR, Code of Federal Regulations, 40 Parts, PART 1065—ENGINE-TESTING PROCEDURES. Available at: http://www.ecfr.gov/cgi-bin/text-idx?tpl=/ecfrbrowse/Title40/40cfr1065_main_02.tpl 2011.

[41] Khalek, I.A. 2007 Diesel Particulate Measurement Research; Coordinating Research Council (CRC) Report E-66 Phase 1; CRC: Alpharetta, GA, 2005; available at http://www.crcao.org/publications/emissions/index.html.

[42] Khalek, I.A. 2007 Diesel Particulate Measurement Research; Coordinating Research Council (CRC) Report E-66 Phase 2; CRC: Alpharetta, GA, 2006; available at http://www.crcao.org/publications/emissions/index.html.

[43] Khalek, I.A. 2007 Diesel Particulate Measurement Research; Coordinating Research Council (CRC) Report E-66 Phase 3; CRC: Alpharetta, GA, 2007; available at http://www.crcao.org/publications/emissions/index.html.

[44] U.S. Environmental Protection Agency, EPA Proposes Tier 3 Tailpipe and Evaporative Emission and Vehicle Fuel Standards. Office of Transportation and Air Quality, EPA 2013, EPA-420-F-13-018a, (Available at: http://www.epa.gov/otaq/documents/tier3/420f13018a.pdf).

[45] CARB, Staff report: LEV III PM, technical support document- development of particulate matter mass standard for future light-duty vehicles. 2012.

[46] CFR, Code of Federal Regulations, 40 Parts, PART 1066—VEHICLE-TESTING PROCEDURES. Available at: http://www.ecfr.gov/cgi-bin/text-idx?tpl=/ecfrbrowse/Title40/40cfr1066_main_02.tpl 2012.

[47] Ntziachristos, L., Samaras, Z., The Potential of a Partial-Flow Constant Dilution Ratio Sampling System as a Candidate for Vehicle Exhaust Aerosol Measurements. J. Air & Waste Manage. Assoc. 60:1223–1236. DOI:10.3155/1047-3289.60.10.1223.

[48] Xue, J., Johnson, K., Durbin, T., Russell, R., Pham, L., Miller, W., Swanson, J., Kittelson, D., Jung, H., 2017, Very Low Particle Matter Mass Measurements from Light-Duty Vehicles, submitted Aerosol Science and Technology, July.

[49] Pui, D. Y. H., Fruin, S., & McMurry, P. H. (1988). Unipolar Diffusion Charging of Ultrafine Aerosols. Aerosol Science and Technology, 8(2), 173-187.

[50] Biskos, G., Reavell, K., & Collings, N. (2005). Unipolar diffusion charging of aerosol particles in the transition regime. Journal of Aerosol Science, 36(2), 247-265.

[51] Filippov, A. V. (1993). Charging of aerosol in the transition regime. Journal of Aerosol Science, 24(4), 423-436.

[52] Keller, A., Fierz, M., Siegmann, K., Siegmann, H. C., & Filippov, A. (2001). Surface science with nanosized particles in a carrier gas. Journal of Vacuum Science & Technology A, 19(1), 1-8.

[53] Pandis, S. N., Baltensperger, U., Wolfenbarger, J. K., & Seinfeld, J. H. (1991). Inversion of aerosol data from the epiphaniometer. Journal of Aerosol Science, 22(4), 417-428.

[54] Jung, H., & Kittelson, D. B. (2005). Characterization of Aerosol Surface Instruments in Transition Regime. Aerosol Science and Technology, 39(9), 902-911.

[55] Kaufman, S., Medved, A., Pöcher, A., Hill, N., Caldow, R., & Quant, F. (2002). An electrical aerosol detector based on the corona-jet charger. Paper presented at the AAAR conference (poster).

[56] Hinds, W. C. (2012). Aerosol technology: properties, behavior, and measurement of airborne particles: John Wiley & Sons.

[57] TSI (2014)

[58] Hatch, T., & Choate, S. P. (1929). Statistical description of the size properties of non uniform particulate substances. Journal of the Franklin Institute, 207(3), 369-387.

[59] Zheng, Z., Durbin, T. D., Xue, J., Johnson, K. C., Li, Y., Hu, S., . . . Jung, H. S. (2014). Comparison of Particle Mass and Solid Particle Number (SPN) Emissions from a Heavy-Duty Diesel Vehicle under On-Road Driving Conditions and a Standard Testing Cycle. Environmental Science & Technology, 48(3), 1779-1786.

[60] Harris, S. J., & Maricq, M. M. (2001). Signature size distributions for diesel and gasoline engine exhaust particulate matter. Journal of Aerosol Science, 32(6), 749-764.

[61] Xue, J., Li, Y., Wang, X., Durbin, T. D., Johnson, K. C., Karavalakis, G., . . . Jung, H. S. (2015). Comparison of Vehicle Exhaust Particle Size Distributions Measured by SMPS and EEPS During Steady-State Conditions. Aerosol Science and Technology, 49(10), 984-996.

[62] MAYNARD, A. D. (2003). Estimating Aerosol Surface Area from Number and Mass Concentration Measurements. Annals of Occupational Hygiene, 47(2), 123-144.

[63] Woo, K.-S., Chen, D.-R., Pui, D. Y. H., & Wilson, W. E. (2001). Use of Continuous Measurements of Integral Aerosol Parameters to Estimate Particle Surface Area. Aerosol Science and Technology, 34(1), 57-65.

[64] Fierz, M., Houle, C., Steigmeier, P., Burtscher, H. (2011). Design, Calibration, and Field Performance of a Miniature Diffusion Size Classifier. Aerosol Science and Technology, 45:1-10

[65] Nguyen, A.; Jung, H. Influence of Wind and Driving Conditions on Self-Polluting Tailpipe Emission 2017, in preparation

[66] Grady, Michael (2013). On-Road Air Quality and the Effect of Partial Recirculation on In-Cabin Air Quality for Vehicles (Master Thesis). Retrieved from https://escholarship.org/uc/item/5343s1pd

[67] Jiménez-Palacios, José Luis. Understanding and Quantifying Motor Vehicle Emissions with Vehicle Specific Power and TILDAS Remote Sensing. Diss. MIT, 1999. Cambridge, MA

[68] Levoni, Chiara; Cervino, Marco; Guzzi, Rodolfo; Torricella, Francesca. Atmospheric aerosol optical properties: a database of radiative characteristics for different components and classes. Applied Optics, 1997, vol. 36, No. 30, 8031-8041.

[69] Zhu, Y.; Hinds, W.; Kim, S.; Shen, S.; Sioutas, C. Study of ultrafine particles near a major highway with heavy-duty diesel traffic. Amos. Env. 2002, 36, 4323-4335.

[70] Barth, M., Scora, G.; Boriboonsomsin, K. Link based PM prediction from traffic data and tailpipe PM emission model, Personal communication, 2010.

[71] Zhu, Y.; Kuhn, T.; Mayo, P.; Hinds, W. Comparison of Daytime and Nighttime Concentration Profiles and Size Distributions of Ultrafine Particles near a Major Highway. Env. Sci. Tech., 2006, 40, 2531-2536.

[72] Zhu, Y.; Pudota, J.; Collins, D.; Allen, D.; Clements, A.; DenBleyker, A.; Fraser, M.; Jia, Y.; McDonald-Buller, E.; Michel, E. Air pollutant concentrations near three Texas roadways, Part I: Ultrafine particles. Amos. Env., 2009, 43, 4513-4522.

[73] Mathis, Urs; Mohr, Martin; Forss, Anna-Maria. Comprehensive particle characterization of modern gasoline and diesel passenger cars at low ambient temperatures. Atmospheric Environment. 39, 2005, 107-117.

[74] Jayaratne, E. R.; Meyer, N. K.; Ristovski, Z. D.; Morawska, L. Volatile Properties of Particles Emitted by Compressed Natural Gas and Diesel Buses during Steady-State and Transient Driving Modes. Env. Sci. Tech., 2012, 46, 196-203.

[75] EPA. 2017. Dynamometer Drive Schedules. https://www.epa.gov/vehicle-and-fuel-emissions-testing/dynamometer-drive-schedules

[76] Hood, J. F.; Silvis, W. M., Predicting and preventing watr condensation in sampled vehicle exhaust for optima CVS dilution. SAE Tech. Pap. 1998, 1998-02-23, (DOI:10.4271/980404).

[77] Maricq, M. M.; Chase, R. E.; Podsiadlik, D. H.; Vogt., R., Vehicle exhaust particle size ditributions: A comparison of tailpipe and dilution tunnel measurements. SAE Tech. Pap. 1999, 1999-01-1461, doi:10.4271/1999-01-1461.

[78] Kittelson, D.; Arnold, M.; Watts, W. F., Final Report: Review of diesel particulate matter sampling methods. Available at: http://www.me.umn.edu/centers/cdr/reports/EPAreport3.pdf

[79] Maricq, M. M., Szente, J. J., Harwell, A. L., & Loos, M. J. (2017). Impact of aggressive drive cycles on motor vehicle exhaust PM emissions. Journal of Aerosol Science, 113, 1-11. doi: http://dx.doi.org/10.1016/j.jaerosci.2017.07.005.